CR 115283

OPEN



AEROTHERM CORPORATION

ADVANCES IN AEROTHERMOCHEMISTRY

Aerotherm Project 6099

Aerotherm
Final Report 71-38

# INVESTIGATION OF THERMAL PROTECTION SYSTEMS EFFECTS ON VISCID AND INVISCID FLOW FIELDS FOR MANNED ENTRY SYSTEMS

by

Eugene P. Bartlett
Howard L. Morse
Henry Tong

prepared for

National Aeronautics and Space Administration

September 22, 1971

Extension to

Contract NAS9-9494

Technical Management
NASA Manned Spacecraft Center
Houston, Texas
Structures and Mechanics Division
Donald M. Curry

## FOREWORD

This report was prepared by the Aerotherm Division of the Acurex Corporation under an extension of NASA/Manned Spacecraft Center Contract NAS9-9494. The period covered by this extension was from 9 March 1971 to 9 September 1971.

The sponsor of the program was the Thermal Protection Section, Structures and Mechanics Division, Manned Spacecraft Center, National Aeronautics and Space Administration, Houston, Texas. Mr. Donald M. Curry was the NASA/MSC technical monitor.

The Aerotherm program manager and principal investigator was Eugene P. Bartlett and this report was prepared with contributions from Howard L. Morse and Henry Tong.

## ABSTRACT

Procedures and methods for predicting aerothermodynamic heating to delta orbiter shuttle vehicles has been reviewed. A number of approximate methods were found to be adequate for large scale parameter studies, but are considered inadequate for final design calculations. It is recommended that final design calculations be based on a computer code which accounts for non-equilibrium chemistry, streamline spreading, entropy swallowing, and turbulence It is further recommended that this code be developed with the intent that it can be directly coupled with an exact inviscid flow field calculation when the latter becomes available.

The recommended procedure for parameter studies is to calculate local pressures based on tangent cone or wedge approximations and heat transfer following Eckert's reference enthalpy method. This procedure is relatively simple and was found to agree favorably with wind tunnel data for a shuttle configuration at angles-of-attack which are of potential interest.

A nonsimilar, equilibrium chemistry computer code (BLIMP) was used to evaluate the effects of entropy swallowing, turbulence, and various three dimensional approximations. These solutions were compared with available wind tunnel data. It was found from this study that, for wind tunnel conditions, the effect of entropy swallowing and three dimensionality are small for laminar boundary layers but entropy swallowing causes a significant increase in turbulent heat transfer. However, it is noted that even small effects (say, 10-20%) may be important for the shuttle reusability concept.

TABLE OF CONTENTS

## LIST OF TABLES



## LIST OF FIGURES

## LIST OF SYMBOLS

| | |
|---|---|
| a | angle between fin chord line and vehicle symmetry plane (see Fig. 5) |
| $C_p$ | specific heat capacity |
| $C_f$ | skin friction coefficient |
| h | heat transfer coefficient |
| $h_2$ | spreading factor |
| H | form factor = displacement thickness/momentum thickness |
| i | enthalpy |
| k | thermal conductivity |
| K | Reynolds analogy factor, also $\sqrt{\frac{R_T}{R_C}}$ |
| m | meridianal coordinate |
| p | pressure |
| q,$\dot{q}$ | heat transfer rate |
| $\bar{q}$ | heat transfer coefficient |
| r | recovery factor |
| $r_o$ | normal distance from centerline to body surface for an axisymmetric body |
| R | nose radius |
| $R_C$ | streamwise radius |
| $R_T$ | transverse radius |
| s | streamwise coordinate |
| t | $i + \frac{u^2 + v^2}{2}$ |
| T | temperature |
| w | streamwise normal velocity |
| v | cross flow velocity |
| x,y,z | coordinates |

## Greek Symbols

| | |
|---|---|
| $\alpha$ | vehicle reference line angle of attack |
| $\bar{\alpha}$ | angle between wing chord line and reference line |
| $\bar{\bar{\alpha}}$ | local surface inclination with respect to chord line |
| $\delta$ | norminal sweep angle of fin (see Fig. 5) |
| $\gamma$ | true angle of incidence on wing; also specific heat ratio |
| $\gamma'$ | true angle of incidence on fin |
| $\zeta$ | semi-apex angle of wing (see Fig. 5) |
| $\theta_B$ | body surface inclination |
| $\Lambda$ | true sweep angle of wing leading edge (see Fig. 5) |
| $\Lambda'$ | true sweep angle of fin leading edge (see Fig. 5) |
| $\mu$ | viscos. $\gamma$ |
| $\rho$ | density |
| $\phi$ | local wing dihedral angle (see Fig. 5) |
| $\phi'$ | tilt angle of fin (see Fig. 5) |

## Subscripts

| | |
|---|---|
| D | dissociation |
| e | boundary layer edge |
| o | stagnation |
| r | reference |
| s | stagnation point or stagnation line |
| $\infty$ | freestream |

## Dimensionless Parameters

| | |
|---|---|
| Le | Lewis number |
| M | Mach number |
| Nu | Nusselt number |
| Pr | Prandtl number |
| St | Stanton number |
| Re | Reynolds number |
| $Re_\theta$ | Reynolds number based on momentum thickness |

## SECTION 1

## INTRODUCTION

The design of an efficient thermal protection system for a shuttle orbiter requires reliable heat transfer prediction methods. Under orbital entry conditions, heating is principally a boundary layer phenomena but even exact boundary layer analyses would be inadequate without sufficient methods for predicting pressure distributions and edge boundary conditions. These predictions of aerodynamic heating and edge conditions may be based on analytic methods, experimental data or a hybrid combination of these two.

Analytical techniques, which are presently available, cannot yield precise predictions for heating distributions everywhere on the body although, with suitable approximations, they can satisfactorily predict heating rates to local regions such as the nose, leading edge and centerline portion of the orbiter. The key here is "suitable approximations." The test of whether or not an approximate is suitable depends on a comparison of predictions with either an exact solution or experimental data. An exact solution for shuttle geometries is not available and wind tunnel data, though highly desirable, is singularly insufficient because of inadequate simultaneous duplication of pertinent parameters in ground test facilities and the lack of complete model scaling laws to permit confidence in extrapolating to flight conditions.

Thus the present capability must rely on approximate analytic or semi-analytic methods fortified by ground facility experimental data. The ideal kind of analysis would be one which is derived from a consideration of all phenomena (including for example, homogeneous chemistry) associated with the flight conditions and which can be generalized to wind tunnel conditions. Then if the analysis adequately predicts the levels of wind tunnel heating, there will be a high degree of confidence in the predicted heating to the flight vehicle.

A very comprehensive review on heat transfer prediction capabilities for Apollo-class vehicles is presented in Reference 1. However, shuttle differs from Apollo in many aspects, each of which increases the prediction requirements. The present discussion will center around these difficulties and prediction methodology which are directly applicable to shuttle requirements. Two of the most outstanding differences between shuttle and Apollo are that shuttle is a true three-dimensional body and is large; a typical configuration would cover

half of a football field. An additional difference which is not readily apparent is in the design philosophy; each Apollo was flown only once so that it was, at least in principle, possible to design early vehicles conservatively and adjust the thermal protection weights on successive vehicles using flight data. Such is not the case with shuttle. To be successful, the "first-off" shuttle should be designed for upwards of 100 flights so that ultra-conservative design procedures would render shuttle impractical.

The choice of a thermal protection system has a significant bearing on the required prediction accuracy. Ablative materials, as were used on Apollo, have a high degree of accommodation or tolerance and can survive through sustained exposure to higher-than-expected heating rates so long as sufficient coating thicknesses are provided. In contrast, the surface temperature of a radiation cooled surface, as is proposed for shuttle applications, is dependent on the heating rates. Metallic surfaces have a maximum service temperature which when exceeded results in rapid deterioration of the material and will reduce the degree of vehicle reusability. Hence prediction accuracy is more critical for shuttle.

The selection of materials for the shuttle thermal protection system depends on the expected peak heating rates which will be maintained lower than those experienced by Apollo. This will be achieved by decelerating the vehicle at higher altitudes but, at the lower densities associated with these altitudes, non-equilibrium chemistry effects are enhanced. These effects may be beneficial in the stagnation region if noncatalytic materials are utilized but a penalty must be paid in increased downstream heating. Nonequilibrium chemistry also increases the concentration of dissociated oxygen near the surface which may drastically increase oxidation rates and hence reduce the life expectancy of the vehicle.

Shuttle size enhances the probability of turbulent flow in the boundary layer which in turn increases heating rates. A serious question is raised regarding where on the vehicle and when during the trajectory transition will occur. Transition during the peak heating phase of the entry may dictate higher temperature materials on the shuttle afterbody. Thus adequate transition criteria must be specified.

Apollo was launched in tandam with the launch vehicle and thermally protected from ascent heating. Shuttle will probably be launched in a piggy-back fashion so that shock interference between the launch vehicle and shuttle may locally increase the thermal protection requirements. Further, during entry maneuvers, various control surfaces will interact with the normal flow field patterns to cause interference heating and flow separation-reattachment problems.

## SECTION 2

## CHARACTER OF FLOW FIELD DURING HEATING

For purposes of convenience and analytic simplification, assumptions regarding the nature of a hypersonic flow field are often divided into the fluid flow and chemistry aspects. Typical assumptions which are made are shown below.

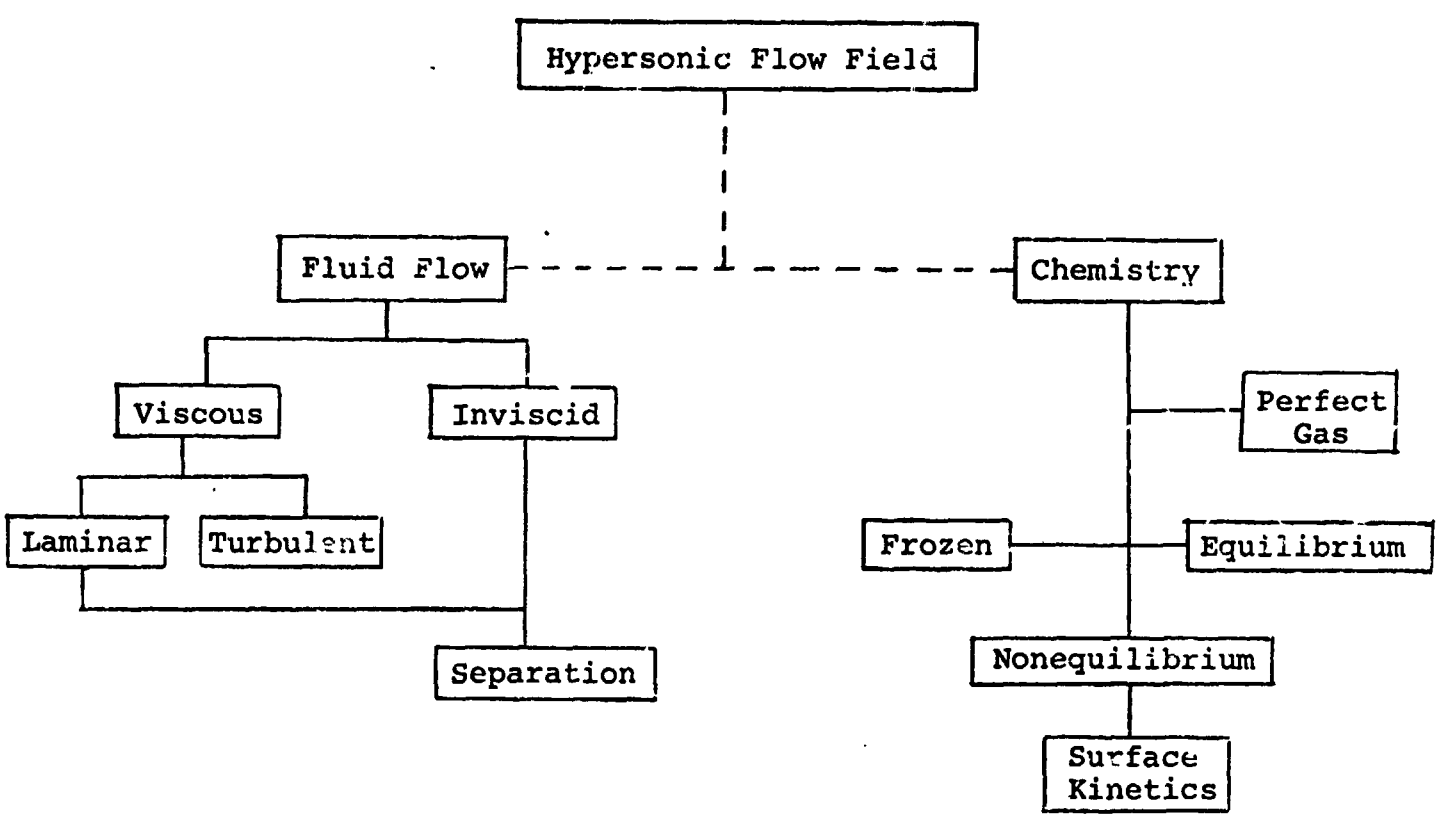


Depending on the entry conditions and location on the vehicle, various combinations may be simultaneously important. For example, at the stagnation point, a laminar boundary layer with nonequilibrium chemistry may occur. The challenge of shuttle is that somewhere in its trajectory there will be separated, inviscid, and viscous flows; the last will involve laminar and turbulent flows and nonequilibrium chemical kinetics will be important. In short, all of the above phenomena at one time or another will be important.

## 2.1 STAGNATION REGION

In the stagnation region of the nose or leading edge and at low altitudes where the density is high, the chemical reaction rates will be rapid enough for equilibrium assumptions to be valid. Further it can be shown that there are negligibly small errors associated with the assumption that a well defined boundary layer exists with zero gradients for edge conditions. Within the confines of these assumptions, several solutions (analytic, correlation and experimental) are available and have proven accuracy.

At moderate altitudes, the equilibrium chemistry assumption is not valid although the boundary layer assumptions still are. Thus the viscous and inviscid fields are still decoupled and can be analyzed separately. In the inviscid shock layer, which is much thicker than the boundary layer, the predominant chemical reaction is dissociation. Dissociation, being a two-body reaction, can achieve equilibrium even though recombination in the boundary layer is near frozen. Thus the boundary layer edge conditions can be readily determined without solving the inviscid field. Because of this simplification, analyses are available for the nonequilibrium stagnation boundary layer. A useful simplification and special case of nonequilibrium is a frozen boundary layer. This assumption has often been used for studies of surface kinetics.

At high altitudes, even dissociation rates are not rapid enough to achieve equilibrium, so if boundary layer assumptions are retained a more careful analysis of the inviscid flow must be used to determine the boundary layer edge conditions. Actually, the boundary layer assumptions commence to breakdown as nonequilibrium chemistry begins to be important so that at high altitudes nonequilibrium viscous shock layer assumptions are used for analysis. Solution methods for these flows are available for simplified air models and recently for general multicomponent models.

At still higher altitudes, the shock wave begins to grow and can no longer be considered as thin. Eventually the shock wave merges with the shock layer to form a viscous merged layer. General chemistry analyses of this flow regime are not available but, fortunately, it does not occur during the shuttle heating cycle.

## 2.2 DOWNSTREAM REGIONS

Regardless of whether the stagnation flow is of the boundary layer type or viscous shock layer type, far enough downstream the windward side of shuttle will approach a viscous and an inviscid layer. Because of the chemical reactions

and effects of shock curvature, the governing differential equations, with boundary layer assumptions, are nonsimilar but can still be analyzed provided the edge boundary conditions are known.

However, at high altitudes and just downstream of the stagnation region, the boundary layer assumptions may not be valid. For these conditions, the complete shock layer may be viscous, chemically reacting and nonsimilar, a condition for which there are apparently no published exact solutions.

When the boundary layer assumptions are valid, solutions are available for general air, chemically reacting flows around simple body shapes. These techniques show promise, with the application of streamline divergence methods, of being suitable for shuttle. Nonetheless, even a perfect boundary layer analysis would be inadequate if appropriate techniques are not available for specifying the edge boundary conditions. Pressure distributions do not seem to be very sensitive to chemistry so they are often determined a priori, by approximation techniques. Subsequently, the other edge conditions are approximated. The ideal approach would be to solve the direct problem for the inviscid field, but present technology* permits this only for simple body shapes and even then calculation times are long and not practical for extended trajectory studies.

As the flow progresses downstream, boundary layer growth may lead to transition into turbulent flow. Although correlation and analogue methods are available for approximate predictions of turbulent heating, the prediction of when transition will occur is in a state of flux. The establishment of a transition criteria is further complicated by its dependence on the state of the gas at the edge of the boundary layer and other boundary layer parameters.

If the windward side of shuttle poses some difficult prediction problems, accurate prediction of the leeward side is virtually impossible. Only a very limited number of studies have been conducted on leeward shuttle heating. At very small angles-of-attack, when the flow remains attached, methods similar to those used for the windward side are applicable, although it should be noted that here the streamlines are converging rather than diverging as on the windward side. However, at high angles of attack, flow separation occurs and the viscous-inviscid interactions are not yet amenable to analysis. Extensive experimental data and conservative extrapolations appear to be the only recourse.

---

*In this context, "present technology" means existing, operational and reliable computer codes.

## SECTION 3

## APPROXIMATE HEAT TRANSFER PREDICTION METHODS

### 3.1 STAGNATION AND LEADING EDGE REGIONS

The state-of-the-art for predicting stagnation region heat transfer rates to planar or axisymmetric bodies is well in hand. Adequate predictions can be made using available solutions[2-11] for both non-catalytic and fully catalytic surfaces so that only a cursory discussion will be presented. Assuming a binary air model, reference 2 also presents general nonequilibrium solutions for surfaces of arbitrary catalycity. Two difficulties occur when arbitrary catalycities are concerned. First, there is very little data on the dependence of surface catalycity on temperature and second, there is no information to adequately define catalytic efficiency for gases with more than one dissociated specie. However, an important conclusion to be reached from examination of these analyses is that for stagnation point flows to surfaces of infinite catalycity at temperatures of interest there is only a negligible difference in heat transfer between assumptions of equilibrium and nonequilibrium chemistry. This conclusion is especially important because of the simple correlation solutions which have been obtained for equilibrium flows. Thus, since experimental evidence shows that metallic surfaces tend to be catalytic, these equilibrium chemistry solutions can be used to predict the heat transfer rates. In addition, for low catalycity surfaces, these predictions represent an upper bound on the expected heating rates.

The accuracy of the above analyses have been adequately proven for both ground test and flight hardware, but in order to apply them to shuttle whose stagnation point may be neither axisymmetric nor planer, some method such as reference 12 must be used to account for three dimensional effects. For instance, for an axisymmetric stagnation point in a dissociating flow[2]

$$\frac{Nu_x}{\sqrt{Re_x}} = 0.76\ Pr^{0.4}\left(\frac{\rho_s \mu_s}{\rho_w \mu_w}\right)^{0.4} \left\{1 + (Le^n - 1)\ \frac{i_D}{i_o}\right\} \qquad (3\text{-}1)$$

where

$$n = \begin{cases} 0.52 & \text{equilibrium chemistry} \\ 0.63 & \text{frozen chemistry} \end{cases}$$

Then for $R_T$ and $R_C$ as the principal radii of curvature of a non-axisymmetric stagnation point, Equation (3-1) is scaled by the expression

$$\left[\frac{Nu_x}{\sqrt{Re_x}}\right]_{R_T,R_C} = \frac{\sqrt{1+K}}{\sqrt{2}}\left[\frac{Nu_x}{\sqrt{Re_x}}\right]_{R_T}$$

where

$$K = \sqrt{\frac{R_T}{R_C}}$$

and $[Nu_x/\sqrt{Re_x}]_{R_T}$ is the stagnation point value for an axisymmetric nose radius equal to $R_T$. Note that for $R_C >> R_T$ the solution degenerates to that for a stagnation line.

The leading edges of the delta wing portion of the vehicle are not stagnation lines and should be considered as swept or yawed cylinders. Solutions for finite length cylinders are not available since this comprises a true three-dimensional body. In addition, nonequilibrium chemistry has not been generally considered. Even so, for catalytic surfaces, adequate predictions can be made by assuming that the leading edge is an infinite swept cylinder. Then, drawing upon stagnation point experience an equilibrium chemistry correlation solution such as Reference 6 can be used. This will be discussed in Section 3.2.2.

Overall, it is generally concluded that, with the exception of surfaces, of finite catalycities, the confidence level is quite high, even for viscous shock layer flows, for the prediction of stagnation and leading edge heat transfer.

## 3.2 DOWNSTREAM REGIONS

Although it may be necessary to consider viscous shock layers in the vicinity of the stagnation point, the major portion of the lower surface of shuttle can be characterized as having an inviscid region and a boundary layer region. Under these conditions it is the boundary layer that is of primary interest, since an adequate analysis of it would provide required design heating rates. However, the inviscid flow, either in a coupled or independent sense, is important because it provides the boundary conditions for the boundary layer equations.

### 3.2.1 INVISCID FLOW

There are presently some solutions[13-20] for the inviscid flow field about symmetric bodies at angles of attack but a general solution for an arbitrary three-dimensional body is not readily available, although some methods[21,22] are in the development state. For a parametric study of entry trajectories, the inviscid flow field or boundary layer edge conditions should be determined by approximate means; more exact methods being reserved for final trajectory calculations. With the inviscid flow field and the boundary layer assumed to be uncoupled, approximate techniques can be used to specify the boundary layer edge conditions and a solution of the inviscid field becomes unnecessary.

It has been noted[23,24] that pressure distributions are relatively insensitive to chemistry and displacement effects at sufficiently high Reynolds numbers so that most approximation methods center first upon obtaining the surface pressure distribution and then using it to determine the chemical, thermodynamic and dynamic states of the fluid at the edge of the boundary layer. For simple axisymmetric bodies, it has been shown[25] that a modified Newtonian pressure distribution is sufficient (within 5% of experimental data) and is the assumption used by several investigators[10,11,25,26]. However for wind tunnel delta winged models, the modified Newtonian pressure was found[27] to be 15 to 20% lower than experimental measurements. For this configuration, Marvin et al show that the elliptic-cone technique is more accurate. However, Fannelop[30] shows that a similar but simpler procedure (effective cone technique) is adequate for symmetric bodies at angle of attack by comparing predictions with the experimental data of Cleary[31]. Laminar heat transfer rates are approximatley proportional to the square root of the pressure so that relative errors in heat transfer rates, due to inaccurate pressures, will be less than the relative pressure errors. Thus, pressure approximations which are accurate to the order of a few percent should be sufficient and more refined approximations would be of second order and would probably be overshadowed by the question of boundary layer edge chemistry. An exception to the above would be for flight conditions for which turbulent flow is expected. Transition phenomena is dependent on the edge Mach number which in turn depends on the pressure distribution. Experimentally determined boundary layer edge Mach numbers on a straight-winged orbiter model were compared with those predicted from a tangent cone pressure distribution in reference 32 and found to be in good agreement. It then appears that a tangent or effective cone approximation for pressures should be sufficient for shuttle centerline predictions. There is insufficient data to reach any conclusions about pressure distributions on the winged portion of the orbiter although here again tangent cone or, more probably, tangent wedge approximations should be adequate.

Given a pressure distribution on the vehicle centerline, one possible approach for determining the edge conditions would be to calculate an isentropic expansion of the flow from the stagnation point to the local body pressure. The chemistry may be considered as being in equilibrium, nonequilibrium or frozen, with the choice depending on flight conditions. For a significant portion of the shuttle trajectory the altitudes will be high enough so that recombination rates will be relatively slow, hence the expansion will be in chemical nonequilibrium. Even so, an equilibrium expansion is often used since, for catalytic surfaces, it is known that stagnation point heating is relatively insensitive to chemistry, and the same is presumed to be true elsewhere on the body. Furthermore, equilibrium calculations are simpler and edge chemistry does not directly enter into some of the heat transfer prediction schemes.[5,33-39] But, for noncatalytic surfaces, nonequilibrium expansions for sphere cones at zero incidence were suggested by Blottner[40] and were shown to be of significant importance by Lewis[25] for a hyperboloid under flight conditions which simulate points on a typical shuttle trajectory.

Even a nonequilibrium adiabatic expansion may be inadequate for shuttle because of its large size. Far downstream of the stagnation point, the boundary layer edge gas does not originate from the normal shock; rather, it originates from an oblique shock. A similar situation arises for flows with large shock curvature since an expansion, of any kind, from the stagnation region presumes that the entropy at the edge of the boundary layer has the high value generated by a normal shock wave. In reality, at a sufficiently far downstream location the stagnation entropy will be gradually swallowed by the boundary layer and the edge entropy will decrease and approach the value behind an oblique shock[41]. Hamilton[42] compares the assumptions of an edge condition determined by expansion from the stagnation point and the state determined by assuming that the flow has just passed through an oblique shock of sufficient strength to get the local pressure. As might be expected, the lower edge entropy for the oblique shock assumption was shown to cause an increase in the predicted heating rates.

Because of the effects induced by shock curvature and entropy swallowing, a complete vorticity interaction analysis would be highly desirable, albeit very difficult. Because of these difficulties, some semi-coupled approximate techniques have been developed. For example, Adams[43] determined the shock shape and pressure distribution in the inviscid flow using an equilibrium chemistry model and the methods described by Lomax and Inouye[44]. Then, assuming that pressures and shock shape are insensitive to chemistry, the nonequilibrium state was determined by integration along streamtubes using this predetermined pressure distribution. Finally, boundary layer solutions were

obtained by iteration of the mass flow within the boundary layer and the absorption of inviscid streamtubes as per Kaplan[45]. It becomes apparent that, even approximate coupling techniques are very complicated and probably very time consuming and application to more complex bodies is hampered still further by the need for an adequate description of a three-dimensional entropy layer.

A more exact accounting of shock curvature and nonequilibrium chemistry effects requires very extensive computer codes which are not available for general three-dimensional bodies. However, codes are available for bodies in chemically equilibrium flows[14,17] but even under these conditions CDC 6600 computational times for sphere-cones at angle of attack are in excess of 5 minutes.[46] For nonequilibrium chemistry and small angles of attack, a perturbation technique which uses available zero incidence solution techniques such as that used by Fannelop[30] could be employed. In general, unless adequate similarity laws are developed, any technique which uses "exact" solutions of the inviscid flow would require a large computer expenditure.

For small angles of attack and far downstream of the stagnation region, the boundary layer edge condition is largely determined by the state behind a weak, oblique shock. Then the degree of dissociation in the inviscid flow will be low and ideal gas assumptions, along with a specified pressure, may be sufficient for determining the edge state. This, of course, does not preclude large amounts of dissociation caused by viscous heating within the boundary layer.

### 3.2.2 BOUNDARY LAYER

With a specified boundary layer edge condition, several approximate methods may be used to predict the heat transfer rates. These include Eckert's reference enthalpy[37,38]; Reynolds analogy[47,48]; rho-mu[49,50]; or swept and modified swept cylinder methods and are representative of methods developed by a combination of theory, experiments and intuition.

Eckert's reference enthalpy method is based on the assumption that incompressible constant property solutions can be used to calculate compressible flow heat transfer if properties are evaluated at an appropriate reference temperature or reference enthalpy. This reference enthalpy is defined as

$$i^* = i_e + 0.5(i_w - i_e) + 0.22(i_r - i_e)$$

At a stagnation point the recovery enthalpy $i_r$ is approximately equal to the edge enthalpy $i_e$ so that

$$i_0^* \simeq 0.5(i_e + i_w)$$

For other regions

$$i_r = i_e + r\frac{u_e^2}{2}$$

For laminar flows $r \sim \sqrt{Pr}$ and for turbulent flows $r \sim \sqrt[3]{Pr}$. Typical imcompressible constant property solutions are:

$$\left.\frac{Nu_x}{\sqrt{Re_x}}\right]_{in} = 0.763(Pr)^{0.4} \qquad \text{(stagnation point)}$$

$$\left.\frac{Nu_x}{\sqrt{Re_x}}\right]_{in} = 0.570(Pr)^{0.4} \qquad \text{(stagnation line)}$$

$$\left.\frac{Nu_x}{\sqrt{Re_x}}\right]_{in} = 0.332(Pr)^{1/3} \qquad \text{(laminar flat plate)}$$

$$Nu_x\Big]_{in} = \frac{0.185\ Re_x Pr^{1/3}}{(\log_{10}Re_x)^{2.584}} \qquad \text{(turbulent flat plate)}$$

where

$$Nu = \frac{hx}{k_e}, \qquad h = \frac{qC_{p,e}}{(i_r - i_w)}, \qquad Re_x = \frac{\rho_e u_e x}{\mu_e}$$

In the reference enthalpy method these are then written as

$$\frac{Nu_x^*}{\sqrt{Re_x^*}} = 0.763(Pr^*)^{0.4} \qquad \text{(stagnation point)}$$

$$\frac{Nu_x^*}{\sqrt{Re_x^*}} = 0.570(Pr^*)^{0.4} \qquad \text{(stagnation line)}$$

$$\frac{Nu_x^*}{\sqrt{Re_x^*}} = 0.332(Pr^*)^{1/3} \qquad \text{(laminar flat plate)}$$

$$Nu_x^* = \frac{0.185\ Re_x^* Pr^{*1/3}}{(\log_{10}Re_x^*)^{2.584}} \qquad \text{(turbulent flat plate)}$$

For dissociated air, the Prandtl number is nearly constant so that the reference enthalpy equations can be written in an alternate form by noting that

$$\frac{Nu_x}{\sqrt{Re_x}} = \frac{Nu_x}{\sqrt{Re_x^*}} \left(\frac{\rho^* \mu^*}{\rho_e \mu_e}\right)^{1/2}$$

Using the experience of the analytic studies performed in Reference 2, the laminar solutions can be corrected for dissociated gases and non-unity Lewis numbers by multiplying the right hand sides by the function

$$1 - (Le^n - 1) \frac{i_D}{i_0}$$

where

$$n = \begin{cases} 0.52 & \text{equilibrium chemistry} \\ 0.63 & \text{frozen chemistry} \\ 0.50 & \text{couette flow} \end{cases}$$

Then, by approximating any point on the body as a stagnation region or a zero pressure gradient wedge/cone, the local heat transfer can be calculated.

The Reynolds analogy method assumes that the velocity and temperature fields are proportional to obtain a simple relationship between heat transfer and skin friction. The Reynolds analogy factor is then defined as

$$K = \frac{2\ St}{C_f}$$

The successful use of the Reynolds analogy depends on an adequate solution for the skin friction coefficient and a method of calculating the Reynolds analogy factor K. Some typical values of K are

$K = 1.0$ — Assumes $Pr = 1$, $M_e \approx 0$

$K = Pr^{-2/3}$ — Empirical determination by Colburn[51]

$$K = \frac{1 + (u_{es}/u_e)}{r + Pr(u_{es}/u_e)}$$

Theoretical value determined by Rubesin[48]

$$\frac{u_{es}}{u_e} = 11.5 \left(\frac{C_f}{2} \frac{T_w}{T_e}\right)^{0.5}$$

$$K = Pr^{-2/3} \exp\left\{1.561 \frac{T_e}{T_s}\left(H - \frac{\gamma - 1}{2} M_e^2\right) - 1.3 \frac{T_w}{T_o}\right\}$$ Empirical determination by Reshotko and Tucker[52]

$$K = \left[1 + 5\sqrt{\frac{C_f^*}{2}}\left(\sigma^* - 1 + \ell n \frac{5\sigma^* + 1}{6}\right)\right]^{-1}$$ Von Kármán

For laminar flow over a flat plate with constant properties, the skin friction coefficient is

$$C_f = \frac{0.664}{\sqrt{Re_x}}$$

For turbulent flows $C_f$ may be determined with methods set forth by Spalding and Chi,[35] Sommer and Short,[53] Van Driest[34] or may use methods such as rho-mu or Eckert's reference enthalpy. The number of possible predictions obtained from a permutation of K and $C_f$ is very large. Select combinations have been compared with experimental data by Pearce[54] for flat plates and by Hopkins and Inouye[55] for flat plates and cones. Pearce concludes that the Spalding-Chi correlation with von Kármán's Reynolds analogy factor is best, whereas Hopkins and Inouye conclude that the Van Driest analysis with a Reynolds analogy factor of 1.0 is best. These differing conclusions are typical for turbulent flows and are indicative of the fact that turbulence is not a well understood phenomena and the results are highly dependent on the particular application.

The swept cylinder methods are based on the analyses of Beckwith,[6] Beckwith and Cohen,[33] and Beckwith and Gallagher.[56] An important conclusion drawn from these solutions is that, even for relatively large sweep angles, the ratio of local heat transfer coefficient to leading edge heat transfer coefficient along a plane perpendicular to the leading edge of a yawed circular cylinder is insensitive to the angle of yaw. For wall temperatures at which there is no dissociation the ratio of heat transfer coefficients based on enthalpy can be expressed as

$$\frac{\bar{q}_w}{\bar{q}_{w,s}} = \left[\frac{\rho_w \mu_w}{(\rho_w \mu_w)_s}\right]^{1/2} \left[\frac{(\beta t_e Pr)_s}{\beta t_e Pr}\right]^{1/2} \left[\frac{du_e/dx}{(du_e/dx)_s}\right]^{1/2} \frac{\theta'_w}{\theta'_{w,s}}$$

where

$$t = i + \frac{u^2 + w^2}{2}$$

$$\beta = \frac{\frac{2}{u_e^2}\frac{t_s}{t_e}\frac{du_e}{dx}}{\rho_w \mu_w r^j} \int_o^x \rho_w \mu_w u_e r^{2j} dx$$

and $\theta'_w$ and $\theta'_{w,s}$ can be determined from tabulated results presented in Reference 33. The local value of heat transfer is then calculated from

$$q_w = \bar{q}_w (i_{Aw} - i_w)$$

with

$$\bar{q}_{w,s} = 0.577 (Pr_w)^{-0.6} (\rho_w \mu_w)^{0.06} (\rho_s \mu_s)^{0.44} \left(\frac{du_e}{dx}\right)_s^{0.5}$$

and

$$i_{Aw} = i_e + r \frac{u_e^2 + v_e^2}{2}$$

The rho-mu method[50] is based on integral solutions of the momentum and energy equations and uses boundary layer thickness parameters and a reference density-viscosity as variable functions. These functions were determined from available exact similarity solutions and, with suitable modifications, account for cross-flow gradients, streamwise gradients, nose bluntness and real gas effects. Hand calculation of the set of rho-mu equations, though possible, is not practical. To facilitate hand calculations, simplified correlation approximations are presented in References 50 and 57 for plates, cones, swept cylinders and the centerlines of sharp delta. In addition, modification procedures for streamline divergence and variable wall temperature cases were described.

## SECTION 4

## CURRENT METHODOLOGY

Current state-of-the-art for predicting shuttle heating rates is not up to the task of considering the vehicle as an entity because of its complex shape. In lieu of this capability, the vehicle is usually segmented into sections for which the heating rates are separately analyzed or approximated. Typical surface regions that are considered are shown in Figure 1. The stagnation region, leading edges and windward surfaces have received the most attention since these regions are expected to be subjected to the highest heating rates and, fortunately, are easier to approximate than the leeward side. However, due to an interaction between separation-reattachment phenomena and transition to turbulence, certain portions of the lee side have been noted to have significant heating rates.

### 4.1 WINDWARD SURFACE

Even though Marvin et. al. show that Newtonian approximations are inadequate for the NAR delta-wing model, the approximation is often favored because it can be expressed in a convenient analytic form. Moreover, Newtonian approximations are known to be adequate for sphere-cones and other simple blunt bodies and are apparently also adequate for lift and drag calculations of delta vehicles.[58] However, one would expect that, since Newtonian approximations (based on body angle) predict the same pressures for cones and wedges, they would be inadequate for regions far from the stagnation point. Hence, depending on the region of interest, different assumptions may be required. Young et. al.,[59] believing that transition to turbulent flow is enhanced by entropy layer swallowing, use a high entropy Newtonian approximation in the laminar flow region and the lower entropy tangent wedge approximation in the turbulent flow region. A tangent wedge approximation was also used in Reference 60 but boundary layer edge approximations were modified with an empirical gas constant. Guard and Schultz[61] based their pressures on a combination of experimental data and blast wave theory of Creager[62] with a correction for nose bluntness. Thomas[63] takes a novel approach; he uses a heat transfer prediction technique and model centerline heating data and works backwards to obtain the pressure distribution which yields the best correlation. With this technique he shows that blast wave correlations with nose bluntness effects are best at slightly negative angles of

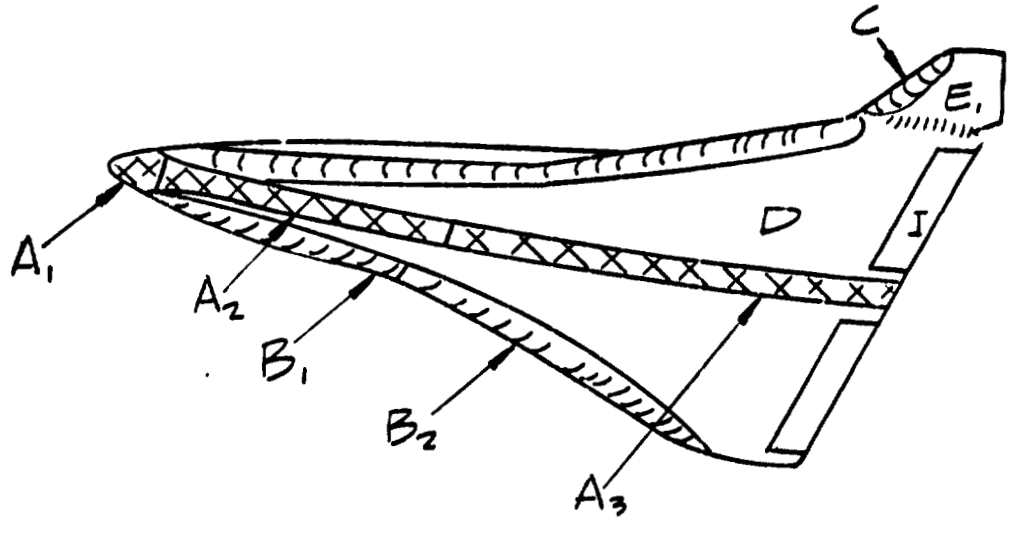


| REGION | DESCRIPTION |
|---|---|
| $A_1$ | STAGNATION REGION |
| $A_2$ | WINDWARD GENERATOR, FORWARD FUSELAGE |
| $A_3$ | WINDWARD GENERATOR, AFT REGION |
| $B_1$ | CHINES |
| $B_2$ | WING LEADING EDGE |
| C | FIN LEADING EDGE |
| D | WING WINDWARD SURFACE |
| $E_1$ | FIN SURFACE, OUTBOARD |
| $E_2$ | FIN SURFACE, INBOARD |
| G | WING LEE SURFACE |
| H | ELEVON LEE SURFACE |
| I | ELEVON WINDWARD SURFACE |

SEE TABLE 1 FOR RECOMMENDED PREDICTION METHODS

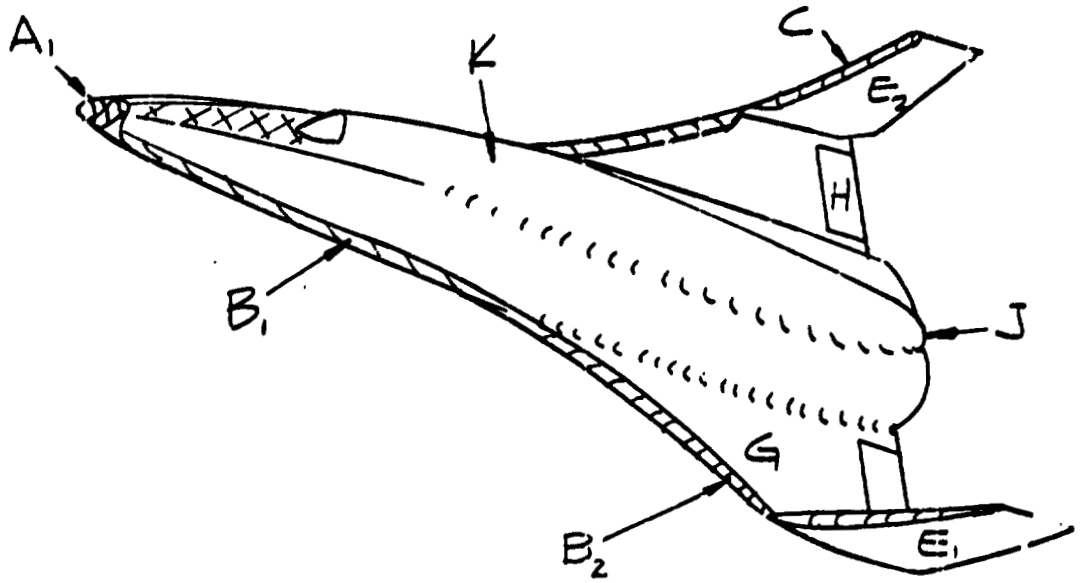


FIGURE 1 TYPICAL HEATING ZONES ON DELTA VEHICLE

A-3807

attack, modified oblique shocks are best at zero incidence and a modified oblique shock accounting for streamline divergence is best at slight positive angles of attack.

Although approximate prediction methods have shown generally good agreement with low enthalpy wind tunnel data, questions dealing with the effects of chemistry, shock curvature and flow interactions need yet to be adequately resolved for flight vehicle prediction confidence. Even for wind tunnel models, pressures along the windward centerline are the most often measured so that more effort needs to be expended on pressure measurements on the remainder of the vehicle.

Given a pressure distribution, an isentropic expansion or oblique shock conditions are the simplest methods for approximating the boundary layer edge flow conditions. However, in efforts to obtain improved approximations, some investigators have employed more sophisticated methods to account for three-dimensional effects.

Marvin et.al. assume that the edge conditions on the vehicle centerline are the same as those behind a swept cylinder inclined at an angle equal to the local body incidence. However, on the wing portion of the vehicle the edge conditions are assumed to be determined by an isentropic expansion from the leading edge. Young et.al. use an isentropic expansion for low angles of attack whereas at high angles of attack they use a swept cylinder theory but correct the stagnation line velocity gradient to account for noncircular cross sections. Masek[64] and Pearce[54] account for the stagnation line cross flow by assuming that the cross-flow velocity gradient is equal to that which occurs on a circular disk with a radius equal to the local wing semi-span and a normal velocity equal to the local normal component of the free stream flow. Pearce points out that the cross flow correction to a plane oblique shock varies from 0 to 13 percent for incidences between 0 and $50^{o}$ which, at least for high angles of attack, makes the correction significant. The data and heating predictions of Marvin et.al and Guard and Schultz represent most of the reported windward side, off centerline heating data for delta vehicles so that not much can be reported on methods applied to the wing portion for determining boundary layer edge conditions. Whereas, Marvin et.al. predict a three-dimensional edge condition, as noted above, Guard and Schultz do not. Guard and Schultz use a planar oblique shock for edge conditions and correct the heat transfer results to account for cross flow.

Current methods for predicting windward-centerline, laminar heat transfer rates are mostly based on adaptations of correlation methods such as Eckert's reference enthalpy or rho-mu theories. Moote,[65] for instance, used the

reference enthalpy method but modified it for conical flows. At low angles of attack Young et.al. also used the reference enthalpy methods but at high angles of attack, a swept cylinder theory (which is a spherical stagnation point theory modified for two dimensionality and sweep) was used. Marvin et.al. used the Beckwith and Cohen cross flow theory to modify the finite difference scheme of Marvin and Sheaffer[66] for streamline divergence effects. This was found to be in good agreement with data for regions aft of the wing-body junction but forward of this point, swept cylinder theory was found to represent the data better.

For laminar flow on the wing of the vehicle, the cross flow theory of Beckwith, and Beckwith and Cohen were used by Marvin et.al. and Young et.al. For lifting body configurations, Guard and Schultz used a similar approach for the underside heating whereas Reference 60 uses Eckert's reference enthalpy method and flat plate solutions with a strip theory correction for cross flow.

For turbulent flow along the vehicle centerline, Hamilton[42] used the Eckert reference enthalpy method with an origin for turbulent flow which is assumed to occur at the start of transition. The Spalding-Chi method was used for simulated shuttle vehicles at low angles of attack by Young et al., Masek and Forney[67] and Moote. The last modified the method used to account for conical flow and real gas effects by using an empirically determined weighting factor of 1.25. At high angles of attack Young et al. chose to use the results of Beckwith and Gallagher, whereas Marvin et al. elected not to be selective and found good agreement between their data and the theories of Spalding-Chi, Sommer-Short and Van Driest for Reynolds analogy factors of 1.0. Hopkins and Inouye recommend Van Driest's method with a factor of 1.0 but note that the Spalding-Chi method with a factor of 1.2 also correlates well with data.

Turbulent flow on the leading edge was predicted by Guard and Schultz by representing it as an isolated swept cylinder and applying the results of Beckwith and Gallagher. Turbulent heating throughout the windward side of a lifting body was predicted by Reference 60 using Eckert's reference enthalpy method with a modified Reynolds analogy and the Schultz-Grunow[68] skin friction law.

It is expected in both laminar and turbulent flows, that the accuracy of the predicted heating rates would be dependent on the accuracy of the specification of the boundary layer edge condition but Young et.al. and Pearce point out that the transition criteria is also dependent on the edge condition. Thus wind tunnel free stream conditions may cause transition to occur earlier on models than might be expected in free flight so that conservative estimates would be obtained by the direct use of the tunnel data.

## 4.2 LEEWARD SURFACE

For very small angles of attack, where the flow on the leeward surface does not separate, the heating predictions have used procedures similar to those used on the windward surface. For example, Guard and Schultz predict the leeward heating for a delta-body vehicle using two-dimensional rho-mu theory and noted good agreement for both laminar and turbulent flows at angles of attack up to $30^{o}$. The good correlations suggest that separation-reattachment phenomena* does not occur in the vicinity where measurements were made. However, the data of Maise[69] for semi-pyramidal shapes at angles-of-attack less than $55^{o}$ and the data of Hefner and Whitehead[70] for a delta-wing orbiter at angles of $20^{o}$ and $40^{o}$ show that the leeward side heating may be nonuniform with regions of "peak" heating. This nonuniform heating is apparently a result of three-dimensional separation-reattachment phenomena complicated by transitional and turbulent flows. Under these conditions it is generally conceded that the prediction of this leeward heating, which requires estimates of pressure and edge flow conditions,** is much too ambitious for current and even near-future technologies. As a first approximation, Reference 60 suggests using tangent cone approximations when the local inclination is positive and use flat plate theory for regions of zero or negative incidence. In this way, transition and turbulent effects can be included but separation-reattachment possibility would cast some doubt on the validity of the predictions.

The only recourse to the above dilemma appears to be semi-empirical techniques utilizing wind tunnel data. Although this would cause a decrease in design confidence, the leeward heating is generally sufficiently low so as not to be serious. Even so, it would not be desirable to be overconservative in the selection of surface material since the leeward area is at least 50 percent of the total vehicle area.

## 4.3 SHORTCOMINGS OF CURRENT METHODOLOGY

With the exception of the stagnation point, the current prediction methods are founded on modifications of solutions which do not, in a physical or mathematical sense, completely account for the real environment to which shuttle will be exposed. This, of course, does not imply that these procedures have been inadequate for preliminary design purposes since a large number of conditions

---

*Which is one of the reasons why the authors chose the delta-body rather than a delta-wing vehicle.

**In passing it should be noted that even the prediction of flow fields for simple shapes such as sphere-cones at angle of attack is no simple task and is the objective of much activity.[69-72]

were studied. However, for final design purposes, the present methods have certain shortcomings that must be minimized or the methods must be replaced by more adequate analyses. A complete inviscid/viscous flow field analysis would be ideal but such a program is not available and its development may not be possible with the resources allotted to shuttle development.

As already discussed, the prediction procedure for the windward side can be considered in three different parts. First, the pressure distribution is determined, then the boundary layer edge conditions are calculated, and finally an appropriate boundary layer solution is used to predict the heating rates. Methods for the prediction of surface pressures are believed, on the whole, to be sufficiently accurate. The other two parts are inadequate for certain critical portions of the shuttle trajectory. In establishing the edge conditions, the two most common assumptions are that the flow originated either from a stagnation region or an oblique shock. The former is valid near and the latter far from the stagnation region. Adams[43] shows that "far" may be as high as 15 nose radii downstream for sphere-cone bodies. In between these extremes, say between 3 and 15 nose radii, a three-dimensional entropy layer will form and swallowing by the boundary layer may be important. None of the above methods accounts for this entropy swallowing effect. In addition, present methods rely on solutions obtained with similar and locally similar assumptions when in fact the boundary layer will be highly nonsimilar.

A somewhat more serious question arises from flow field chemistry. The present methodology makes use of analyses developed for ideal gas flows and corrects for real gas effects by empirical methods (e.g., Eckert's reference enthalpy method). Although these precedures have been shown to yield good agreement for stagnation flows with equilibrium chemistry, their application to downstream flows of complex bodies is not fully justified and in nonequilibrium chemistry with noncatalytic surfaces, these methods fail except to bracket the probable heating range. Moreover the prediction methods are based on similarity or local similarity assumptions which are generally invalid for nonequilibrium chemistry boundary layers.

Turbulent boundary layer heat transfer predictions may be very important for shuttle. As noted though, there are several prospectively good approximation methods; the choice of which may depend on the particular geometry and/or environmental conditions. None of these methods is believed to be universally correct; in fact, since none of these methods directly account for nonsimilarity and thermochemistry effect , they may be seriously in error for shuttle even though they adequately predict wind tunnel heating rates.

## 4.4 RECOMMENDED CURRENT STATE-OF-THE-ART METHODOLOGY

It has been noted that pressure distributions are relatively insensitive to chemistry so that pressures can be determined from ideal gas flows in the form of experimental correlations or analyses. Modified Newtonian flow methods are the simplest to use since the pressure can be expressed analytically, but it was shown in wind tunnel measurements on a scale delta-wing vehicle that the predicted centerline pressures are about 15-20 percent lower than measured values. Nonetheless, for rough-cut calculations on the vehicle centerline, this should be sufficient. For more accurate predictions a tangent cone method is recommended over the more complex elliptic cone method. A comparison of these two predictions and the data of Marvin et.al. is shown in Figure 2 and good agreement is obtained up to an angle-of-attack of $40^{o}$. At $53.5^{o}$ the tangent cone method overpredicts the pressure by about 10 percent whereas the elliptic cone method underpredicts by about 5 percent. Thus the tangent cone approximation will lead to conservative (higher) heat transfer predictions. In retrospect, the failure of the tangent cone approximation at $53.5^{o}$ should be expected since this angle approaches the maximum cone angle that will support an attached shock and, at these high angles, the precedure would begin to fail even for slightly blunted cones.

If an approximate analytic equation is desired, a modified tangent cone/wedge method can be developed as follows. The Newtonian pressure is given as

$$p - p_{\infty} = \rho_{\infty} U_{\infty}^{2} \sin^{2}\alpha$$

where $\alpha$ is the angle of the surface with respect to the free stream vector. At a stagnation point the Newtonian pressure is higher than the actual pressure whereas on sharp wedges and sharp cones it is lower. The modified Newtonian pressure adjusts the predicted value to be correct at the stagnation point; then the pressure is given by

$$\frac{p - p_{\infty}}{p_{s} - p_{\infty}} = \sin^{2}\alpha$$

This modified Newtonian pressures does a very good job of predicting the pressure distribution on the forward portion of blunt bodies, but far from the nose region this procedure predicts a slightly lower pressure than the unmodified method. Thus the discrepancy is widened further. Since the Newtonian formulation is analytically convenient the following procedure is recommended for large ratios of surface distance to nose radius. Let

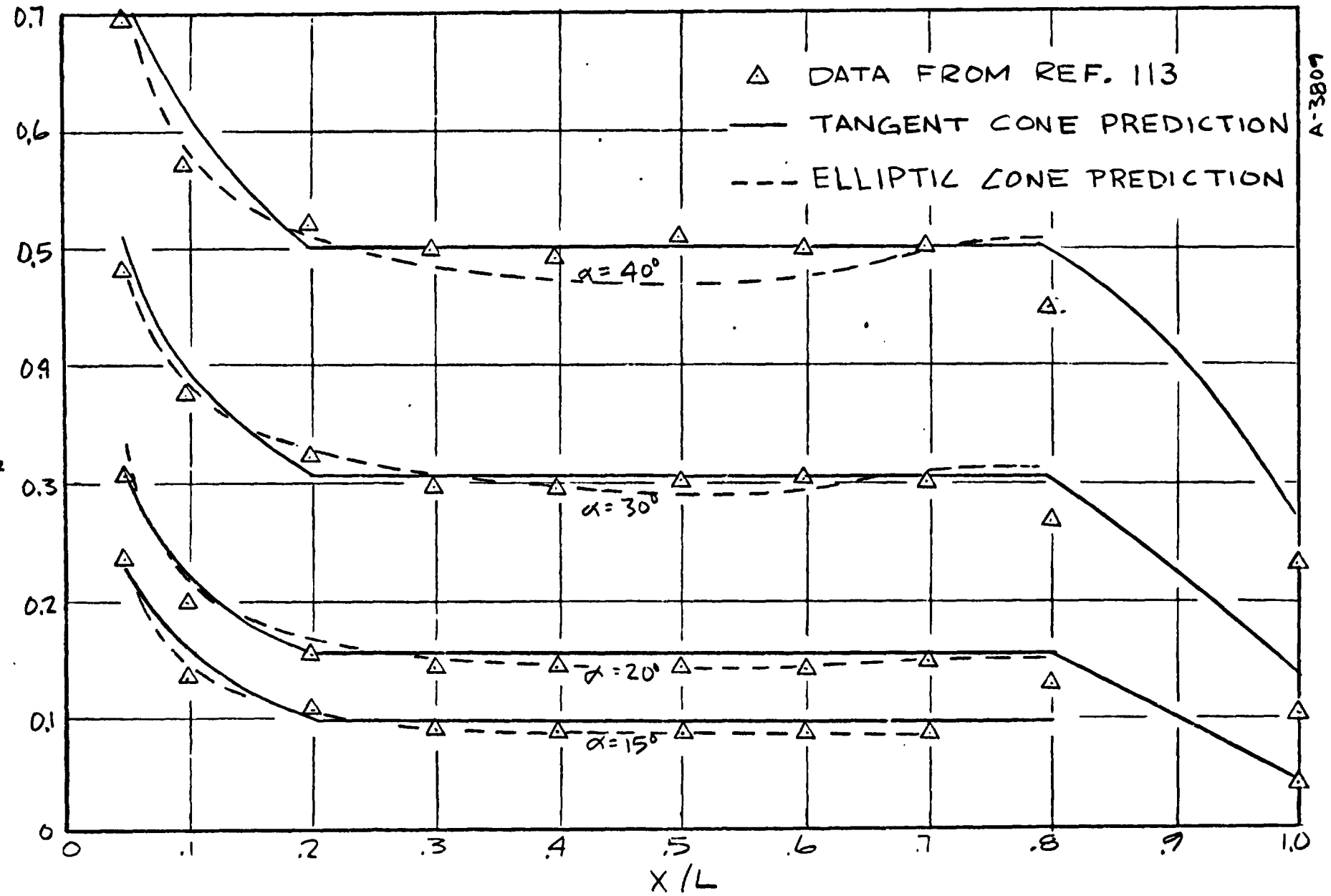


FIGURE 2 COMPARISON OF PREDICTED AND MEASURED PRESSURES ON WINDWARD GENERATOR OF NAR MODEL 134 B

$$\frac{p - p_\infty}{p_r - p_\infty} = \frac{\sin^2\alpha}{\sin^2\alpha_r}$$

where $p_r$ is the pressure on a reference surface oriented at the angle $\alpha_r$. This equation can be written in the form

$$\frac{p}{p_\infty} = 1 + \left(\frac{p_r}{p_\infty} - 1\right) \frac{\sin^2\alpha}{\sin^2\alpha_r} \qquad (4\text{-}1)$$

which is then a Newtonian tangent cone/wedge equation. To illustrate the use of this equation, consider an airfoil at angle of attack as shown below

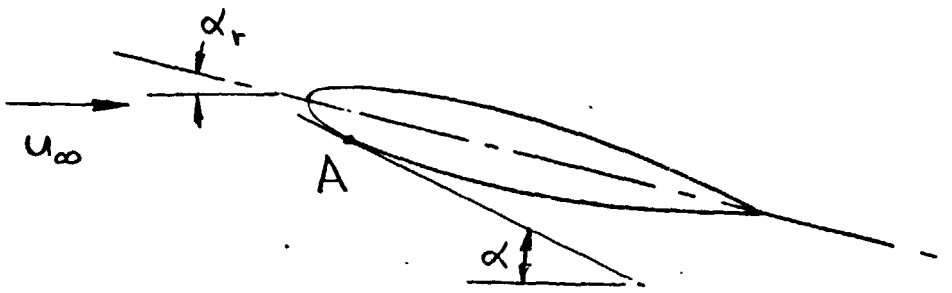


The chord line will be used as $\alpha_r$ and, depending on the nature of the flow around the airfoil and whatever body is attached to it, the pressure $p_r$ can be determined for a wedge or cone at angle $\alpha_r$. The pressure at A which has a local angle of incidence equal to $\alpha$ can then be calculated from Equation (4-1). For a typical shuttle vehicle this procedure will yield pressures comparable to tangent wedge or tangent cone values as shown in Figure 3. Note, however, that a qualitative decision must still be made regarding which, tangent cone or tangent wedge, is most applicable. Note also that the procedure would not be valid in the limit as $\alpha_r$ approaches zero.

At low angles-of-attack the transverse curvature of the shock wave on the windward side will not be significant except near the centerline of the vehicle. The flow across the wing is then akin to that around a yawed-blunted wedge so that the pressures should be adequately predicted with tangent wedge approximations. At higher angles-of-attack the shock wave, even over the wing, will have significant transverse curvature so that tangent cone approximations should be used. It is apparent then, that a decision must be made as to when each assumption is valid. Based on the Marvin data, the following rule-of-thumb is recommended: If the angle-of-attack is somewhat greater than the half-angle of the delta, then use the tangent cone approximation; and if the angle-of-attack is approximately equal to or less than the half-angle, use the tangent wedge approximation.

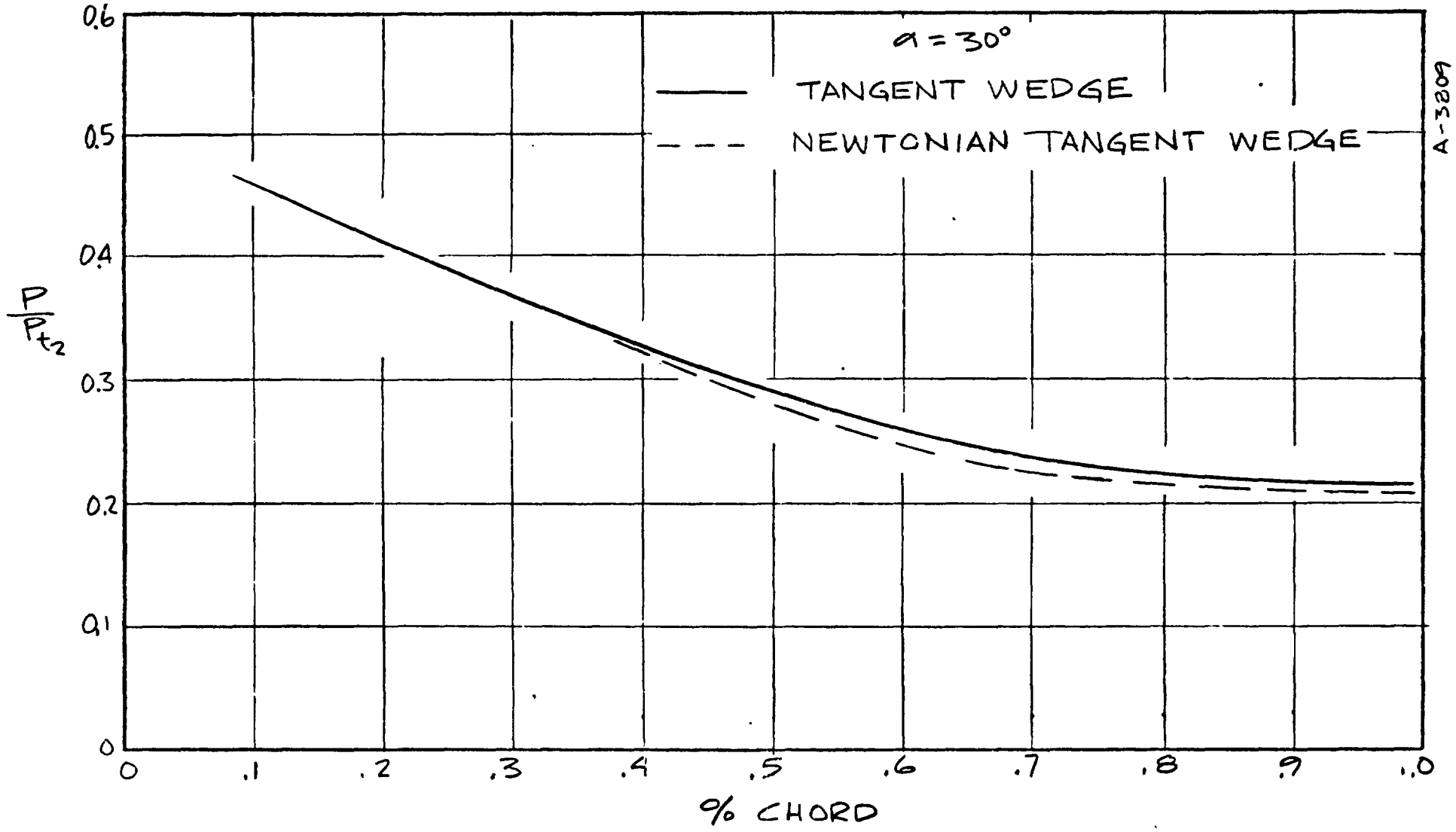


FIGURE 3 COMPARISON OF TANGENT WEDGE AND NEWTONIAN-TANGENT WEDGE PRESSURE ON WING OF NAR MODEL 134 B AT 20% SEMISPAN, $\alpha = 30°$ LAMINAR FLOW

Regardless of which approximation is used on the wing, the combination of the airfoil shape and dihedral causes the true local angle of incidence to be different from the vehicle angle-of-attack. For small values of the sum $(\bar{\alpha} + \bar{\bar{\alpha}})$, a geometric analysis will yield the following results for chordwise stations greater than a few percent.

$$\sin \gamma = \cos \phi \sin(\alpha + \bar{\alpha} + \bar{\bar{\alpha}})$$

where

$\alpha$ = vehicle reference line of attack

$\bar{\alpha}$ = angle between chord line and reference line

$\bar{\bar{\alpha}}$ = local surface inclination with respect to chord line

$\phi$ = local wing dihedral angle

$\gamma$ = true angle of incidence on wing

Calculations using $\gamma$ in the tangent wedge approximations are compared with the Marvin data in Figure 4. It should be noted that the general decrease in pressure going outboard is due primarily to a change in $\bar{\alpha}$ rather than a three-dimensional end flow effect.

The fins can be handled in much the same way as the wings where once again the true incidence of the fin must be determined. Assuming that the fin is a flat plate with no airfoil shape, this incidence is given by

$$\sin \gamma' = \cos \phi' \sqrt{\sin^2 a + \tan^2 \phi'} \sin(\xi + \alpha)$$

$$\sin \xi = \frac{\sin a}{\sqrt{\sin^2 a + \tan^2 \phi'}}$$

where

$a$ = angle between fin chord line and vehicle symmetry plane

$\phi'$ = angle of tilt of fin

$\gamma'$ = true angle of incidence

There is no available data on fin pressure distributions to use for comparisons of predicted values.

The pressure along the stagnation line of both the fin and the wings are calculated as the pressure on a swept cylinder with a correction for angle-

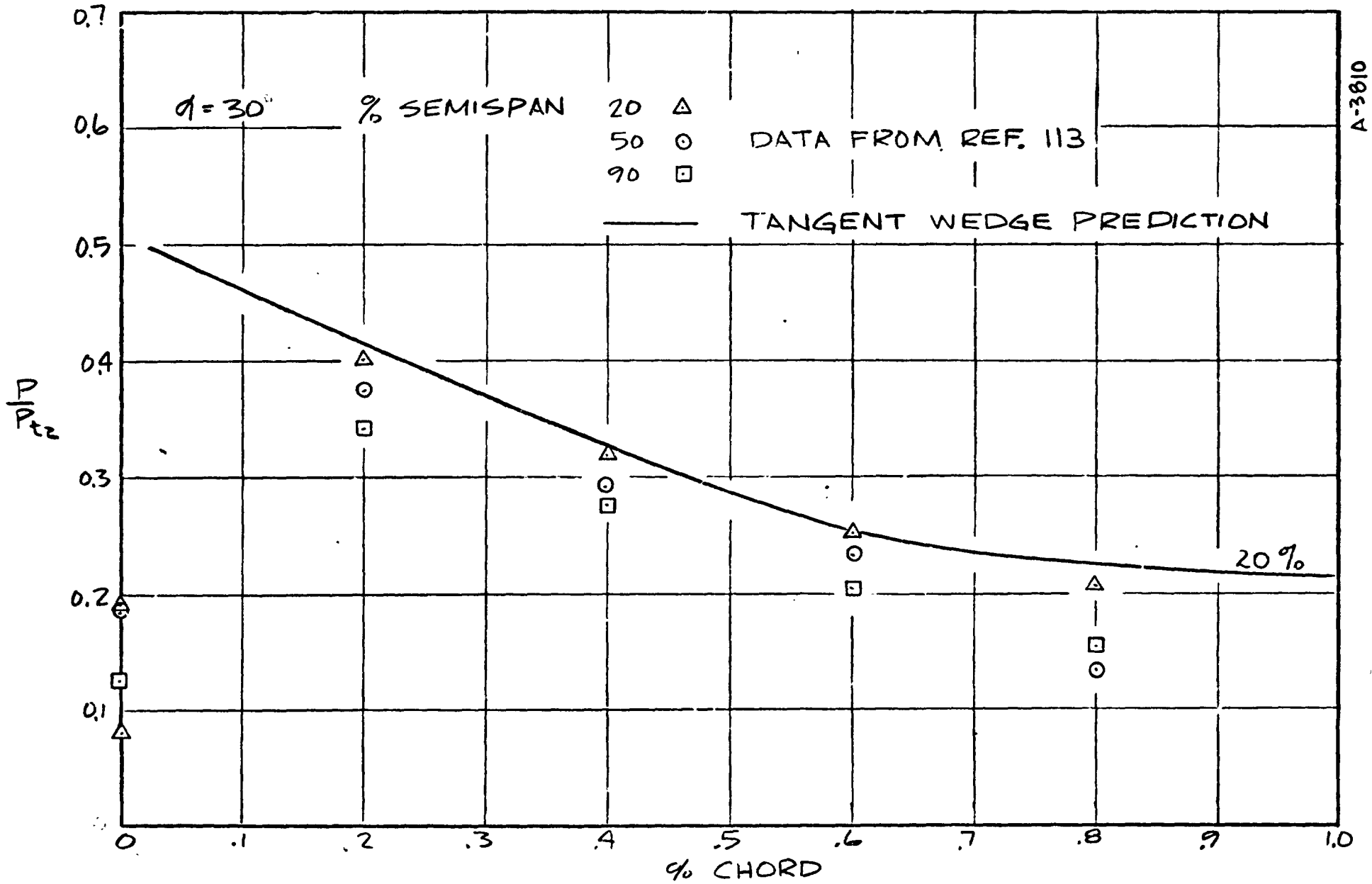


FIGURE 4 COMPARISON OF PREDICTED AND MEASURED PRESSURE ON WING OF NAR MODEL 134 B, $\alpha = 30°$ (LAMINAR FLOW)

of-attack to obtain the true yaw angle. That is, for the wing, with a small dihedral angle

$$\cos \Lambda = \cos \alpha \cos \zeta$$

where

$\zeta$ = semi-apex of wing

$\Lambda$ = true angle of wing leading ledge

and for the leading edge of the fins

$$\cos \Lambda' = r \sin(\delta + \alpha)$$

where

$$r = \left[1 + (\sin \delta \tan a + \cos \delta \tan \phi')^2\right]^{-1/2}$$

$\delta$ = nominal sweep angle of fin measured on vehicle symmetry plane

$\Lambda'$ = true angle of attack of fin leading edge

The above angles for the wing and fin are shown in Figure 5 and the above relationships are derived in Appendix 1.

As far as the leeward side is concerned, short of a complete flow field analysis, there are no adequate means of predicting surface pressures. Based on the analysis of Reference 73 and experimental data,[74] it is recommended that laminar heating rates be calculated as 0.56 of the laminar flat plate value and turbulent rates at 0.84 of the turbulent flat plate value.

For the low velocity-low altitude portion of the shuttle trajectory. the predicted pressure can be used with equilibrium gas assumptions to obtain adequate boundary layer edge conditions. But during the earlier portions of the trajectory, accurate predictions of the edge condition must include the effects of nonequilibrium chemistry, especially if surface kinetics are to be considered. However, for a "first cut" design calculation, equilibrium chemistry can be assumed with the knowledge that the use of noncatalytic surfaces affect the heating rates both at the non-catalytic surface and downstream of it. For a distance up to several nose radii downstream, the edge condition can be determined by a streamline expansion.

$$u_e \frac{du_e}{dx} = - \frac{1}{\rho_e} \frac{dp_e}{dx}$$

$$i_t = i_e + \frac{u_e^2}{2} = \text{constant}$$

$$i_e = i_e(p_e, \rho_e)$$

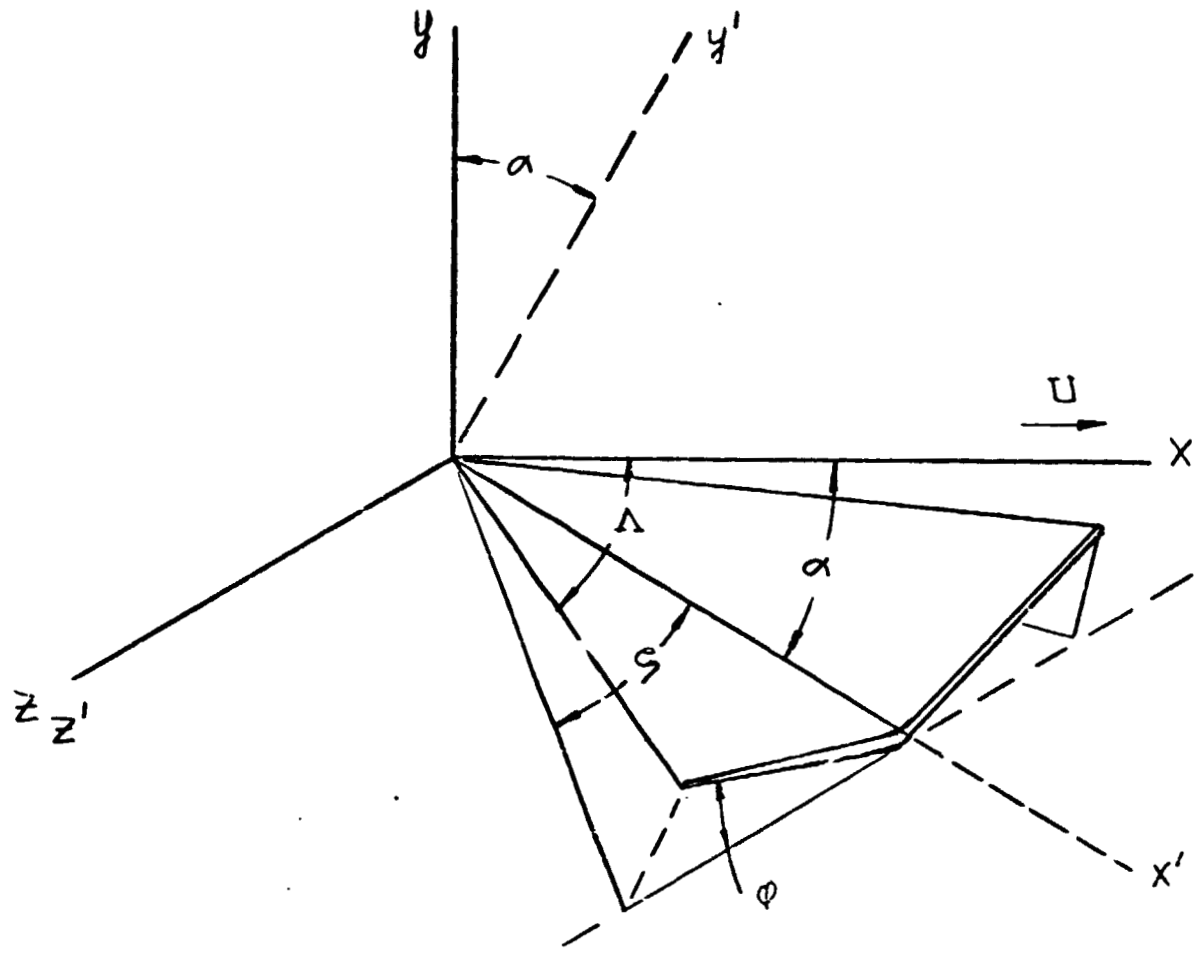


DELTA WING NOMENCLATURE

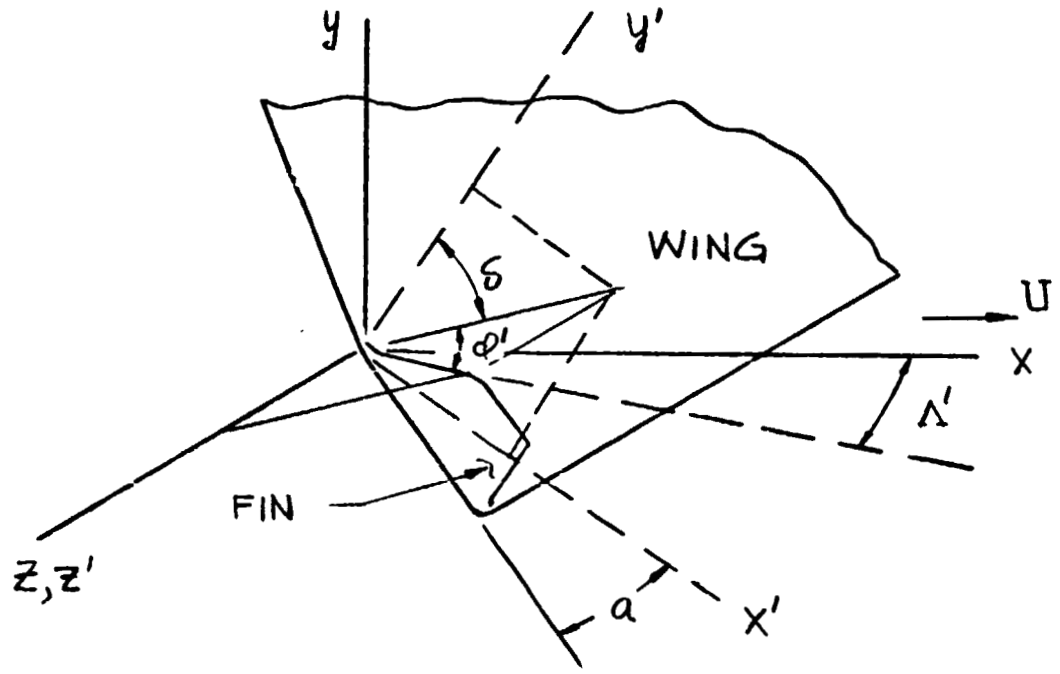


OUTBOARD FIN NOMENCLATURE

FIGURE 5 BODY REFERENCE ANALYSIS

Far downstream (say a distance in the order of tens of nose radii) the edge condition can be assumed to be the same as that which would exist behind an oblique shock with $p_2$ equal to the local surface pressure. Thus with $p_2/p_1$ known, equilibrium normal shock tables* can be used to determine the equivalent free stream Mach number, $M_{equiv.}$, which is equal to $M_\infty \sin \theta$. The tables will also yield all static properties and the normal component of velocity; thus with the tangential terms unchanged the edge velocity can be calculated to complete the edge conditions. For intermediate distances, there will be a transition from the high entropy stagnation state to the low entropy oblique shock state. The rate of transition depends on the shock wave shape and is further complicated by three dimensional effects. Since the heat transfer prediction methods to be recommended use similarity or local similarity assumptions, the results are not sensitive to the smoothness of the edge conditions. Thus it is suggested that, for moderate distances from the stagnation point, the solution be bracketed by solving both the normal shock expansion and the oblique shock conditions.

It is believed that the particular choice of an approximation method to be used to predict the heat transfer rates is not critical since a degree of empiricism is built into each method. In line with the tangent cone/wedge method used to predict pressures, it is recommended that the heat transfer be predicted using, for example, Eckert's reference enthalpy method for conical or wedge flow where the local body incidence is used as the cone or wedge angle. This procedure, of course, would not be valid near the nose or leading edge but would be applicable at large S/R. Calculations, as described are compared with the Marvin's centerline data for $\alpha = 15°$ and $\alpha = 30°$ in Figures 6 and 7 respectively. The 53.5° case is not compared since, as noted, this is too close to the limiting cone angle. The agreement at $\alpha = 30°$ is very good for $X/L \geq 0.2$ but at $\alpha = 15°$ the predicted values are conservatively higher than measured values.

Stagnation point heat transfer can also be calculated using the reference enthalpy method but between the stagnation point and $x/L \sim 0.2$ the method of Lees[76] is suggested. Briefly, the ratio of local heat transfer to stagnation heat transfer is given as

$$\frac{q}{q_o} = \frac{F(s)}{F(o)}$$

---

* e.g., Reference 75.

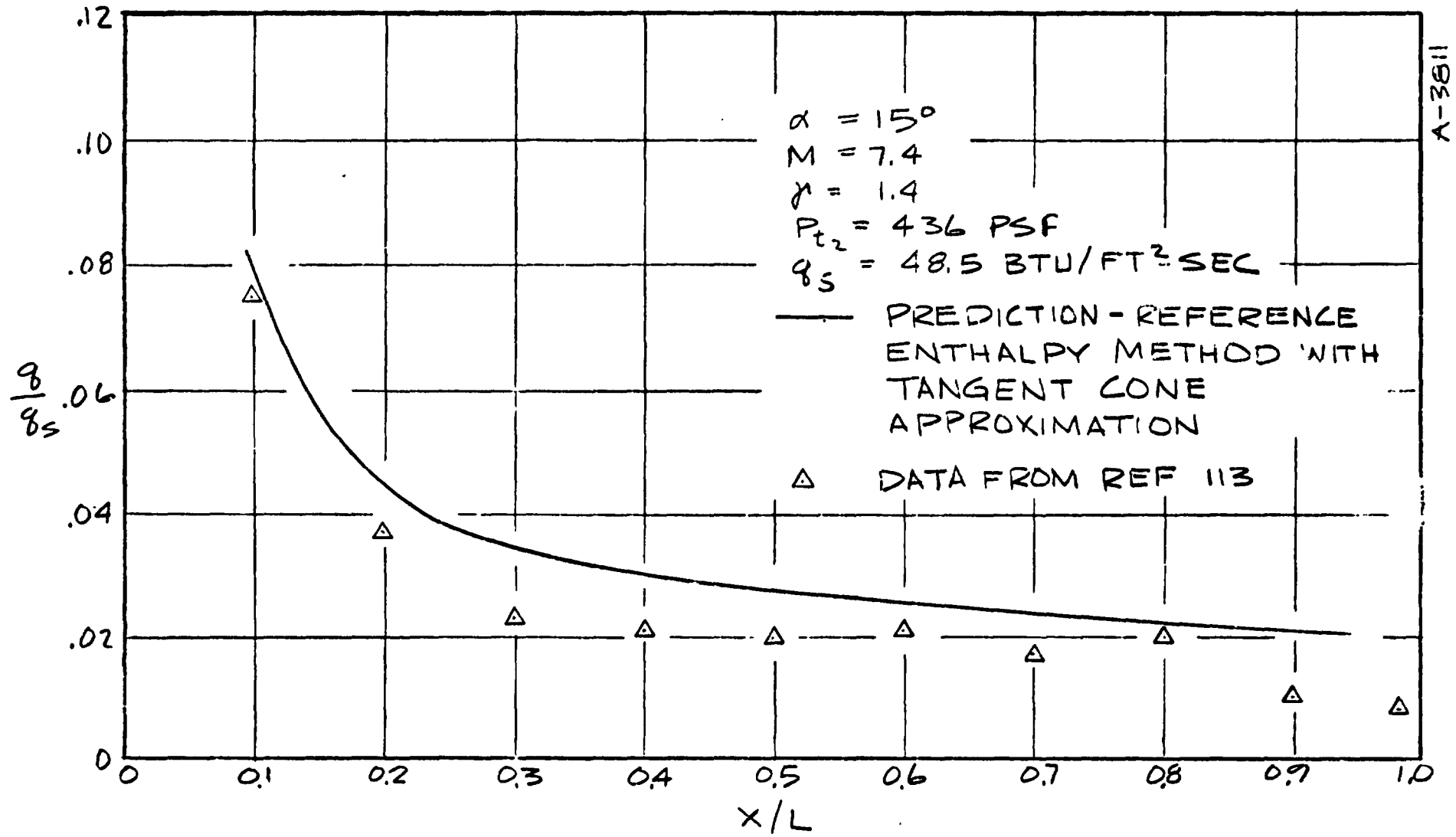


FIGURE 6 COMPARISON OF PREDICTED AND MEASURED HEAT TRANSFER ON WINDWARD GENERATOR OF NAR MODEL 134 B $\alpha = 15°$ (LAMINAR FLOW)

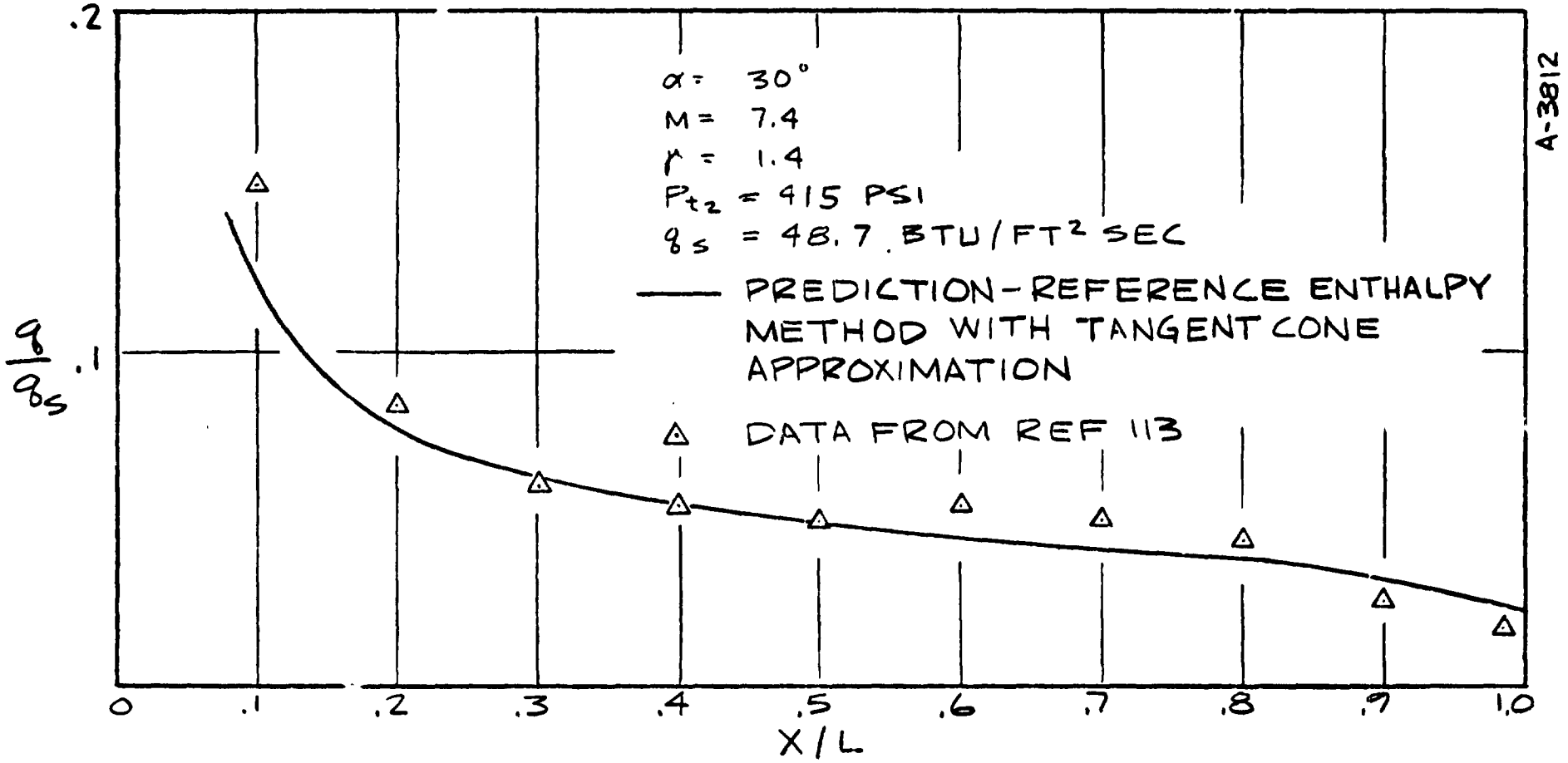


FIGURE 7 COMPARISON OF PREDICTED AND MEASURED HEAT TRANSFER ON WINDWARD GENERATOR OF NAR MODEL 134 B, $\alpha = 30°$ (LAMINAR FLOW)

where

$$F(s) = \frac{\left(\frac{\rho_e \mu_e}{\rho_o \mu_o}\right) r^k \left(\frac{u_e}{u_\infty}\right)}{\left[2 \int_o^s \left(\frac{\rho_e \mu_e}{\rho_o \mu_o}\right) r^{2k} \left(\frac{u_e}{u_\infty}\right) ds\right]^{\frac{1}{2}}}$$

$$F(o) = 2^{\frac{k}{2}} \left[\frac{1}{u_\infty}\left(\frac{du_e}{ds}\right)_o\right]^{\frac{1}{2}}$$

$$k = \begin{cases} 0 & \text{two-dimensional} \\ 1 & \text{axisymmetric} \end{cases}$$

and the coordinates are defined by the following sketch:

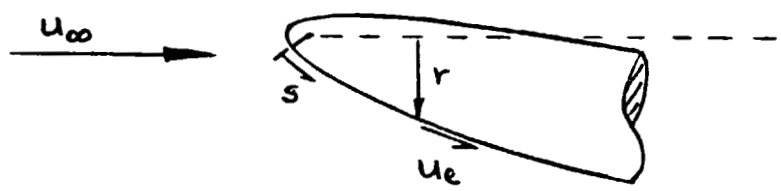


An alternative approach for regions not too close to the nose is that used by Guard and Schultz. On the windward centerline this procedure calculates the two-dimensional heating rate and scales it with methods developed by Dunavant[77] and Thomas, et. al.[57] For example, the local heating can be predicted by Eckert's method for flow over a plate or wedge, i.e.,

$$\frac{Nu_x^*}{\sqrt{Re_x^*}} = 0.332 (Pr^*)^{\frac{1}{3}}$$

then the ratio of heat trasnfer coefficients is

$$\left(\frac{h}{h_{2_D}}\right)_{Lam} = \sqrt{1 + 2j} \tag{4-2}$$

$$\left(\frac{h}{h_{2_D}}\right)_{turb} = \left(1 + \frac{5}{4}j\right)^{0.2} \tag{4-3}$$

where

$$j = \frac{0.745\ \sqrt{1 + \frac{\gamma - 1}{2}\ (M_\infty \sin \alpha)^2}}{2(\tan \varepsilon)(M_\infty \cos \alpha)}$$

and $\varepsilon$ is the half angle of the delta wing. The above procedure would be valid only for the centerline of the delta portion of the vehicle. When turbulent flow is expected, it is observed from Equation (4-3) that the effect of streamline divergence is very small and can probably be neglected.

For some vehicle configurations, (e.g., NAR configurations 129 and 134) the delta portion is preceded by a cylindrical fuselage. In this region, the swept cylinder theory of Beckwith, and Beckwith and Gallagher should be used. On the wing and at low angles-of-attack, two dimensional methods are probably sufficient but at higher angles, cross flow effects should be included following the procedure of Beckwith and Cohen.

To be conservative, it is recommended that "spot" calculations be made to determine upper and/or lower bounds in terms of 2D/3D and laminar/turbulent predictions. This of course would not be necessary if exact solutions were available. In addition the degree of confidence in the overall predictions is increased as exact methods for local predictions become available. The recommended procedures, which are summarized in Table 1, are not expected to be applicable to all possible vehicle configurations but are considered adequate for the current delta configurations. In using the recommended procedures or any other approximation scheme, it should be noted that, although a number of possible "improvements" are available, the increased complication is often not warranted in view of the fact that these improvements are building onto solutions that do not account for all of the important phenomena. The test of the accuracy of approximation methods is a comparison with exact solutions or flight data. Because of the budgetary and political constraints imposed on

TABLE 1

RECOMMENDED METHODS FOR APPROXIMATE HEAT TRANSFER PREDICTIONS TO DELTA SHUTTLE VEHICLES

| Region* | Pressure | Edge Conditions | Heat Transfer |
|---|---|---|---|
| $A_1$ | Stagnation point and Newtonian | Equilibrium stagnation, isentropic expansion | Fay and Riddell correlations (or Ref. 5)<br>$q_0 = 0.94(\rho_w\mu_w)^{0.5}\left(\frac{\rho_s\mu_s}{\rho_w\mu_w}\right)^{0.4}\left\{1 + (Le^{0.52} - 1)\frac{i_D}{i_0}\right\}\left[\frac{1}{R}\sqrt{\frac{2(p_s - p_\infty)}{\rho_s}}\right]^{1/2}(i_0 - i_w)$<br>or Reference enthalpy<br>$\frac{Nu^*}{\sqrt{Re^*}} = 0.76(Pr^*)^{0.4}\left\{1 + (Le^{0.52} - 1)\frac{i_D}{i_0}\right\}$ |
| $A_2, A_3$ | Tangent cone | Oblique shock conditions (tangent cone) | Reference enthalpy, tangent cone<br>$q_{tc} = 0.575\ Pr^{*-2/3}\sqrt{\rho^*\mu^*}\sqrt{\frac{u_e}{x}}\left(i_e - i_w + r\frac{u_e^2}{2}\right)\left\{1 + (Le^{0.52} - 1)\frac{i_D}{i_0}\right\}$ |
| $B_1, B_2, C$ | Swept cylinder stagnation line | Swept cylinder stagnation line, isentropic expansion | Swept cylinder - Beckwith<br>$\frac{Nu}{\sqrt{Re}} = 0.5\left(\frac{\rho_s\mu_s}{\rho_w\mu_w}\right)^{0.44}\left\{1 + (Le^{0.52} - 1)\frac{i_D}{i_0}\right\}$<br>or<br>$q_{sc} = 0.75\ q_0(\sin\Lambda)^{1.2}$ |
| $D, E_1$ | Tangent cone for $\alpha_{eff} \gtrsim$ semi-apex angle<br>Tangent wedge for $\alpha_{eff} <$ semi-apex angle | Oblique shock conditions, tangent cone $\alpha_{eff} \gtrsim$ semi-apex angle<br>Tangent wedge $\alpha_{eff} <$ semi-apex angle | Tangent cone $\alpha_{eff} \gtrsim$ semi-apex angle<br>$q_{tc}$ as in region $A_2$, $A_3$<br>Tangent wedge $\alpha_{eff} <$ semi-apex angle<br>$q_{tw} = \frac{1}{\sqrt{3}}\ q_{tc}$<br>or crossflow theory, Ref. 33, 39 |
| $K, G, E_2$ | Approximations based on experimental data | --- | Approximation from experimental data |

*See Figure 1

shuttle, it is not practical to wait for flight data, hence the development of exact or near-exact computer codes (at least for specific regions of the shuttle surface) is the key to a successful shuttle design.

## SECTION 5

## CANDIDATE ADVANCED BOUNDARY LAYER TECHNIQUES

During the past few years with the advent of large scale computer machinery a number of computer codes have been developed which yield numerical solutions to the boundary layer equations. These codes are relatively expensive to operate and are often tempermental. For these reasons it is not envisioned that they should take the place of experiments or simple engineering relations for predicting heat-transfer rates when such methods are available. However, they are very useful in auxiliary studies where they can be used to validate or calibrate engineering relations, to extend engineering relations to include additional effects, to extrapolate wind-tunnel tests to flight conditions, and to develop correlations for use with simple engineering relations. A classic example of this last approach is the correlation of stagnation point boundary layer solutions by Fay and Riddell.[2]

While boundary layer computational technology has come a long way, no code is available (nor would it be practical to develop a code) which treats the complete shuttle boundary layer precisely. This would require consideration of a three-dimensional boundary layer with separated flow and viscid-inviscid coupling over the leeward side of the vehicle. The only three-dimensional code available today which is oriented to flight vehicle geometries and which treats the equations precisely is that of Der.[71] However, this code uses an explicit approach and therefore is very expensive to operate. Also, it does not consider separated flow, viscid-inviscid coupling, turbulence, or chemical reactions.

A rather extensive review of boundary layer computatic technology was presented recently in Reference 78. This report discussed in detail the various numerical procedures presently in use (e.g., shoot and hunt, quasilinearization, streamwise integration, implicit and explicit finite difference procedures, and successive approximation and Newton-Raphson iteration methods). It also discussed the current status of all then known codes for treating the chemical state, coupling to inviscid flow, coupling to surface phenomena, molecular transport, turbulent transport, and three-dimensional flows. While a few new codes have appeared since this report was written in late 1968 and some of the codes discussed therein have been developed somewhat further, the basic conclusions of the report are not changed. Therefore, the reader is referred to Reference 78 for a comprehensive comparison of candidate codes.

Based on the results of this survey, it would appear to be practical to develop a code for shuttle application with the following features:

1. Considers the full nonsimilar axisymmetric or planar boundary layer equations (i.e., it contains no similarity approximations).
2. Solves the boundary layer equations "exactly" in a numerical sense (i.e., without the use of linearization, assumed profile shapes, etc).
3. Considers laminar, transitional, and turbulent flows including rather sophisticated models for transition length and turbulent eddy viscosity
4. Performs calculations along inviscid streamlines with approximate treatment of three-dimensional effects through use of small cross-flow theory (the axisymmetric analogy).
5. Considers regions of attached flow only.
6. Considers nonisentropic boundary-layer edge expansions (i.e., entropy layer effects).
7. Considers detailed nonequilibrium chemistry including surface-catalyzed reactions or equilibrium chemistry when the situation dictates.
8. Permits consideration of surface ablation materials through use of a relatively general chemistry model and general ablating wall boundary conditions.
9. Performs each streamline solution around the body in a matter of a few minutes on a relatively high speed computer such as the Univac 1108.

There are possibly several dozen separate codes in the country today which perform Items 1 and 2 above, that is, which yield "exact" numerical solutions to various sets of boundary layer equations. However, most of these are limited to incompressible or compressible single-component boundary layers or have some other major shortcoming that rules them out of consideration for application to Shuttle. Experience in developing the BLIMP code at Aerotherm would suggest that the development of an operational compressible single-component code is a trivial fraction of the effort needed to develop a code of the type needed for Shuttle.

Limiting attention, then, to reacting, nonsimilar boundary layer codes, there are about six codes (or classes of codes) which would appear to have some potential for application to shuttle. These are

1. Implicit method of Blottner as extended and used by several investigators
2. Shoot and hunt method of Smith
3. Implicit method of Cebeci

4. Multiple strip method of Pallone

5. Implicit method of Spalding

6. Newton-Raphson method of Kendall (BLIMP program)

Probably the earliest nonsimilar nonequilibrium boundary layer code was developed by Blottner while at General Electric.[10] In Reference 10 he extended the implicit finite difference procedure developed while a Flugge-Lotz student[79] to binary nonequilibrium (atoms-molecules). The basic computational approach developed under this thesis was used later by several subsequent students including Fannelop[80] and Davis.[81] The Blottner binary nonequilibrium code was obtained by Boeing and extended by Tong to multicomponent air nonequilibrium.[82] Blottner also extended his code to a nonequilibrium air model.[11] This code has been used and extended at ARO by Adams,[43,83] Davis[84] and Lewis[85] in studies of chemical nonequilibrium, mass transfer, viscous interaction and turbulent flow (equilibrium only). The General Electric version has also been extended to include ablation products[86,87] and to apply to the thin shock layer equations.[88]

Another early nonsimilar boundary layer code which has gotten extensive use was developed by Smith and Clutter[89] of McDonnell Douglas. This code uses a shoot and hunt method.[78] It was extended to nonequilibrium air in Reference 90 and to include binary (foreign gas) injection (but for equilibrium) in Reference 91. This latter version has been used, for example, by Mayne and coworkers.[92] Further extension of these codes seems to have stopped with the advent of an improved implicit finite difference method by Smith and Cebeci.[93,94] This code has been used rather extensively by Cebeci (e.g., Ref. 95) in turbulent model studies including air-to-air injection but while still retaining a nonreacting compressible boundary layer framework. Other compressible turbulent nonreacting boundary layer codes have been developed and used in turbulent model studies, the most noteworthy being Bushnell and Beckwith[96] and Herring and Mellor.[97]

A third early approach for solving the nonequilibrium, nonsimilar boundary layer equations was developed by Pallone and coworkers.[98] They employed a multiple strip integral method.[78] This code does not appear to have been used too extensively, but some calculations are reported in Reference 99 considering teflon ablation products and further solutions are promised (but not presented) in Reference 100.

In 1967 Spalding and Patankar published a book[101] containing listings and instructions for use of a skeletal computer program based on an implicit finite difference procedure for solving chemically reacting laminar or turbulent flows, the idea being that the user would supply the necessary subroutines

(chemistry, turbulent model, etc.) to solve his specific problems. This method has been used extensively by Professor Kays of Stanford University and his students in studies of the turbulent (principally incompressible) boundary layer.[102] It was also used by Mayne and Adams[103] in a study of streamline swallowing in laminar boundary layers. No other American references could be found. Certainly a lot of effort would be required to develop this method to the point where nonequilibrium chemistry is included.

In 1966 a novel implicit procedure employing Newton-Raphson iteration[78] was developed by Kendall and Bartlett of Aerotherm.[104] This method has been used extensively to study equilibrium chemically-reacting laminar and turbulent boundary layers with and without surface ablation, including entropy layer effects, and including the axisymmetric analogy to three-dimensional flow. A fairly recent version of the program which is termed BLIMP is described in Reference 105. While the code is currently operational for general equilibrium flows only, subroutines governing homogeneous nonequilibrium are currently built into the code which, while not fully operational within BLIMP, are operational as a separate nonequilibrium streamtube code.

Additional code developments worthy of mention include those of Galowin and Gould of GASL,[106,107] Mondrzyk of Boeing,[108] Moore and Lee of TRW,[109,110] Chenoweth of Sandia,[111] and Marvin and Sheaffer of NASA Ames.[66] The first two codes treat nonequilibrium but employ time consuming explicit procedures. They appear to have been used very sparingly. Moore and Lee present solutions for discontinuous inert injection into a nonequilibrium laminar boundary layer but no solutions seem to have been reported since their initial efforts. Chenoweth presented plans for a nonequilibrium turbulent boundary layer code but it is not clear that the code has ever been developed. The code of Marvin and Sheaffer, while limited to a binary equilibrium mixture, is mentioned since it is being used to evaluate shuttle heating data.[112,27]

While the codes mentioned above consider for the most part reacting nonsimilar flows, they are not all ideally suited for application to shuttle. Some apply only to sharp bodies[108] and some require special starting procedures (eg., marching from a known solution).[98] Many are currently limited to laminar flow (e.g., Refs 86, 99 and 110) and little experience has been gained with some (e.g., Refs 101, 106, 110 and 111). Many consider only air chemistry[11,90,98] While this would be sufficient for nonablating heat shields, it would be severely limiting in the event that replacable ablation panels come into vogue. There are several other considerations such as calculational speed, ease of setting up and running problems, and generality -- in other words, usability.

Taking all of these factors into consideration it appears that there are two major candidates for a shuttle boundary layer code -- the BLIMP code and a recent version of the Blottner code.

Extension of the BLIMP code would require the implementation of the homogeneous kinetics subroutine and other technical but straightforward modifications required to achieve nonequilibrium solutions with nominally the same accuracy, stability, and computational speed with which equilibrium solutions are currently generated. Extension of a Blottner code would require (depending upon the specific starting point) the implementation of a transitional and turbulent heating model, addition of the axisymmetric analogy, and the addition of a general ablation capability. Judging from the number of codes which were developed in the early 1960's to include nonequilibrium[11,90,98] and the fact that turbulence and ablation phenomena have been included only recently, it would appear that the extension of BLIMP to nonequilibrium would be substantially easier. Secondly, the resulting code would be apt to be considerably more general and flexible since this is the major advantage of the BLIMP code over other codes today. Finally, based on the experience of one of the authors (HT) who has used both codes, the BLIMP code would be expected to be easier to use and less expensive to operate.

## SECTION 6

## BLIMP PREDICTION CAPABILITY

BLIMP is a nonsimilar, chemical equilibrium computer code which uses a spline fit technique for approximating the distribution of flow variables within the boundary layer. The present capability includes an arbitrary edge pressure distribution, surface kinetics, laminar and turbulent flows, two-dimensional entropy layers and cross flow (axisymmetric analogy). All of the above features have been validated either on wind tunnel models or Apollo flight data. The spline fit technique is very efficient in terms of computational times when compared with finite difference methods.

In its present state, BLIMP can be used to predict pitchplane heating rates to the windward and leeward (for no separation) surfaces during the equilibrium chemistry portion of the trajectory. To make BLIMP applicable to the rest of the trajectory, nonequilibrium chemistry and three-dimensional entropy layers should be included. Even without these modifications it is believed that nonequilibrium heating rates to catalytic surfaces are not significantly different from equilibrium heating rates, so that with a bit of empiricism, BLIMP could be used for the full trajectory provided the shuttle surfaces are catalytic.

For noncatalytic surfaces, BLIMP in its present state is inadequate and nonequilibrium chemistry of some sort is essential. Since the primary driving function for heat transfer is enthalpy, an elaborate multi-component representation is probably not required. It has been shown that binary models are sufficient in most cases, but for shuttle, since oxidation is important, a minimum model would require at least three species, namely atomic oxygen, atomic nitrogen, and molecular "air". With nonequilibrium chemistry, BLIMP would then be able to handle surfaces with discontinuous surface catalycity and oxidation rates.

BLIMP, like other boundary layer codes, requires a means of either determining or specifying the edge conditions. A scheme such as that used by Adams can be used since BLIMP's present capability allows for streamline absorption into the boundary layer. Alternatively, the methods described in Section 4.4 can be used.

Since BLIMP accounts for most of the phenomena associated with entry vehicle heating, a favorable comparison with wind tunnel test data generates a high degree of confidence in flight predictions. The accuracy of these flight predictions have been proven for Apollo class vehicles and this experience suggests that a code such as BLIMP should be used in a sensitivity study and the results compared with wind tunnel data to determine which basic assumptions and phenomena will be of significant importance in flight. It should be stressed, though, that wind tunnel conditions will generally not include chemical dissociation-recombination effects so that the ability of a code to adequately account for these effects must be determined from extensive experience with the code.

To assess the effects of various three-dimensional and entropy layer assumptions, a matrix of heat transfer solutions were obtained for the windward generator of the NAR Model 134B and compared with the wind tunnel data of Reference 27 and 113. Additional supporting data were obtained by direct communications with the authors of Reference 27. The body geometry of the NAR Model 134B was obtained from Reference 114 and shock shape was measured from shadowgraphs of the flow about NAR Model 129[115] (which is slightly larger than Model 134B). These shadowgraphs were obtained from J. Cleary of NASA Ames.

Since the wind tunnel test conditions were at relatively low temperatures, the homogeneous version of BLIMP which consumes substantially less computer time than the chemically reacting version was used. These short run times make homogeneous BLIMP an economically practical tool for extensive studies of wind tunnel test conditions. Several check runs were made with the chemical code to verify the accuracy of the homogeneous results and in all cases, predicted heat fluxes were found to agree within $\pm$ 2%.

## 6.1 PRESSURE DATA FOR BLIMP INPUT

Pressure ratio data ($P/P_{t_2}$) were taken directly from the pressure ratio plots in Reference 113. The total pressure behind the shock was obtained assuming an ideal gas with $\gamma = 1.4$ and $M = 7.4$. It is noted that there is undoubtedly some error introduced by interpolating from such a plot; however, the uncertainty introduced into the heat flux predictions will be only about 50 percent of the uncertainty in pressure and thus this source of error is considered small (no more than 3 percent at the lowest angle of attack). For the purposes of the BLIMP code input, additional pressure data were required, particularly in the nose regions. These data were generated by assuming a Newtonian pressure distribution from the stagnation point and calculating the pressure ratio from the measured slope of the windward generator (see Section 6.1.2). The pressure

distributions used in the predictions are given in Appendix 2 and consisted of these computed values faired into the forwardmost reported measured values. Pressure gradient data ($\partial(P/P_T)/\partial s$) for the spreading factor calculation were obtained by measuring slopes from the pressure ratio vs. s plots.

Heating data were obtained from the normalized plots in Reference 113. in a similar manner. Actual heating values were computed using the calculated stagnation point heat flux values listed in Table 2. These values were computed by Marvin based on a 0.006 foot radius sphere and were used to normalize his data. These values are not measured stagnation fluxes.

## 6.2 MODEL GEOMETRY

The side profile and several frontal cross sections of the NAR Model 134B are shown in Figure 8 to provide a general indication of the model configuration. Pertinent geometric variables are

- $s$ , distance along the windward generator at each angle of attack. Here it was assumed the stagnation point was located at the intersection of the windward generator and a radial line through the center of the nose sphere at the particular angle of attack. The body centerline was taken from the drawing to be a line through the center of the nose sphere and parallel to the straight sections of the upper and lower fuselage.
- $R_c$ , radius of curvature of the windward generator
- $R_T$ , radius of curvature at the windward generator in the plane transverse to the generator. This plane is locally perpendicular to the generator.
- $r_o$ , the perpendicular distance from the windward generator to the angle of attack axis, i.e., the local radius of an axisymmetric body generated by rotation of the windward generator about the angle of attack axis.

## 6.3 SHOCK WAVE GEOMETRY FOR ENTROPY LAYER PREDICTIONS

Shock wave geometry was obtained from full scale shadowgraphs of Model 129 which were obtained at the same freestream conditions as used in heat transfer and pressure tests. Angle-of-attack conditions included $\alpha$ = 15°, 30°, 45° and 60°. Data for the $\alpha$ = 53.5° test condition were obtained from interpolation between the $\alpha$ = 45° and 60° cases.

TABLE 2

TEST CONDITIONS FOR THE PREDICTED CASES

| Case | Free Stream | | Wall Temperature ($^{\circ}R$) | Wall Temperature @ Stagnation Point ($^{\circ}R$) | Reference Stagnation Point Heat Flux* (Btu/ft$^2$sec) |
|---|---|---|---|---|---|
| | Total Pressure (psia) | Total Temperature ($^{\circ}R$) | | | |
| $\alpha = 15^{\circ}$, Laminar | 252 | 1,466 | 545 | 571 | 48.54 |
| $\alpha = 30^{\circ}$, Laminar | 239 | 1,500 | 540 | 581 | 48.72 |
| $\alpha = 30^{\circ}$, Turbulent | 1,494 | 1,409 | 570 | 650 | 99.82 |
| $\alpha = 53.5^{\circ}$, Laminar | 257 | 1,431 | 560 | 621 | 44.18 |

*Calculated by NASA/Ames personnel; based on a 0.006 ft radius sphere.

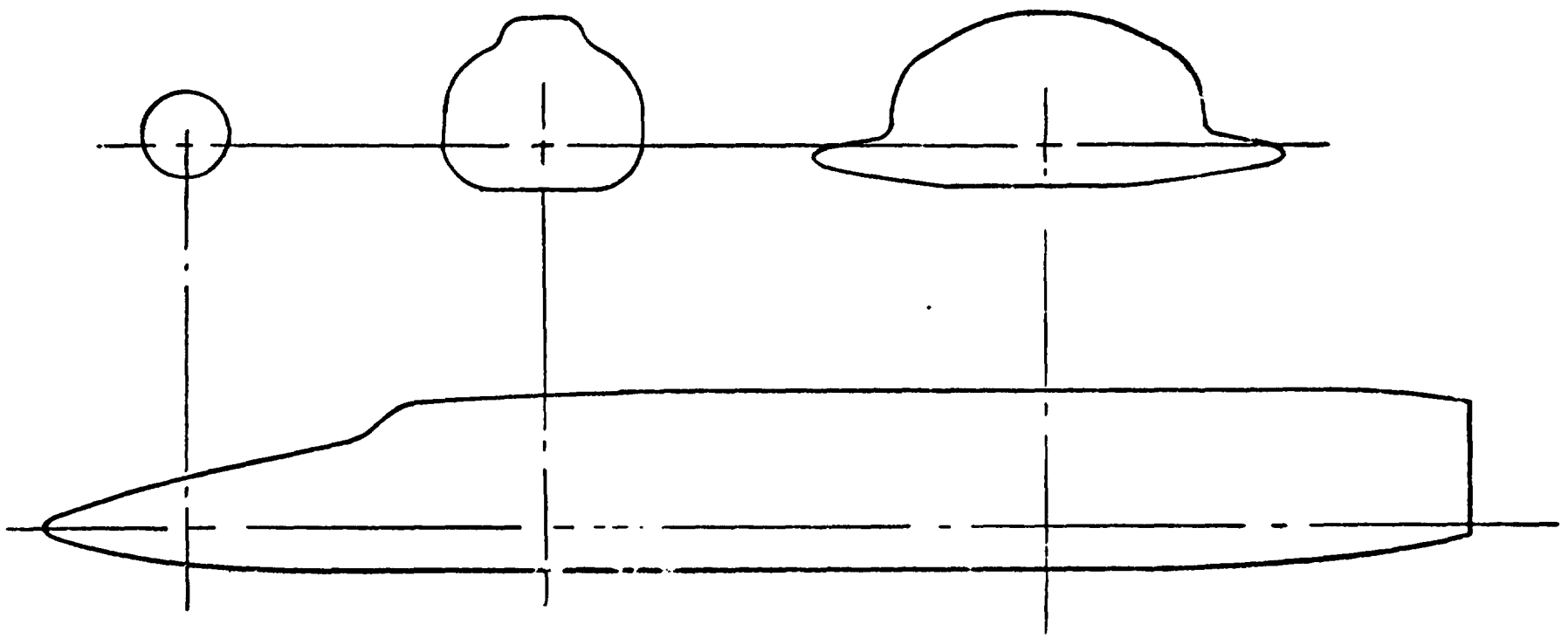

FIGURE 8 REPRESENTATIVE PROFILES OF NAR MODEL 134B

A-3812

The shock angle (given in Appendix 2) relative to the angle of attack axis was measured as a function of the radial distance from the angle of attack axis to the shock and then converted into total pressure ratio across an oblique shock by the relation

$$\frac{P_{t_2}}{P_{t_1}} = \left[\frac{(\gamma + 1)M_1 \sin^2\theta}{(\gamma - 1)M_1^2 \sin^2\theta + 2}\right]^{\frac{\gamma}{\gamma-1}} \left[\frac{\gamma + 1}{2\gamma M_1^2 \sin^2\theta - (\gamma - 1)}\right]^{\frac{1}{\gamma-1}} \tag{6-1}$$

This ratio together with the shock radius was used for the entropy layer input for the homogeneous code.

## 6.4 APPROXIMATION OF THREE-DIMENSIONAL FLOW EFFECTS

Three dimensional effects can be approximated in the BLIMP code by an axisymmetric analogy or in terms of a streamline spreading factor $h_2$.* In the former approximation, the heat transfer rates are calculated by assuming that the body is axisymmetric with a longitudinal profile specified as the windward generator. The continuity equation is then given by

$$\frac{\partial}{\partial s}(h_2 \rho u) + \frac{\partial}{\partial y}(h_2 \rho w) = 0$$

For a spherical surface such as on the face of an Apollo vehicle, $h_2$ is given[116] by the equation

$$\frac{d^2 h_2}{ds^2} - \frac{1}{\rho u^2}\frac{\partial P}{\partial s}\frac{dh_2}{ds} + \frac{1}{R_c^2}\left[1 - 2\frac{P_T}{\rho u^2}\cos^2\theta_B\right] h_2 = 0 \tag{6-2}$$

where $\theta_B$ is the angle between the local surface normal and the free stream velocity vector

$P_T$ is the total pressure

$R_C$ is the local surface radius of curvature

For this case, there is no ambiguity in the variable $R_C$ since the surface is spherical, but for a general three-dimensional body such as a shuttle vehicle

*$h_2$ is also the metric coefficient of the streamwise coordinate

the above formulation does not account for the difference in surface curvature as measured in the transverse and longitudinal directions A new derivation, presented in Appendix 3, shows that for non-spherical surfaces the spreading factor should really be defined by the equation

$$\frac{d^2h_2}{ds^2} - \frac{1}{\rho u^2}\frac{\partial P}{\partial s}\frac{dh_2}{ds} + \left[\frac{1}{R_C^2} - \frac{2P_T}{\rho u^2}\frac{\cos^2\theta_B}{R_T^2}\right]h_2 = 0 \qquad (6\text{-}3)$$

Equation (6-3) was integrated using a Runge-Kutta method for a single second order equation. The dynamic pressure term was evaluated from the perfect gas relation

$$\frac{\rho u^2}{P_T} = \frac{(\gamma - 1)\left(\frac{P}{P_T}\right)}{2\gamma\left[\left(\frac{P_T}{P}\right)^{\frac{\gamma-1}{\gamma}} - 1\right]} \qquad (6\text{-}4)$$

resulting in the equation being a function of the two surface radii of curvature, the pressure ratio, and the pressure ratio gradient which was evaluated from a plot of the measured pressure supplemented by the calculated Newtonian pressure gradient distribution near the nose. Calculated values of $h_2$ are given in Appendix 2.

## 6.5 BLIMP PREDICTION MATRIX

Experimental data were available for laminar flow at $\alpha$ = 15°, 30° and 53.5° and turbulent flow at $\alpha$ = 30°; the matrix of BLIMP solutions, shown in Table 3, is limited to these angles-of-attack and the test conditions shown in Table 2.

## 6.6 RESULTS AND DISCUSSION OF BLIMP STUDIES

Figures 9 through 12 show the influence of various assumptions on the predicted heating rates. The small crossflow results shown are all based upon $P/P_T$ replacing $\cos^2\theta_B$ in the spreading factor equation (Equation (6-3)) and $R_T = \infty$ in the aft or wing region of the fuselage. All predictions for a given case used the same stations, pressure ratios, and wall temperatures input distributions. Three-point differencing was used throughout to obtain streamwise derivatives except for the turbulent case which used two-point differencing.*

*A run using three-point differencing was also made with negligible difference in the results in the laminar region. Two-point differencing was used to provide more flexibility through the transition region than afforded by the limit of 4, two-point difference stations in the three-point difference option.

TABLE 3

MATRIX OF BLIMP PREDICTIONS

| Case | —·—·— Planar Blunt | ——— Axisymmetric Blunt | — - — Small Crossflow Blunt | - - - - Axisymmetric Blunt Entropy Layer |
|---|---|---|---|---|
| $\alpha = 15^{\circ}$, Laminar | X | X | X | X |
| $\alpha = 30^{\circ}$, Laminar | X | X | X | X |
| $\alpha = 30^{\circ}$, Turbulent | | X | X | |
| $\alpha = 53.5^{\circ}$, Laminar | | X | X | |

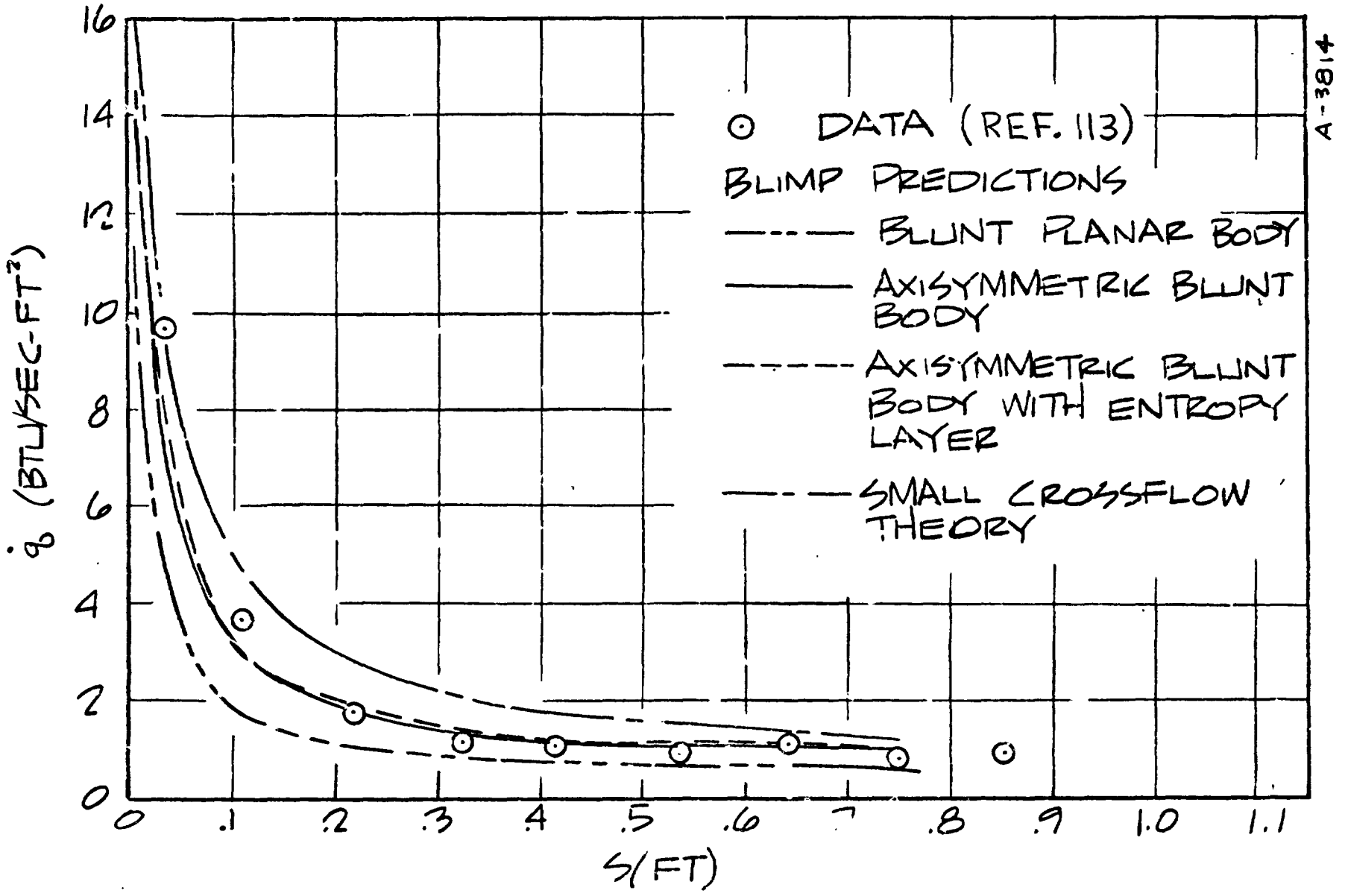


FIGURE 9 WINDWARD GENERATOR HEATING FOR THE NAR DELTA WING SHUTTLE MODEL (134B) $\alpha = 15°$, (LAMINAR FLOW ONLY)

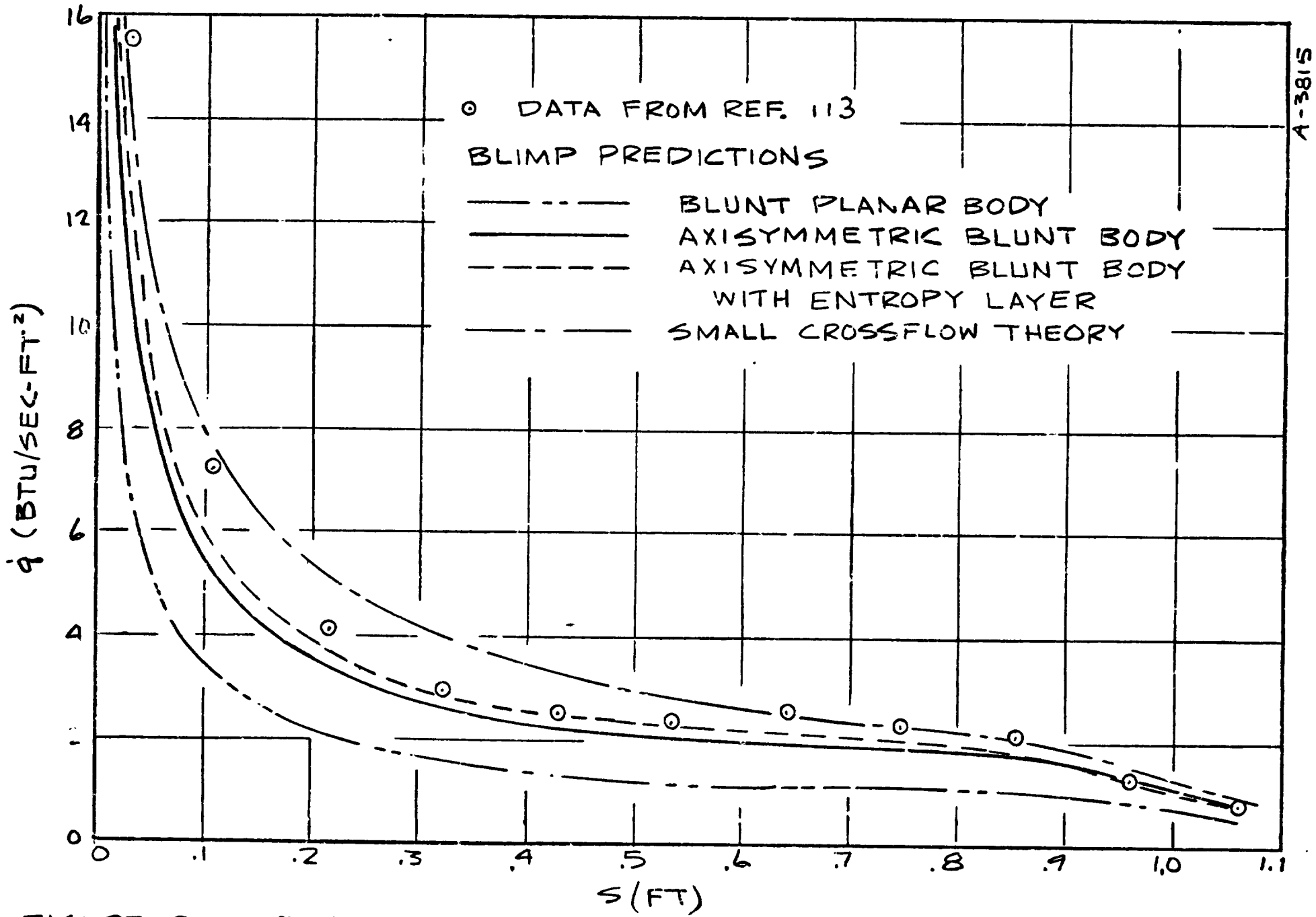


FIGURE 10 WINDWARD GENERATOR HEATING FOR THE NAR DELTA WING SHUTTLE (MODEL 134 B) $\alpha = 30°$, (LAMINAR FLOW ONLY)

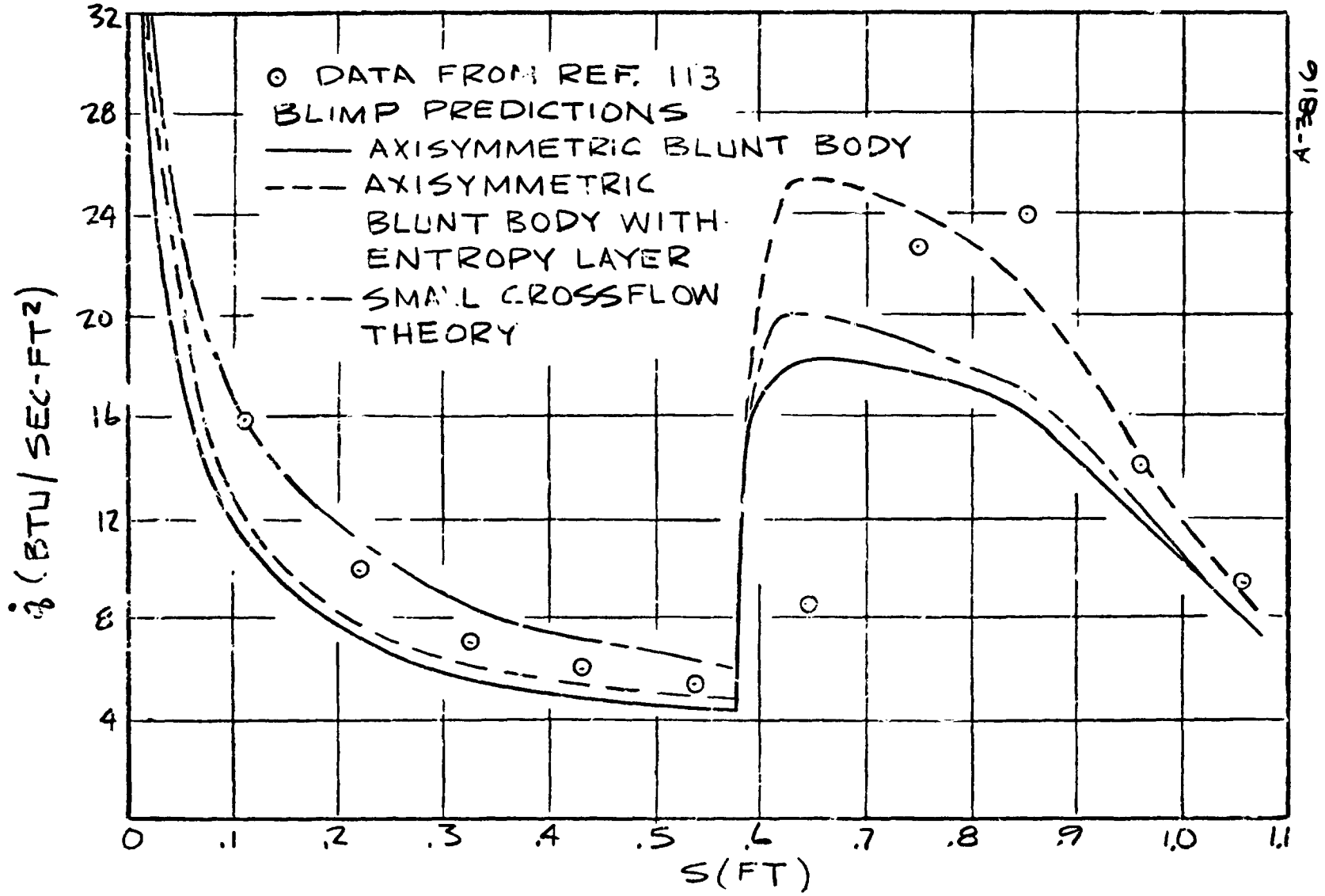


FIGURE 11 WINDWARD GENERATOR HEATING FOR NAR DELTA WING SHUTTLE (MODEL 134 B) $\alpha = 30°$ (LAMINAR AND TURBULENT FLOW)

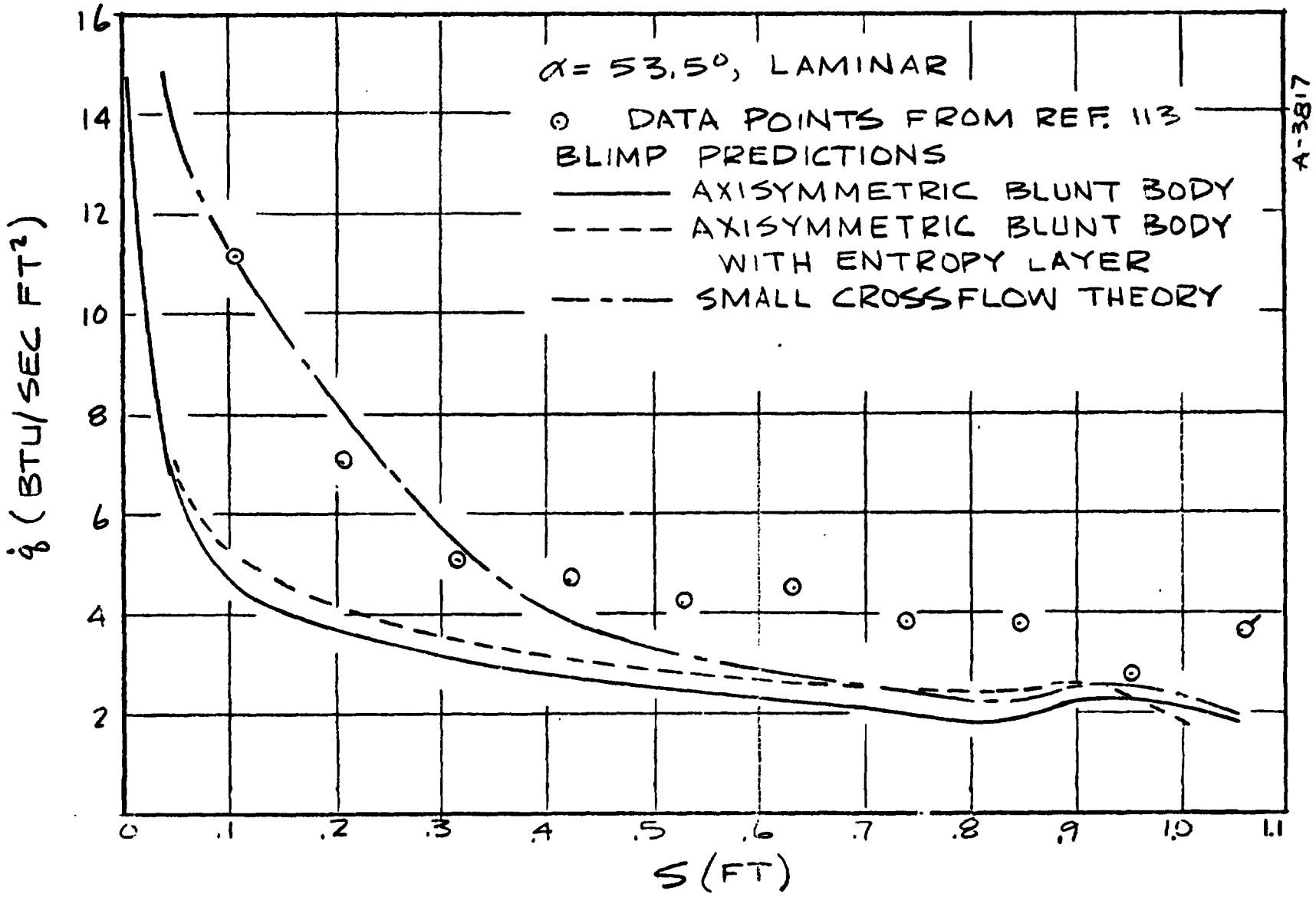


FIGURE 12 WINDWARD GENERATOR HEATING FOR THE NAR DELTA WING SHUTTLE (MODEL 134 B) $\alpha = 53.5°$, (LAMINAR FLOW ONLY)

Laminar Flow Results

The blunt planar body predictions made for the $\alpha$ = 15° and 30° (Figures 9 and 10) laminar cases underpredict heating over the entire length of the windward generator. The differences increase with angle of attack to roughly 50% for $\alpha$ = 30°. These trends are consistent with the over-prediction of boundary layer growth resulting from the planar approximation as compared to an axisymmetric treatment. Although the planar blunt body assumption may be useful in establishing a lower limit on the predicted heat transfer rates, its use is not justified since there is no significant reduction in time to either set-up the input data or run the code. However, since no wing heat transfer predictions were attempted, no conclusions can be reached on the validity of this assumption in these regions.

The predictions based on an isentropic expansion around a blunt axisymmetric body compare favorably with the data for the $\alpha$ = 15° and 30° cases (Figures 9 and 10), particularly over the aft regions of the fuselage. In the nose and forward regions of the fuselage, the predictions are somewhat low; an apparent effect of the lower degree of streamline spreading caused by the assumed axisymmetric body as compared to that which should exist over the smaller transverse curvature of the actual body. This lower spreading of the flow causes a more rapid boundary layer growth and consequently reduced heating. This effect is confirmed and amplified in the $\alpha$ = 53.5° case (Figure 11) where the predictions are about 50% low in the forward region. In addition, it appears that the history of this thicker boundary layer also causes an underprediction of the heating along the aft regions.

The results of the third assumption, that of the small crossflow theory, show excellent agreement with data in the forward regions for all three angles of attack. There is a tendency to overpredict wing region heating at $\alpha$ = 15°. At $\alpha$ = 30°, only the first half of the wing region shows any disagreement. Finally, at $\alpha$ = 53.5° the small crossflow prediction is low along the latter half of the body by an average of 25%. It is noted that Marvin, et. al., (Reference 113) suspect that the final data point at $\alpha$ = 53.5° (flagged in Figure 11) is in a region of transition to turbulent flow. BLIMP-predicted values of $Re_\theta$ at this location were of the order of 200 to 250. Based on the correlations given by Masek[64] for the dependence of the transition parameter $Re_\theta/[M_e \cdot (Re/L)]^{0.2}$ with angle of attack, transition might be expected at $Re_\theta$ of approximately 150 to 175. If the flow were laminar, the heat flux at this last body location would be less than that of the previous upstream location.

For a blunt axisymmetric body assumption, accounting for an entropy layer (as opposed to an isentropic expansion) results in an increase in the predicted

heating rates of about 10%, 15% and 25% respectively for the $\alpha$ = 15°, 30° and 53.5° cases. Inclusion of an entropy layer appears to be only a small improvement over the isentropic expansion case, but even these small effects may have significant influences on a shuttle vehicle design. A measure of the rate at which flow from the high entropy stagnation region shock is swallowed by the boundary layer is obtained by comparing the shock wave angle through which the boundary layer edge streamline originated. For $\alpha$ = 30%, this shock wave angle is plotted in Figure 13 as a function of the surface coordinate s and it can be observed that the swallowing process is essentially complete before s $\sim$ 0.1 ft. The continuing but slow decrease of the shock angle, and thus the entropy, is primarily due to the continual decrease of the shock angle along the entire body length (see Appendix 2). Figures 14 and 15 show typical boundary layer velocity profiles (solid lines) for $\alpha$ = 15° and 30° at x/L of 0.7 to 0.8. The dashed curve represents the shock angle of the streamline as a function of y, the normal distance from the wall. These plots also indicate that the entropy layer has been swallowed well forward on the body.

Predictions combining the entropy layer with the small-cross flow theory were not made as this system has not been incorporated into the current version of the BLIMP code (this is conceptually straightforward but requires some code modification). However, by extrapolating the available results, small-crossflow with entropy layer will slightly increase the isentropic small-crossflow results for $\alpha$ = 15° and 30° and should substantially improve the prediction over the latter half of the body for the $\alpha$ = 53.5° case.

Turbulent Flow Results

The turbulent flow results for $\alpha$ = 30° are presented in Figure 11. Transition to turbulent flow in the wind tunnel experiments of Reference 113 was reported to occur at x/L = 0.54. Transition to the fully turbulent model in the BLIMP code was made to occur at the same location, thus the apparent instantaneous increase in turbulent heating levels. The interesting result here is the effect of the entropy layer on turbulent heating. Whereas in the laminar region the increase, above the isentropic axisymmetric value, is limited to about 10%, in the turbulent region the increase is 40% resulting in good agreement with the data downstream of the actual transition region. This difference in relative effects is most probably due to the greater dependence of transport properties near the wall on edge conditions in turbulent flow as compared to laminar flow. At the transition station edge gradients still persist primarily due to shock curvature along the body as shown by Figure 16 which includes the laminar velocity profile and the streamline shock angle at the final laminar station. The reported transition momentum thickness Reynolds number, $Re_{\theta}$, in Reference 113 was approximately 450. Predicted values for the fixed transition location were 470 for the axisymmetric run and 330 for the small crossflow theory.

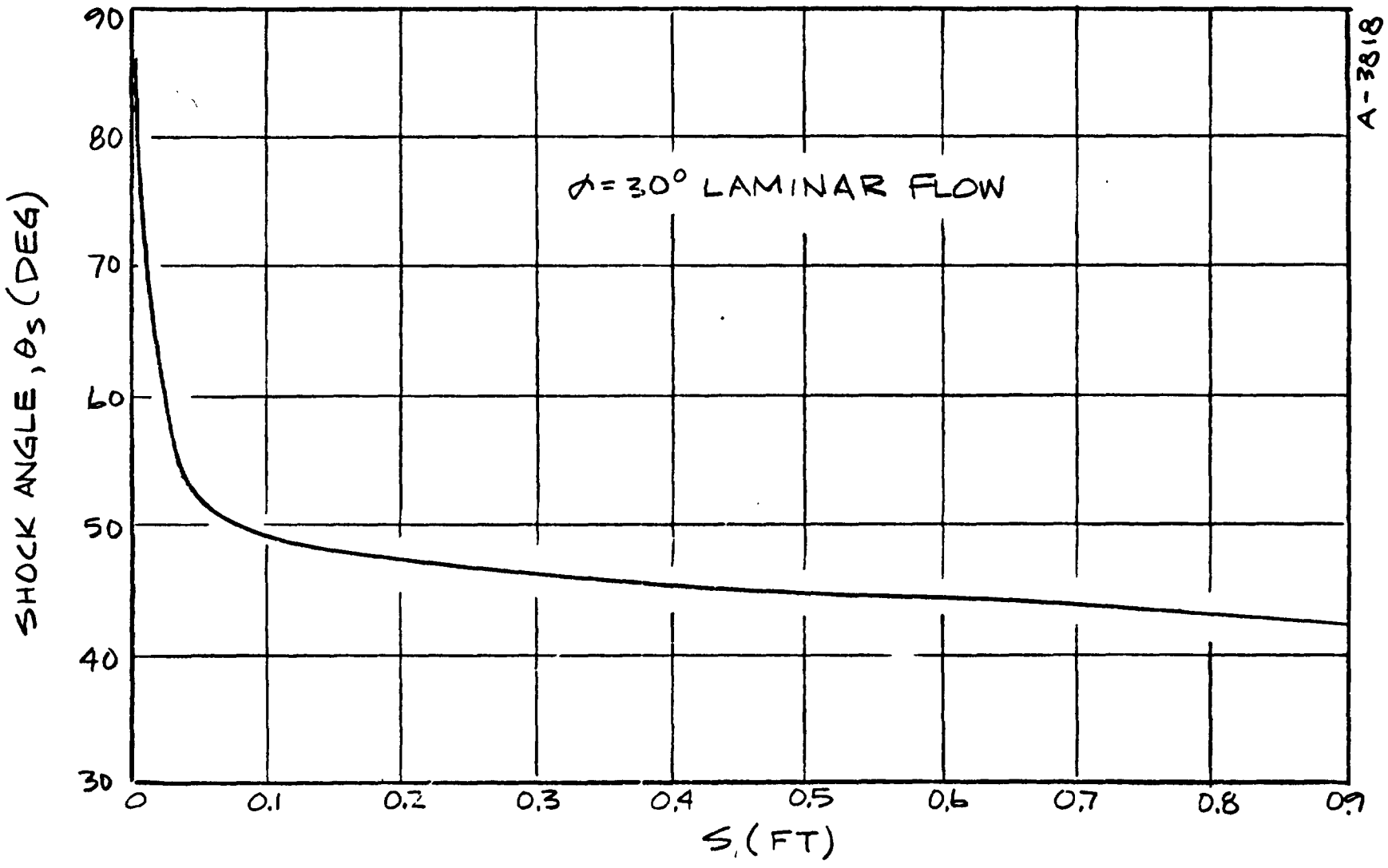


FIGURE 13 SHOCK ANGLE OF STREAMLINE IN VICINITY OF BOUNDARY LAYER EDGE

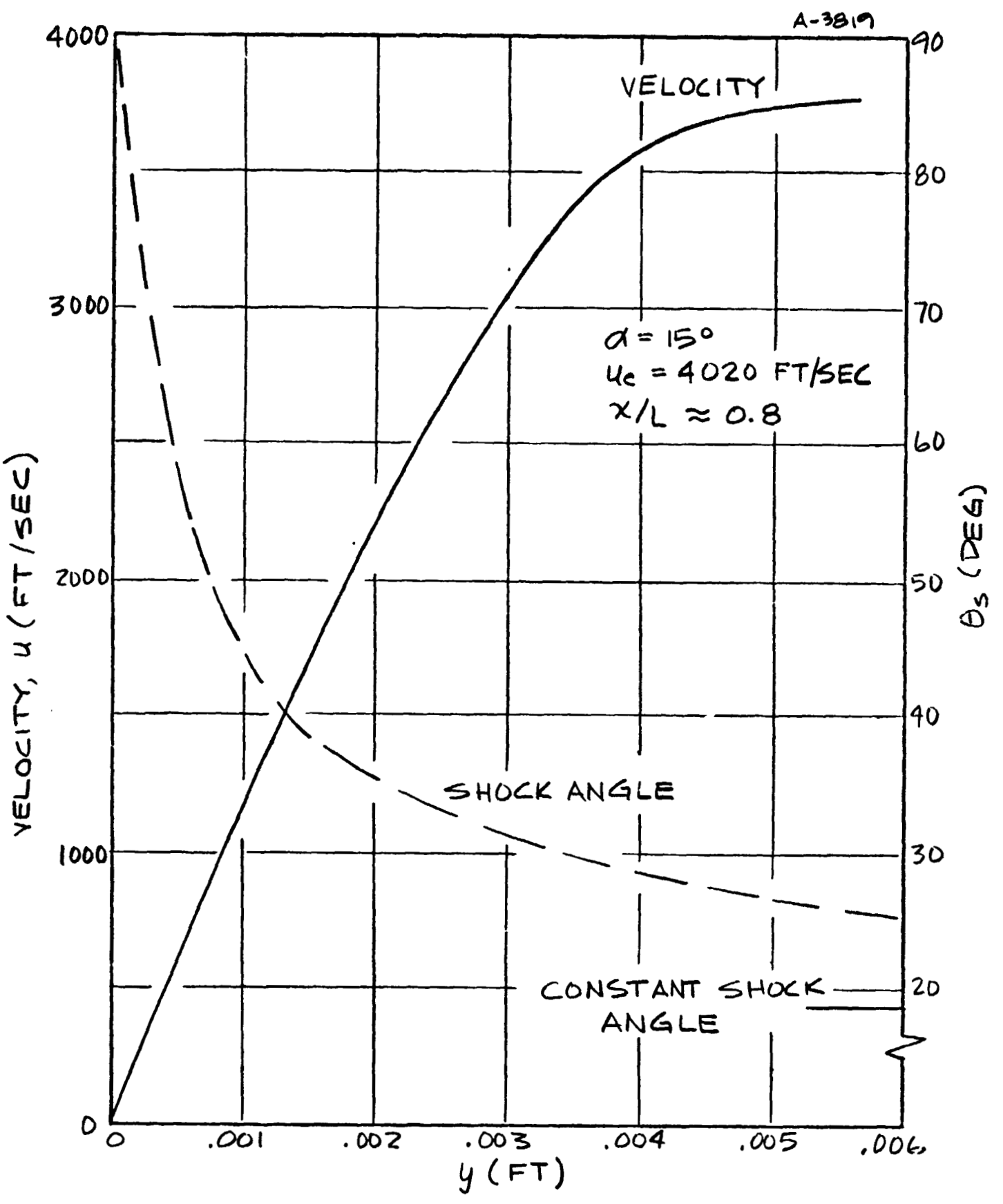


FIGURE 14 VELOCITY AND STREAMLINE ORIGIN PROFILES, $\alpha = 15°$ (LAMINAR FLOW)

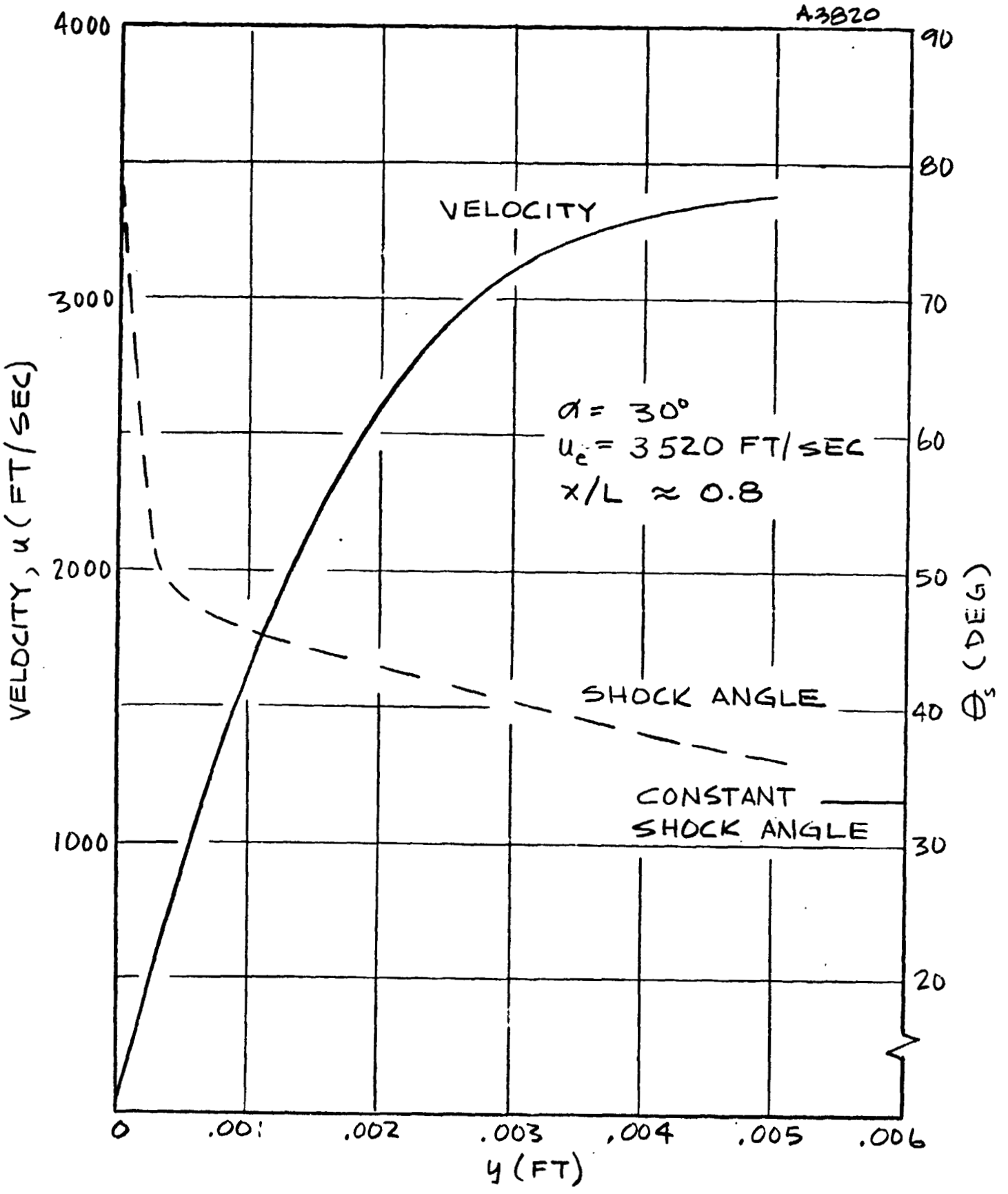


FIGURE 15 VELOCITY AND STREAMLINE ORIGIN PROFILES, $\alpha = 30°$ (LAMINAR FLOW)

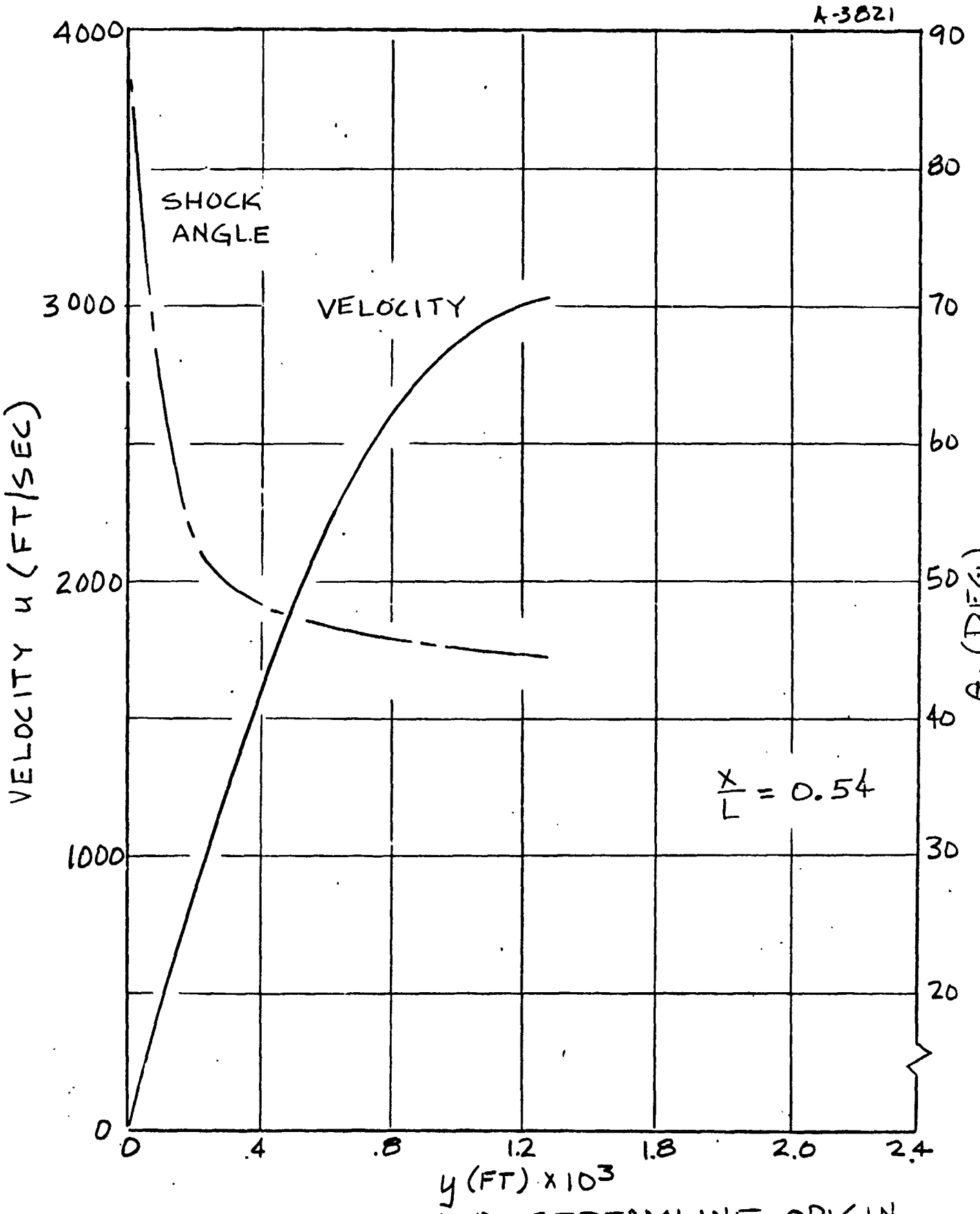


FIGURE 16 VELOCITY AND STREAMLINE ORIGIN PROFILES, $\alpha = 30°$ (TURBULENT FLOW)

OTHER RESULTS

Equations (6-2) and (6-3) were derived with a Newtonian pressure assumption. For shuttle configurations, this is not quite correct so that the validity of these equations might be questioned. In Equation (6-3), the Newtonian assumption appears solely in the second term of the $h_2$ coefficient where $P_T\cos^2\theta_B$ represents the Newtonian pressure at s on the plane of symmetry. At a given $\theta_B$ the actual pressure will be slightly higher; in particular, as $\theta_B$ approaches 90°, $P_T\cos^2\theta_B$ goes to zero whereas the real pressure does not. Consequently, replacing the term $P_T\cos^2\theta_B$ with the actual surface pressure would increase the magnitude of the corresponding term in Equation (6-3).

To investigate this point further, two solutions were obtained for the $\alpha = 50°$ spreading factor case, one with an $h_2$ distribution based on $P_T\cos^2\theta_B$ and the other on the measured pressure on the symmetry axis. The two results were identical from the stagnation point to an x/L of 0.1. From this point to the beginning of the fla at x/L = 0.2 the heat fluxes based on the measured pressure increased to 5 percent above the $P_T\cos^2\theta_B$ value. Over the remaining (wing) portion of the body the measured values were from 0 to 2 percent higher than $P_T\cos^2\theta_B$. Thus, it is concluded that for the shuttle configuration, this effect is of a minor order. For all angles of attack, the reported results are based on use of the local pressure which should overpredict local heating by no more than 2 percent.

The effect of transverse curvature in the aft region was evaluated by assuming that $R_T$ was (a) infinite and (b) equal to that of a cone locally tangent to the surface and coaxial with the angle-of-attack axis. For $\alpha = 30°$, the tangent cone approximation resulted in an increase in heat fluxes from 5-10%.

Additional comparisons which would be beneficial are shown in Figures 17, 18 and 19. In these figures the BLIMP axisymmetric blunt body predictions are compared with the tangent cone approximations recommended in Section 4.4. The data of Reference 113 are also included. At all three angles-of-attack (15°, 30°, 53.5°) the tangent cone approximations are slightly higher than the BLIMP prediction but both are in generally good mutual agreement. However, at $\alpha = 53.5°$ both predictions are noticeably lower than the data and would suggest that other factors such as three dimensional entropy swallowing or variable transverse curvature effects are important, especially at high angles-of-attack. These effects are presently approximated in the BLIMP code. Although these approximations do not necessarily represent optimum approaches, improved methods will probably rely on the development of near-exact inviscid solutions such as the work of References 21 and 22. Consequently an important consideration in the development of a boundary layer code is the inclusion of an option for integral coupling with an inviscid code.

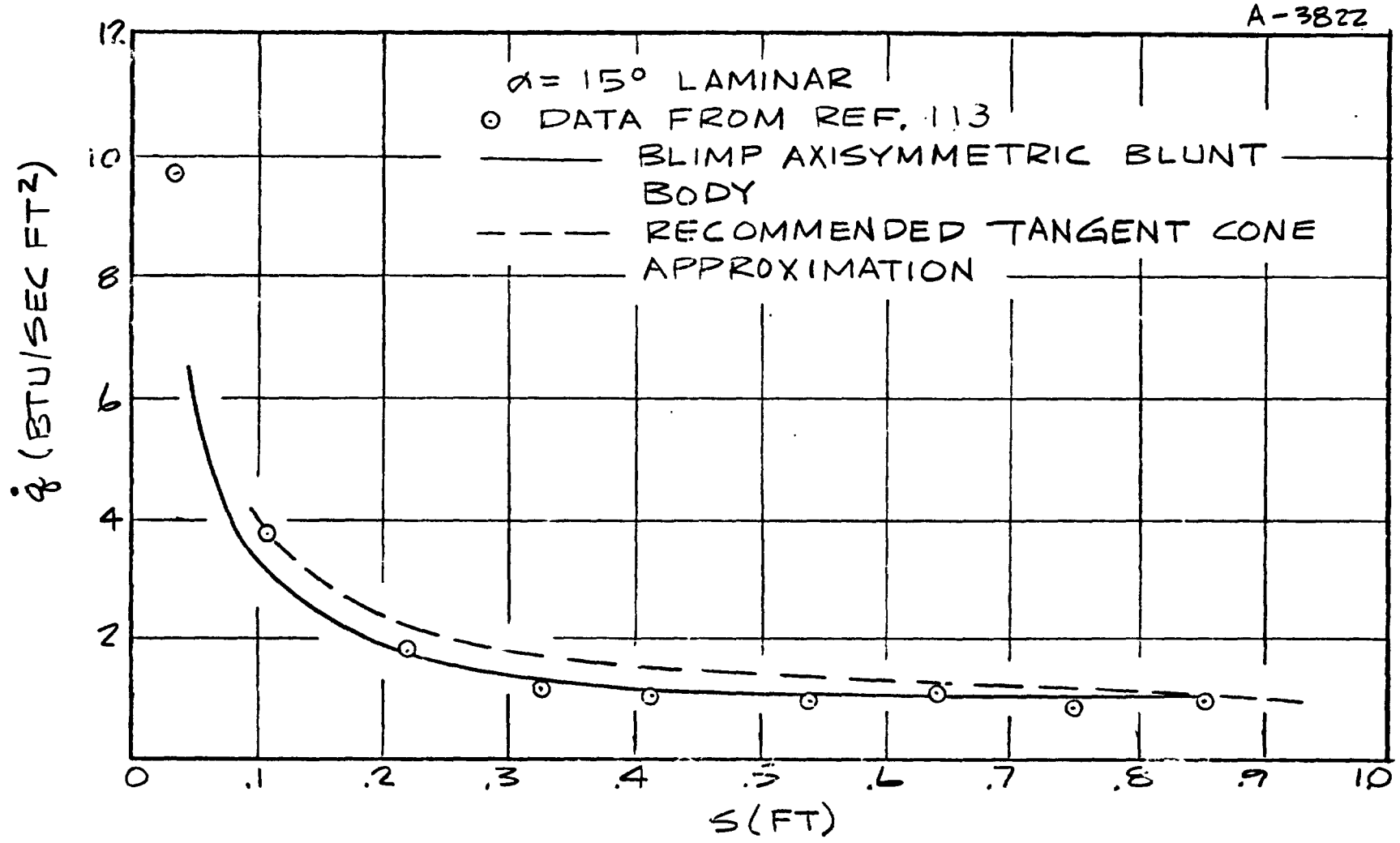


FIGURE 17 COMPARISON OF BLIMP AND TANGENT CONE APPROXIMATIONS, $\alpha = 15°$ (LAMINAR FLOW)

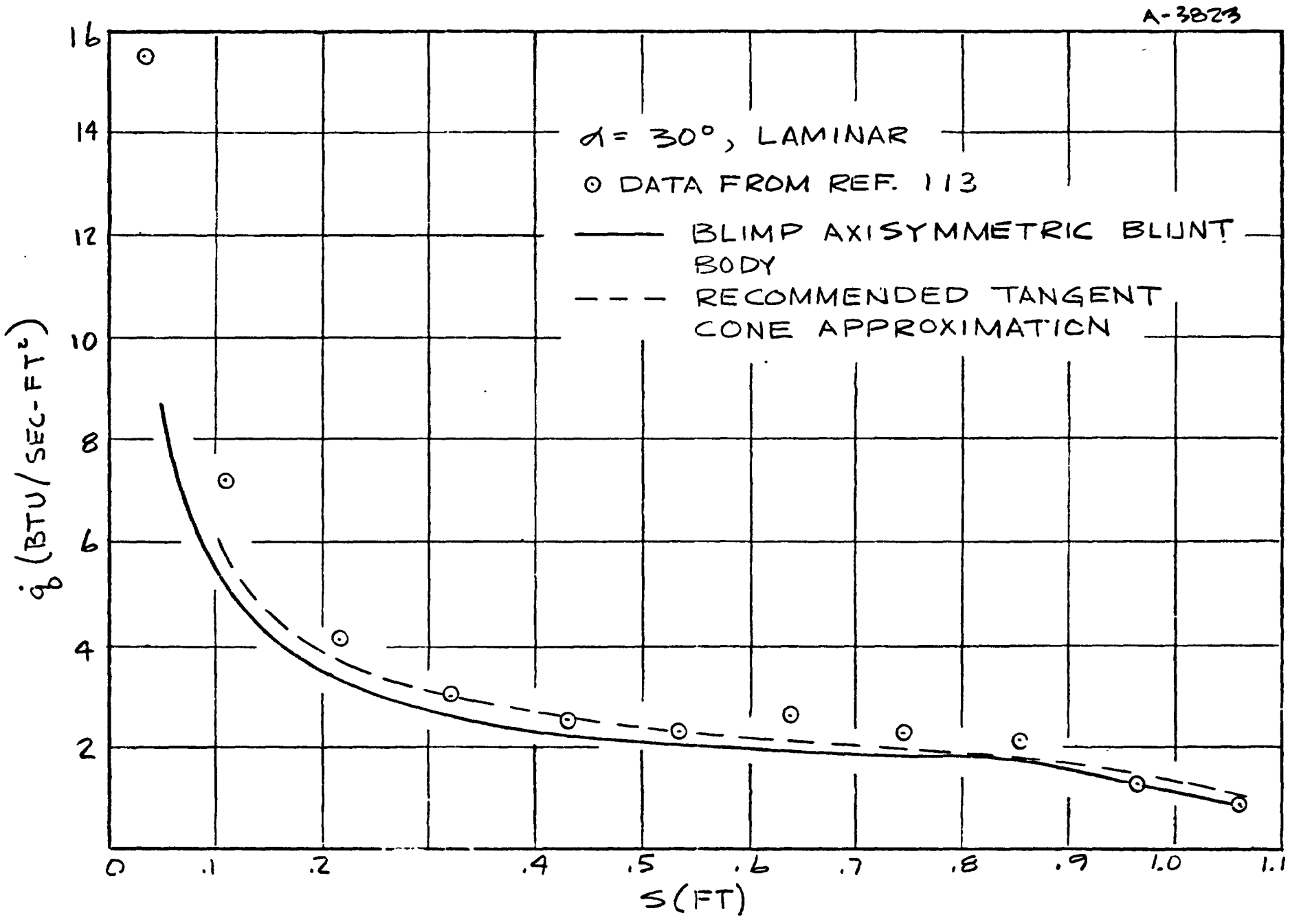


FIGURE 18 COMPARISON OF BLIMP AND TANGENT CONE APPROXIMATION, $\alpha = 30°$ (LAMINAR FLOW)

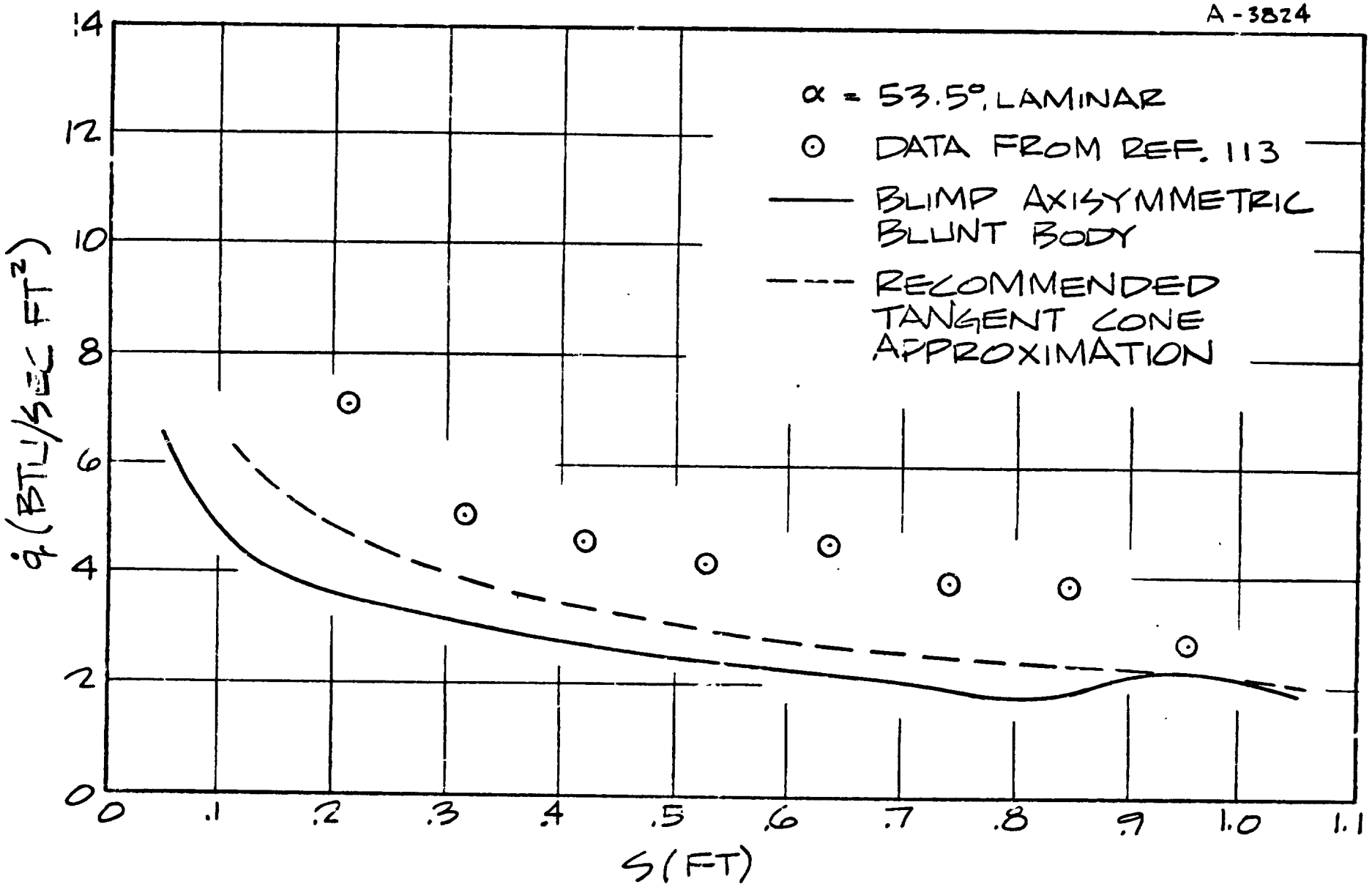


FIGURE 19 COMPARISON OF BLIMP AND TANGENT CONE APPROXIMATION, $\alpha = 53.5°$ (LAMINAR FLOW)

## SECTION 7

## RECOMMENDATIONS FOR FURTHER DEVELOPMENT OF HEATING PREDICTION CAPABILITY FOR SHUTTLE VEHICLES

Although it is possible to predict the approximate magnitude of the heat transfer to be expected on a delta shuttle vehicle, the reusability concept dictates a higher level of accuracy. The following are some recommendations on methods and procedures to improve accuracies of present methods.

1. The BLIMP code should be modified to account for nonequilibrium homogeneous chemistry.
2. Nonequilibrium BLIMP should be used to evaluate the influence of locally noncatalytic surfaces on downstream heat transfer.
3. The BLIMP code should be used to evaluate the influence of various approximations of streamline spreading and entropy swallowing effects for typical shuttle flight conditions.
4. A critical examination and evaluation of transition-to-turbulence information should be performed to define a viable transition criteria.

The present BLIMP code has options for integral coupling with inviscid flow field calculations and surface reaction chemistry. Any modifications and improvements to this code should be developed so as to retain these options.

## REFERENCES


1. Bartlett, E. P., Rindal, R. A., and Kendall, R. M., "A Critical Evaluation of Recent Developments and Future Requirements for the Prediction of Ablation of Manned Reentry Vehicles at Superorbital Velocities," Vidya Report No. 174, February 1965.

2. Fay, J. A. and Riddell, F. R., "Theory of Stagnation Point Heat Transfer in Dissociated Air," JAS, 25, 2, p.73-85, February 1958.

3. Fay, J. A. and Kemp, N. H., "Theory of Stagnation-Point Heat Transfer in a Partially Ionized Diatomic Gas," AIAA Jour., 1, 12, p.2741-2751, December 1963.

4. Blottner, F. G., "Viscous Shock Layer at the Stagnation Point with Nonequilibrium Air Chemistry," AIAA Jour., 7, 12, p.2281-2288, December 1969.

5. Detra, R. W. and Hildago, H., "Generalized Heat Transfer Formula and Graphs," AVCO RR 72, March 1960.

6. Beckwith, I. E., "Similar Solutions for the Compressible Boundary Layer on a Yawed Cylinder with Transpiration Cooling," NASA TR R-42, 1959.

7. Chung, P. M., "Hypersonic Viscous Shock Layer of Nonequilibrium Dissociating Gas," NASA TR R-109, 1961.

8. Moore, J. A. and Pallone, A., "Similar Solutions to the Laminar Boundary Layer Equations for Nonequilibrium Air," AVCO Memo RAD TM-62-59, July 1962.

9. Scala, S. M., "Hypersonic Stagnation Point Heat Transfer to Surfaces Having Finite Catalytic Efficiency," Proc. 3rd U.S. Congress on Applied Mechanics.

10. Blottner, F. G., "Chemical Non-Equilibrium Boundary Layer," AIAA Jour., 2, 2, p.232-240, February 1964.

11. Blottner, F. G., "Nonequilibrium Laminar Boundary-Layer Flow of Ionized Air," AIAA Jour., 2, 11, p.1921-1927, November 1964.

12. Reshotko, Eli, "Heat Transfer to a General Three Dimensional Stagnation Point," Jet Propulsion, 28, 1, p. 58-59, January 1958.

13. Rakich, J. V., "A Method of Characteristics for Steady Three Dimensional Supersonic Flow with Application to Inclined Bodies of Revolution," NASA TN D-5341, October 1969.

14. Rakich, J. V. and Cleary, J. W., "Theoretical and Experimental Study of Supersonic Flow Around Incline Bodies of Revolution," AIAA Jour., 8, 3, p. 511-518, March 1970.

15. Abbett, M. J., "Inviscid Equilibrium Air Flow About Blunted Cones at Incidence - Analysis and User's Manual," Aerotherm Report UM-70-20, June 1970.

16. Sanlorenzo, E. and Petri, F., "Programs for the Analyses of Flow Fields Around Spherically Capped Three Dimensional Bodies at Angles of Attack, Part 1 - Analysis and Typical Results," GASL TR-462, September 1964.

17. Moretti, G. et.al., "Flow Field Analysis of Reentry Configurations by a General Three Dimensional Method of Characteristics," GASL TR-247-Vol.III, April 1962.

18. Bohachevsky, I. O. and Mates, R. E., "A Direct Method for Calculation of the Flow About an Axisymmetric Blunt Body at Angle of Attack," AIAA Jour., 4, 5, p. 776-782, May 1966.

19. Moretti, G. and Bleich, G., "Three-Dimensional Flow Around Blunt Bodies," AIAA Paper No. 67-222, January 1967.

20. Stallings, R. L., Jr., and Campbell, J. F., "An Approximate Method for Predicting Pressure Distributions on Blunt Bodies at Angle of Attack," J. Spacecraft, 7, 11, p. 1306-1310, November 1970.

21. Grossman, B., Marconi, F. Jr., and Moretti, G., "A Numerical Procedure to Calculate the Inviscid Flow Field About a Space Shuttle Orbiter Travelling at a Supersonic/Hypersonic Velocity," NASA TM X-2272, p.158-183, April 1971.

22. Kutler, P., Lomax, H., Warming, R. F., "Computation of Space Shuttle Flow Fields Using Noncentered Finite Difference Schemes," Paper Submitted to AIAA 10th Aerospace Sciences Meeting, San Diego, California, January 17-19, 1972.

23. Wood, A. D., Springfield, J. F., and Pallone, A. J., "Chemical and Vibrational Relaxation of an Inviscid Hypersonic Flow," AIAA Jour., 2, 10, p.1697-1705, October 1964.

24. Curtis, J. T., Burke, A. F., and Hayman, R. A., "An Analytical and Experimental Study of the Ionized Flow Field About a Hemisphere Cylinder and Its Effect on the Radiation Pattern of a Slot Antenna," Cornell Aeronautical Laboratories Report AFCRL-63-339.

25. Lewis, C. H., "Numerical Methods for Nonreacting and Chemically Reacting Laminar Flows - Tests and Comparisons," J. Spacecraft, 8, 2, p.117-122, February 1971.

26. Hamilton, R. K., "Correlation of Space Shuttle Applicable Experimental Hypersonic Aerodynamic Characteristics with Theory," NASA TM X-2272, p. 455-4592, April 1971.

27. Marvin, J. G., et.al., "Surface Flow Patterns and Aerodynamic Heating on Space Shuttle Vehicles," AIAA Paper No. 71-594, June 1971.

28. Kaattari, G. E., "A Method for Predicting Pressures on Elliptic Cones at Supersonic Speeds," NASA TN D-5952, August 1970.

29. Kattari, G. G., "Estimation of Shock Layer Thickness and Pressure Distribution on Conical Bodies," NASA TM X-62031, 1971.

30. Fannelop, T. K. and Waldman, G. D., "Displacement Interaction and Flow Separation on Cones at Incidence to a Hypersonic Stream," AGARD Specialists' Meeting on Hypersonic Boundary Layers and Flow Fields, London, Paper No. 21, May 1968.

31. Cleary, J. W., "Effects of Angle of Attack and Nose Bluntness on the Hypersonic Flow Over Cones," AIAA Paper No. 66-414, June 1966.

32. Johnson, C. B., "Boundary-Layer Transition and Heating Criteria Applicable to Space Shuttle Configurations from Flight and Ground Tests," NASA TM X-2272, p.97-156, April 1971.

33. Beckwith, I. E. and Cohen, N. B., "Application of Similar Solutions to Calculation of Laminar Heat Transfer on Bodies with Yaw and Large Pressure Gradient in High Speed Flow," NASA TN D-625, January 1961.

34. van Driest, E. R., "Turbulent Boundary Layer in Compressible Fluids," Jour. Aero. Sciences, 18, 3, p. 145, 1951.

35. Spalding, D B. and Chi, S. W., "Skin Friction Exerted by a Compressible Fluid Stream on a Flat Plate," AIAA Jour., 1, 9 , p.2160-2161, September 1963.

36. Eckert, E. R. G. and Tewfik, O. E., "Use of Reference Enthalpy in Specifying the Laminar Heat-Transfer Distribution Around Blunt Bodies in Dissociated Air," Jour. Aero/Space Sciences, 27, 6, p.464-466, June 1960.

37. Romig, M. F., "Stagnation Point Heat Transfer for Hypersonic Flow," Jet. Prop. 26, 12, p.1098-1101, December 1956.

38. Eckert, E.R.G., "Survey on Heat Transfer at High Speeds," WADC Tech. Report 59-624, April 1960.

39. Bekcwith, I. E., "Similar Solutions for the Compressible Boundary Layer on a Yawed Cylinder with Transpiration Cooling," NASA TR R-42, 1959.

40. Blottner, F. G., "Finite Difference Methods of Solution of the Boundary-Layer Equations," AIAA Jour., 8, 2, p. 193-204, February 1970.

41. Zakkay, V. and Krause, E., "Boundary Conditions at the Outer Edge of the Boundary Layer on Blunted Conical Bodies," AIAA Jour., 1, 7, p.1671-1672, July 1963.

42. Hamilton, H. H. "Turbulent Heating on Space Shuttle Orbiters During Reentry," NASA TM X-52876, p.463-484, July 1970.

43. Adams, J. C. Jr., "Chemical Nonequilibrium Boundary Layer Effects on a Simulated Space Shuttle Configuration During Re-Entry," J. Spacecraft, 8, 6, p.683-684, June 1971.

44. Lomax, H. and Inouye, M., "Numerical Analysis of Flow Properties About Blunt Bodies Moving at Supersonic Speeds in an Equilibrium Gas," NASA TR R-204, July 1964.

45. Kaplan, B., "The Non-Equilibrium Air Boundary Layer on a Blunt Nosed Body," General Electric Report TIS 68SD227, April 1968.

46. Eaton, R. R., "Three Dimensional Numerical and Experimental Flowfield Comparisons for Sphere-Cones," J. Spacecraft, 7, 2, p.203-204, February 1970.

47. Cary, A.M.Jr., "Summary of Available Information on Reynolds Analogy for Zero-Pressure-Gradient, Compressible Turbulent-Boundary-Layer Flow," NASA TND 5560, January 1970.

48. Rubesin, M. W., "A Modified Reynolds Analogy for the Compressible Turbulent Boundary Layer on a Flat Plate," NACA TN 2917, March 1953.

49. Thomas, A. C., et.al., "Application of Ground Test Data to Reentry Vehicle Design," AFFDL TR-229, January 1967.

50. Savage, R. T. and Jaeck, C. L., "Investigation of Turbulent Heat Transfer at Hypersonic Speeds, Vol. 1, Analytical Methods," AFFDL TR 67-144, Vol. 1, December 1967.

51. Colburn, A. P., "A Method of Correlating Forced Convection Heat Transfer Data and a Comparison with Fluid Friction," Trans. AIChE, Vol. XXIX, p.174-211, 1933.

52. Reshotko, E. and Tucker, M., "Approximate Calculation of the Compressible Turbulent Boundary Layer with Heat Transfer and Arbitrary Pressure Gradient," NACA TN 4154, December 1957.

53. Sommer, S. C. and Short, B. J., "Free Flight Measurements of Turbulent-Boundary-Layer Skin Friction in the Presence of Severe Aerodynamic Heating at Mach Numbers from 2.8 to 7.0," NACA TN 3391, March 1955.

54. Pearce, B. E., "A Comparison of Simple Turbulent Heating Estimates and Boundary Layer Transition Criteria with Application to Large, Lifting Entry Vehicles," NASA TM X-52876, Vol. 1, p. 485-508, July 1970.

55. Hopkins, E. J. and Inouye, M., "An Evaluation of Theories for Predicting Turbulent Skin Friction and Heat Transfer on Flat Plates at Supersonic and Hypersonic Mach Numbers," AIAA Jour., 9, 6, p.993-1003, June 1971.

56. Beckwith, I. E. and Gallagher, J. J., "Local Heat Transfer and Recovery Temperatures on a Yawed Cylinder at a Mach Number of 4.15 and High Reynolds Numbers," NASA TR R-104, 1961.

57. Thomas, A., Perbachs, A., and Nagel, A., "Advanced Reentry Systems Heat Transfer Manual for Hypersonic Flight," AFFDL-TR-65-195, Ocrober 1966.

58. Katzen, E. D., et.al., "Static Aerodynamics, Flow Fields and Aerodynamic Heating of Space Shuttle Orbiters," NASA TM X-52876, Vol. 1, p. 142-194, July 1970.

59. Young, C. H., Reda, D. C., and Roberge, A. M., "Transitional and Turbulent Heat Transfer Correlations for a Lifting Entry Vehicle at M = 10," NASA TM X 52876, Vol. 1, p. 418-444, July 1970.

60. Anon. (General Dynamic/Convair), "Space Shuttle, Volume 4: Technical Analysis and Performance, Final Technical Report," NASA CR 102552, Vol. 4, Section 4, October 1969.

61. Guard, F. L. and Schultz, H. D., "Space Shuttle Aerodynamic Heating Considerations," ASME 70-HT/SpT-10, June 1970.

62. Creager, M. O., "The Effect of Leading Edge Sweep and Surface Inclination on Hypersonic Flow Field Over a Blunt Flat Plate, NASA Memo 12-26-58A, 1959.

63. Thomas, A. C., "Interference and Radiation Blockage Effects on Surface Temperatures of Composite Flight Vehicles," NASA TM X-52876, Vol. 1, p.390-417, July 1970.

64. Masek, R. V., "Boundary Layer Transition on Lifting Entry Vehicle Configurations at High Angles of Attack," NASA TM X-52876, Vol. 1, p. 445-462, July 1970.

65. Moote, J. D., "A Minimum Heating Flight Mode for High Lateral Range Space Shutcle Entries Including the Effects of Transition," NASA TM X-52876, p.531-546, July 1970.

66. Marvin, J. G. and Sheaffer, Y. S., "A Method for Solving the Nonsimilar Laminar Boundary Layer Equations Including Foreign Gas Injection," NASA TN D-5516, November 1969.

67. Masek, R. V. and Forney, J. A., "An Analysis of Predicted Space Shuttle Temperatures and Their Impact on Thermal Protection Systems," NASA TM X-2272, Vol. 1, p. 75-96, April 1971.

68. Schlichting, H., Boundary Layer Theory, Chap. XXI, McGraw Hill, New York, New York, 1960.

69. Maise, G., "Lee-Side Heating Investigations of Simple Body-Like Configurations," NASA TM X-2272, Vol. I, p. 289-309, April 1971.

70. Hefner, J. N. and Whitehead, A. H. Jr., "Experimental Lee-Side Heating Studies on a Delta-Wing Orbiter," NASA TM X-2272, Vol. I, p. 267-288, April 1970.

71. Der, J. Jr., "A Study of General Three-Dimensional Boundary-Layer Problems by an Exact Numerical Method," AIAA Jour., 9, 7, p.1294-1302, July 1971.

72. Schlichting, H., "A Survey of Some Recent Research Investigations on Boundary Layers and Heat Transfer," Jour. App. Mech., 38, Ser. E, 2, p. 289-300, June 1971.

73. Chapman, D. R., "A Theoretical Analysis of Heat Transfer Regions of Separated Flow," NACA TN 3792, 1956.

74. Schadt, G. H., "Aerodynamic Heating Problems and Their Influence on Earth Orbit Lifting Entry Spacecraft," AIAA Paper No. 68-1126, October 1968.

75. Feldman, S., "Hypersonic Gas Dynamic Charts for Equilibrium Air," AVCO RR-40, January 1957.

76. Lees, L., "Laminar Heat Transfer Over Blunt-Nosed Bodies at Hypersonic Flight Speeds," Jet Propulsion, p.259-274, April 1956.

77. Dunavant, J. C., "Investigation of Heat Transfer and Pressures on Highly Swept Flat and Dihedraled Delta Wings at Mach Numbers of 6.8 and 9.6 and Angles of Attack to 90°," NASA TM X-688, June 1962.

78. Bartlett, E. P., "An Evaluation of Design Analysis Techniques for High Performance Ballistic Vehicle Graphite Nose Tips, Appendix C, Boundary Layer Transport Phenomena," AFML-TR-69-73, Vol. III, January 1970.

79. Flügge-Lotz, I. and Blottner, F. G., "Computation of the Compressible Laminar Boundary-Layer Flow including Displacement Thickness Interaction using Finite-Difference Methods," Stanford University, Div. of Eng. Mech., TR 131, January 1962.

80. Fannelop, T. K. and Flügge-Lotz, I., "Two-Dimensional Viscous Hypersonic Flow over Simple Blunt Bodies including Second-Order Effects," Stanford University, Div. of Eng. Mech., TR 144, June 1964.

81. Davis, R. T. and Flugge-Lotz, I., "Laminar Compressible Flow Past Axisymmetric Blunt Bodies (Results of a Second-Order Theory)," Journal of Fluid Mechanics, 20, 4, pp. 593-623, 1964.

82. Tong, H., "Multicomponent Nonequilibrium Boundary Layer Program," Boeing Rept. D2-23929-1, 1966.

83. Adams, J. C., Lewis, C. H., et. al., "Effects of Chemical Nonequilibrium, Mass Transfer, and Viscous Interaction on Spherically Blunted Cones at Hypersonic Conditions," AEDC-TR-69-237, January 1970.

84. Davis, R. T., "Numerical Solutions to the Viscous Shock-Layer Blunt Body Problem with Inert Gas Injection," Sandia SC-CR-70-6162, January 1971.

85. Lewis, C. H., Anderson, E. C., and Miner, E. W., "Nonreacting and Equilibrium CHemically Reacting Turbulent Boundary-Layer Flows," AIAA Paper No. 71-597, June 1971.

86. Lew, H. G., "The Ionized Flow Field over Re-entry Bodies," General Electric TIS R67 SD 70, December 1967.

87. Braun, E. R., "Effects of a Fully Catalytic Wall on a Non-equilibrium Boundary Layer Including Ablation Products," General Electric TIS 70 SD 253, June 1970.

88. Dellinger, T. C., "Nonequilibrium Air Ionization in Fully Viscous Shock Layers," AIAA Paper No. 70-806, June 1970.

89. Smith, A.M.O. and Clutter, D. W., "Machine Calculation of a Compressible Laminar Boundary Layers," AIAA Journal, 3, 4, pp. 639-647, April 1965.

90. Smith, A.M.O. and Jaffe, N. A., "General Method for Solving the Laminar Nonequilibrium Boundary-Layer Equations of a Dissociating Gas," AIAA Journal, 4, 4, pp. 611-620, April 1966.

91. Jaffe, N. A., Lind, R. C., and Smith, A.M.O., "Solution to the Binary Diffusion Laminar Boundary-Layer Equations with Second-Order Transverse Curvature," AIAA Journal, 5, 9, pp. 1563-1569, September 1967.

92. Mayne, A. W., Jr., Gilley, G. E., and Lewis, C. H., "Binary Boundary Layers on Sharp Cones in Low Density Supersonic and Hypersonic Flow," AIAA Paper No. 68-66, January 1968.

93. Smith, A.M.O., and Cebeci, T., "Numerical Solution of the Turbulent-Boundary-Layer Equations," Douglas Report No. DAC 33735, May 1967.

94. Cebeci, T., Smith, A.M.O., and Wang, L. C., "A Finite-Difference Method for Calculating Compressible Laminar and Turbulent Boundary Layers," McDonnell Douglas Rept. No. DAC-67131, March 1969.

95. Cebeci, T., "Calculation of Compressible Turbulent Boundary Layers with Heat and Mass Transfer," AIAA Jour., 9, 6, pp. 1091-1097, June 1971.

96. Bushnell, D. M. and Beckwith, I. E., "Calculation of Nonequilibrium* Hypersonic Turbulent Boundary Layers and Comparisons with Experimental Data," AIAA Jour., 8, 8, pp. 1462-1469, August 1970.

97. Herring, H. J. and Mellor, G. L., "A Method of Calculating Compressible Turbulent Boundary Layers," NASA CR-1144, September 1968.

98. Pallone, A. J., Moore, J. A., and Erdos, J. I., "Nonequilibrium, Nonsimilar Solutions of the Boundary-Layer Equations," AIAA Jour., 2, 10, pp. 1706-1713, October.

99. Luceri, J. A., "Reentry Environment and Systems Technology (REST) Semiannual Progress Report 1 January-30 June 1966, Vol. II -- Aerophysics Appendices," BSD-TR-66-231, Vol. II, July 1966.

*Nonequilibrium as used here means turbulent flows with pressure gradient.

100. Erdos, J., and Pallone, A. J., "Interaction of a Chemically Reacting Laminar Boundary Layer and an Ablating Surface, Part I: Analysis," ARL 68-0029, February 1968.

101. Spalding, D. B., and Patankar, S. V., Heat and Mass Transfer in Boundary Layers, C.R.C. Press: Cleveland, 1968.

102. Kays, W. M., "Heat Transfer to the Transpired Turbulent Boundary Layer," paper to be presented at ASME Heat Transfer Conference 1971 (Copies available upon request from Stanford Univ., Mech. Eng. Dept.)

103. Mayne, A. W., Jr., and Adams, J. C., Jr., "Streamline Swallowing by Laminar Boundary Layers in Hypersonic Flow," AEDC-TR-71-32, March 1971.

104. Kendall, R. M., and Bartlett, E. P., "Nonsimilar Solution of the Multicomponent Laminar Boundary Layer by an Integral-Matrix Method," AIAA Jour., 6, 6, pp. 1089-1097, June 1968.

105. Aerotherm Corporation, Mountain View, California, "User's Manual Boundary Layer Integral Matrix Procedure, Version C (BLIMPC)," Report No. UM-70-20, June 1970.

106. Galowin, L. S., and Gould, H. E., "A Finite Difference Method Solution of Non-similar, Non-equilibrium Air, Laminar and Turbulent Boundary Layer Flows," Parts I, II, and II, General Applied Science Laboratories, Tech. Rept. No. 422, March 1964.

107. Galowin, L. S., and Gould, H. E., "Examples of Exact Numerical Solution of the Laminar Boundary Layer Equations by Explicit Finite Difference Methods," General Applied Science Laboratories, Tech. Rept. No. 502, February 1965.

108. Mondrzyk, R. J., "Nonsimilar, Nonequilibrium Laminar Boundary Layers for Sharp Conical Bodies," Boeing Rept. D2-36398-1, December 1965.

109. Lee, J. T., Langlet, T. J., and Moore, J. A., "Nonequilibrium Laminar Boundary Layer Calculations on a Slightly Blunted 11.5 Degree Cone-Cylinder," TRW Systems Rept. 4509-6015-T, January 1966.

110. Moore, J. A., and Lee, J. T., "Discontinuous Injection of Inert Gases into the Non-equilibrium Laminar Boundary Layer," TRW Systems Rept. 06388-6018-R000, July 1967.

111. Chenoweth, D. R., "Finite Difference Solution of the Boundary-Layer Equations," Sandia SCL-DR-67-32, May 1967.

112. Marvin, J. G., NASA Ames Research Center, Moffett Field, California, private communication, July 1971.

113. Marvin, J. G., et. al., "Flow Fields and Aerodynamic Heating of Space Shuttle Orbiters," NASA TM X-2272, pp. 21-73, April 1971.

114. North American Rockwell, "Wind Tunnel Model Contours-134 B," NAR Drawing 3-930, 30 October 1970.

115. North American Rockwell, "Wind Tunnel Model Contours-129," NAR Drawing 9992-22, 1 June 1970

116. Hearne, L. F., Chin, J. H., and Woodruff, L. W., "Final Report: Study of Aerothermodynamic Phenomena Associated with Reentry of Manned Spacecraft," Lockheed Missile and Space Co., Sunnyvale, Calif., May 1966.

# APPENDIX 1

## LOCAL SURFACE INCIDENCE RELATIVE TO FREE STREAM DIRECTION

## APPENDIX 1

## LOCAL SURFACE INCIDENCE RELATIVE TO FREE STREAM DIRECTION

### Local Surface Incidence of Wing Surface

Defining pertinent angle as

$\alpha$ = vehicle reference angle of attack

$\bar{\alpha}$ = angle between chord line and reference line

$\tilde{\alpha}$ = local surface inclination with respect to chord line

$\phi$ = local dihedral angle

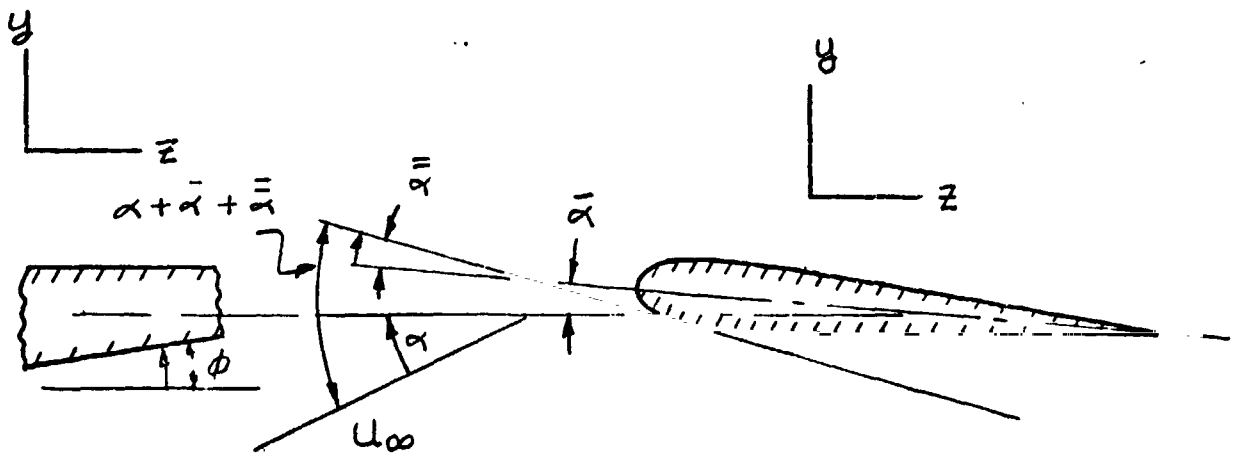


then at $\alpha = 0$, the unit vector which is tangent to the surface and lies in the chord section plane is

$$\hat{U}_1 = \cos(\bar{\alpha} + \tilde{\alpha})\hat{i} - \sin \tilde{\alpha}\, \hat{j}$$

and the unit vector which is tangent to the surface but which lies in the plane perpendicular to the reference line is

$$\hat{U}_2 = \sin \phi\, \hat{j} + \cos \phi\, \hat{k}$$

The cross product of these two vectors is normal to the local tangent plane and in normalized form is

$$\hat{U}_3 = -\frac{\sin(\bar{\alpha} + \bar{\bar{\alpha}})\cos\phi}{N}\hat{i} - \frac{\cos(\bar{\alpha} + \bar{\bar{\alpha}})\cos\phi}{N}\hat{j} + \frac{\cos(\bar{\alpha} + \bar{\bar{\alpha}})\sin\phi}{N}\hat{k}$$

where

$$N^2 = \sin^2(\bar{\alpha} + \bar{\bar{\alpha}})\cos^2\phi + \cos^2(\bar{\alpha} + \bar{\bar{\alpha}})\cos^2\phi + \cos^2(\bar{\alpha} + \bar{\bar{\alpha}})\sin^2\phi$$

$$= \cos^2\phi + \cos^2(\bar{\alpha} + \bar{\bar{\alpha}})\sin^2\phi$$

Rotating $\hat{U}_3$ through an angle of attack $\alpha$

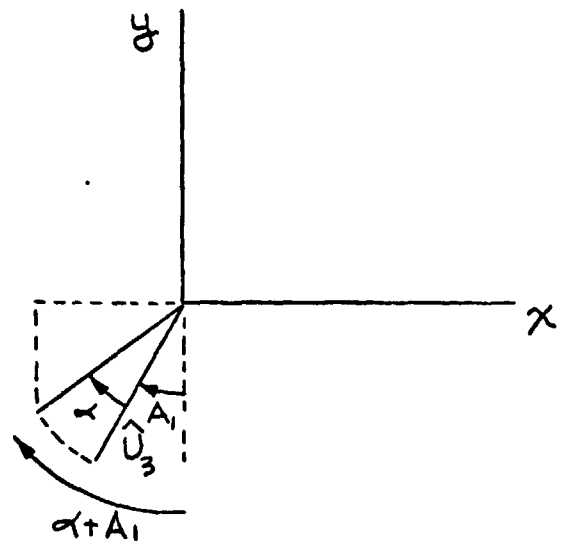


The length of the projection of $\hat{U}_3$ onto the x-y plane is

$$L = \frac{\cos\phi}{N}$$

and

$$A_1 = \bar{\alpha} + \bar{\bar{\alpha}}$$

The unit normal vector which defines the local tangent plane at angle of attack $\alpha$ is then

$$\hat{U}_4 = -\frac{\sin(\alpha + \bar{\alpha} + \bar{\bar{\alpha}})\cos\phi}{N}\hat{i} - \frac{\cos(\alpha + \bar{\alpha} + \bar{\bar{\alpha}})\cos\phi}{N}\hat{j} + \frac{\cos(\alpha + \bar{\alpha} + \bar{\bar{\alpha}})\sin\phi}{N}\hat{k}$$

The dot product of $\hat{U}_4$ with $\hat{i}$ is the sine of the effective incidence. Defining $\gamma$ as the effective incidence

$$\sin\gamma = \frac{\cos\phi\,\sin(\alpha + \bar{\alpha} \quad \bar{\bar{\alpha}})}{N}$$

where the sign was changed to yield a positive angle.

For small $\bar{\alpha} + \bar{\bar{\alpha}}$ this reduces to

$$\sin\gamma \approx \cos\phi\,\sin(\alpha + \bar{\alpha} + \bar{\bar{\alpha}})$$

Local Surface Incidence of Outboard Fin Surface

Defining pertinent angles as

a = angle between fin chord line and vehicle symmetry plane

$\phi'$ = angle of tilt of fin

$\bar{\alpha}'$ = local profile angle relative to chord line

then at $\alpha = 0$, the unit vector at an angle $\phi'$ from the vertical and in a plane perpendicular to the fin chord line is

$$\hat{U}_1 = -\sin\phi'\sin a\,\hat{i} + \cos\phi'\hat{j} + \sin\phi'\cos a\,\hat{k}$$

The unit vector which is tangent to the fin surface and lies in a horizontal plane is

$$\hat{U}_2 = \cos(a + \bar{\alpha}')\hat{i} + \sin(a + \bar{\alpha}')\hat{k}$$

The cross product of $\hat{U}_1$ and $\hat{U}_2$, after normalization yields the unit normal vector which defines the tangent plane. Thus

$$\hat{U}_3 = - \frac{\cos \phi' \sin(a + \bar{\alpha}')}{N_1} \hat{i} - \frac{1}{N_1} \Big\{ \sin \phi' \sin a \sin(a + \bar{\alpha}') + \sin \phi' \cos a \cos(a + \bar{\alpha}') \Big\} \hat{j} + \frac{\cos \phi' \cos(a + \bar{\alpha}')}{N_1} \hat{k}$$

where

$$N_1^2 = \cos \phi' + \sin^2 \phi' \Big\{ \sin a \sin(a + \bar{\alpha}') + \cos a \cos(a + \bar{\alpha}') \Big\}^2$$

Using the same procedure as before, $\hat{U}_3$ is rotated through an angle $\alpha$. The unit normal vector which defines the local surface tangent at angle of attack $\alpha$ is then

$$\hat{U}_4 = - L \sin(\alpha + \xi)\hat{i} - L \cos(\alpha + \xi)\hat{j} + \frac{\cos \phi' \cos(a + \bar{\alpha}')}{N_1} \hat{k}$$

where

$$L^2 = \frac{\cos^2 \phi' \sin^2(a + \bar{\alpha}')}{N_1^2} + \frac{1}{N_1^2} \Big\{ \sin \phi' \sin a \sin(a + \bar{\alpha}') + \sin \phi' \cos a \cos(a + \bar{\alpha}') \Big\}^2$$

$$\tan \xi = \frac{\cos \phi' \sin(a + \bar{\alpha}')}{\Big\{ \sin \phi' \sin a \sin(a + \bar{\alpha}') + \sin \phi' \cos a \cos(a + \bar{\alpha}') \Big\}}$$

Again, the dot product of $\hat{U}_4$ and $\hat{i}$ is the sine of the effective angle of incidence $\gamma'$. With the sign changed to yield a positive angle,

$$\sin \gamma' = L \sin(\alpha + \xi)$$

and L and $\xi$ can be expressed as

$$L = \left\{ \frac{\cos^2 \phi' \sin^2(a + \bar{\alpha}') + \sin^2 \phi' \cos^2 \bar{\alpha}'}{\cos^2 \phi' + \sin^2 \phi' \cos^2(\bar{\alpha}')} \right\}^{\frac{1}{2}}$$

$$\xi = \tan^{-1} \left[ \frac{\sin(a + \bar{\alpha}')}{\cos \bar{\alpha}' \tan \phi'} \right]$$

For small angle $\bar{\alpha}'$ this set of equations reduce to

$$\sin \gamma' = \cos \phi' \sqrt{\sin^2 a + \tan^2 \phi'} \sin(\xi + \alpha)$$

$$\sin \xi = \frac{\sin a}{\sqrt{\sin^2 a + \tan^2 \phi'}}$$

True Sweep Angle of Wing Leading Edge

Define

$\zeta$ = semi-apex angle of wing

$\phi$ = dihedral angle

Then consider the unit vector which is the axis of a hypothetical cylindrical leading edge. This unit vector is

$$\hat{U}_1 = \frac{\cos \zeta}{N_1} \hat{i} + \frac{\sin \zeta \tan \phi}{N_1} \hat{j} + \frac{\sin \zeta}{N_1} \hat{k}$$

where

$$N_1^2 = 1 + \sin^2 \zeta \tan^2 \phi$$

Rotating this vector through an angle of attack $\alpha$, the unit vector becomes

$$\hat{U}_2 = L \cos(\alpha - A_2)\hat{i} - L \sin(\alpha - A_2)\hat{j} + \frac{\sin \zeta}{N_1} \hat{k}$$

where

$$L^2 = \frac{\cos^2 \zeta + \sin^2 \zeta \tan^2 \phi}{N_1^2}$$

$$\tan A_2 = \tan \zeta \tan \phi$$

the dot product of $\hat{U}_2$ and $\hat{i}$ is the cosine of the effective angle of attack $\Lambda$. Thus

$$\cos \Lambda = L \cos(\alpha - A_2)$$

For small angles $\phi$ this reduces to

$$\cos \Lambda \sim \cos \zeta \cos \alpha$$

True Sweep Angle of Outboard Fins

Define

$\delta$ = nominal sweep angle of fins measured on vehicle symmetry plane

also $\phi'$ and a are as previously defined. Then the unit vector which represents the axis of a hypothetical cylindrical leading edge is

$$\hat{U}_1 = \frac{\sin\delta}{N_1}\hat{i} + \frac{\cos\delta}{N_1}\hat{j} + \frac{(\sin\delta\tan a + \cos\delta\tan\phi')}{N_1}\hat{k}$$

where

$$N^2 = 1 + (\sin\delta\tan a + \cos\delta\tan\phi')^2$$

Rotating through an angle of attack $\alpha$, the unit vector becomes

$$\hat{U}_2 = \frac{1}{N_1}\sin(\alpha+\delta)\hat{i} + \frac{1}{N_1}\cos(\alpha+\delta)\hat{j} + \frac{\sin\delta\tan a + \cos\delta\tan\phi'}{N_1}\hat{k}$$

and the effective angle of attack of the fin leading edge is

$$\cos\Lambda' = \frac{\sin(\alpha+\delta)}{\sqrt{1 + (\sin\delta\tan a + \cos\delta\tan\phi')^2}}$$

# APPENDIX 2

# INPUT DATA FOR BLIMP TEST CASES

INPUT DATA FOR BLIMP TEST CASES

$\alpha = 15°$

| Surface Data | | | | Shock Wave Data | |
|---|---|---|---|---|---|
| S(ft) | $r_o^k$(ft) | $h_2$(ft) | $P/P_T$ | $r_s$(ft) | $\theta_s$(deg) |
| 0.0 | 0.0 | 0.0 | 1.000 | 0.0 | 90.0 |
| 0.001 | 0.000995 | 0.000995 | 0.9725 | 0.000995 | 82.2 |
| 0.002 | 0.00196 | 0.00197 | 0.890 | 0.00196 | 74.5 |
| 0.003 | 0.002875 | 0.00291 | 0.730 | 0.002875 | 68.2 |
| 0.004 | 0.00376 | 0.00380 | 0.655 | 0.00376 | 62.7 |
| 0.005 | 0.00450 | 0.00475 | 0.600 | 0.0045 | 59.1 |
| 0.006 | 0.00517 | 0.00560 | 0.547 | 0.00583 | 53.5 |
| 0.007 | 0.00583 | 0.00665 | 0.502 | 0.00783 | 47.2 |
| 0.010 | 0.00783 | 0.0100 | 0.420 | 0.00974 | 42.9 |
| 0.013 | 0.00974 | 0.0140 | 0.375 | 0.0139 | 37.6 |
| 0.016 | 0.01159 | 0.0187 | 0.358 | 0.0196 | 34.2 |
| 0.020 | 0.0139 | 0.0270 | 0.335 | 0.0279 | 31.0 |
| 0.025 | 0.0167 | 0.0400 | 0.312 | 0.0368 | 28.5 |
| 0.030 | 0.0196 | 0.0550 | 0.293 | 0.0516 | 25.5 |
| 0.040 | 0.0250 | 0.0950 | 0.260 | 0.0683 | 23.3 |
| 0.0471 | 0.0279 | 0.132 | 0.232 | 0.114 | 21.1 |
| 0.070 | 0.0368 | 0.310 | 0.188 | 0.169 | 19.7 |
| 0.090 | 0.0441 | 0.530 | 0.156 | 0.224 | 18.7 |
| 0.111 | 0.0516 | 0.860 | 0.132 | | |
| 0.160 | 0.0683 | 2.20 | 0.114 | | |
| 0.219 | 0.0865 | 4.40 | 0.104 | | |
| 0.325 | 0.114 | 8.70 | 0.090 | | |
| 0.431 | 0.1415 | 13.0 | 0.088 | | |
| 0.537 | 0.169 | 17.0 | 0.088 | | |
| 0.643 | 0.197 | 21.3 | 0.088 | | |
| 0.749 | 0.224 | 26.3 | 0.088 | | |

## INPUT DATA FOR BLIMP TEST CASES

$\alpha = 30°$

| Surface Data | | | | Shock Wave Data | |
|---|---|---|---|---|---|
| S(ft) | $r_o^k$(ft) | $h_2$(ft) | $P/P_T$ | $r_s$(st) | $\theta_s$(deg) |
| 0.0 | 0.0000 | 0.0 | 1.000 | 0.0 | 90.0 |
| 0.001 | 0.000995 | 0.001 | 0.97213 | 0.000833 | 83.1 |
| 0.002 | 0.00197 | 0.002 | 0.8885 | 0.001667 | 76.4 |
| 0.003 | 0.00294 | 0.003 | 0.828 | 0.0025 | 70.3 |
| 0.004 | 0.00383 | 0.0042 | 0.787 | 0.003333 | 65.5 |
| 0.005 | 0.0047 | 0.0056 | 0.762 | 0.004167 | 61.6 |
| 0.006 | 0.0055 | 0.0071 | 0.745 | 0.005833 | 55.6 |
| 0.007 | 0.0063 | 0.0092 | 0.730 | 0.0075 | 52.1 |
| 0.010 | 0.00879 | 0.016 | 0.687 | 0.010 | 49.1 |
| 0.013 | 0.01117 | 0.0245 | 0.654 | 0.01667 | 47.3 |
| 0.016 | 0.01346 | 0.0360 | 0.625 | 0.03333 | 44.9 |
| 0.020 | 0.01652 | 0.0540 | 0.595 | 0.05833 | 41.2 |
| 0.025 | 0.02095 | 0.08 | 0.566 | 0.08333 | 37.6 |
| 0.030 | 0.0240 | 0.12 | 0.541 | 0.125 | 35.0 |
| 0.040 | 0.0310 | 0.217 | 0.500 | 0.250 | 34.0 |
| 0.04552 | 0.03465 | 0.290 | 0.480 | 0.5667 | 33.2 |
| 0.070 | 0.050 | 0.73 | 0.425 | 0.6250 | 32.0 |
| 0.090 | 0.0613 | 1.30 | 0.395 | 0.6917 | 29.5 |
| 0.1094 | 0.0733 | 2.07 | 0.373 | | |
| 0.160 | 0.102 | 5.3 | 0.339 | | |
| 0.2174 | 0.1313 | 11.4 | 0.319 | | |
| 0.3234 | 0.1845 | 29.0 | 0.290 | | |
| 0.4294 | 0.2485 | 53.0 | 0.290 | | |
| 0.5354 | 0.2905 | 79.0 | 0.300 | | |
| 0.6414 | 0.343 | 103.0 | 0.302 | | |
| 0.7474 | 0.397 | 130.0 | 0.298 | | |
| 0.8534 | 0.450 | 158.0 | 0.262 | | |
| 0.9597 | 0.497 | 182.0 | 0.171 | | |
| 1.0587 | 0.537 | 205.0 | 0.101 | | |

INPUT DATA FOR BLIMP TEST CASES

$\alpha = 53.5°$

| Surface Data | | | | Shock Wave Data | |
|---|---|---|---|---|---|
| S(ft) | $r_o^k$(ft) | $h_2$(ft) | $P/P_T$ | $r_s$(ft) | $\theta_s$(deg) |
| 0.0 | 0.0 | 0.0 | 1.0 | 0.0 | 90.0 |
| 0.0005 | 0.000475 | 0.0005 | .9955 | 0.00833 | 83.6 |
| 0.001 | 0.00095 | 0.001 | .9875 | 0.01667 | 78.3 |
| 0.002 | 0.00190 | 0.00235 | .978 | 0.02500 | 74.0 |
| 0.003 | 0.00285 | 0.0047 | .970 | 0.03333 | 70.5 |
| 0.004 | 0.00380 | 0.0093 | .964 | 0.04167 | 67.6 |
| 0.006 | 0.00570 | 0.030 | .950 | 0.05000 | 65.2 |
| 0.008 | 0.00760 | 0.073 | .940 | 0.06667 | 62.2 |
| 0.010 | 0.00950 | 0.175 | .932 | 0.08333 | 60.4 |
| 0.015 | 0.0140 | 0.900 | .915 | 0.1250 | 60.0 |
| 0.0211 | 0.0200 | 4.2 | .900 | 0.1667 | 59.4 |
| 0.050 | 0.0475 | 450.0 | .848 | 0.2500 | 59.0 |
| 0.080 | 0.0740 | 5900.0 | .810 | 0.4167 | 58.4 |
| 0.1065 | 0.0980 | $3.2 \times 10^5$ | .788 | 0.5417 | 58.1 |
| 0.160 | 0.144 | $6.1 \times 10^6$ | .761 | 0.6250 | 58.5 |
| 0.2095 | 0.186 | $3.3 \times 10^7$ | .741 | 0.7208 | 59.6 |
| 0.3155 | 0.2705 | $1.6 \times 10^8$ | .724 | 0.8333 | 56.7 |
| 0.4215 | 0.355 | $2.9 \times 10^8$ | .716 | 0.9167 | 55.5 |
| 0.5275 | 0.4395 | $4.2 \times 10^8$ | .717 | 1.0000 | 55.3 |
| 0.6335 | 0.524 | $5.4 \times 10^8$ | .719 | | |
| 0.7395 | 0.6085 | $6.7 \times 10^8$ | .730 | | |
| 0.8455 | 0.693 | $8.0 \times 10^8$ | .739 | | |
| 0.9518 | 0.775 | $9.1 \times 10^8$ | .540 | | |
| 1.0508 | 0.845 | $1.0 \times 10^9$ | .409 | | |

# APPENDIX 3

## SPREADING FACTOR FOR NONEQUAL BODY CURVATURE

## APPENDIX 3

### SPREADING FACTOR FOR NONEQUAL BODY CURVATURE

The variable $R_c$ in Equation (6-2) is not ambiguous since it applies only to a sphere, the application being the Apollo reentry heat shield. For shuttle application, Equation (6-2) is not valid since it does not account for the unequal surface curvatures which exist forward of the wing region. The derivation of Reference 116 assumes Newtonian flow along a streamline and transverse to it in arriving at an expression for the crossflow pressure gradient in the meridianal direction.

$$\frac{\partial P}{\partial m} = - \frac{2z}{R_c^2} \cos^2\theta_B P_T \qquad \text{(A-1)}$$

where $z$ is the distance from the plane of symmetry.

For a non-spherical surface, it is necessary to return to the basic assumption of Newtonian flow, namely

$$\frac{P(s,z)}{P(s,0)} = \frac{\cos^2\psi(s,z)}{\cos^2\psi(s,0)} \qquad \text{(A-2)}$$

where $\psi$ is the angle between the local surface normal and the free stream velocity vector.

Referring to the sketch, the circle with radius $R_T$ represents

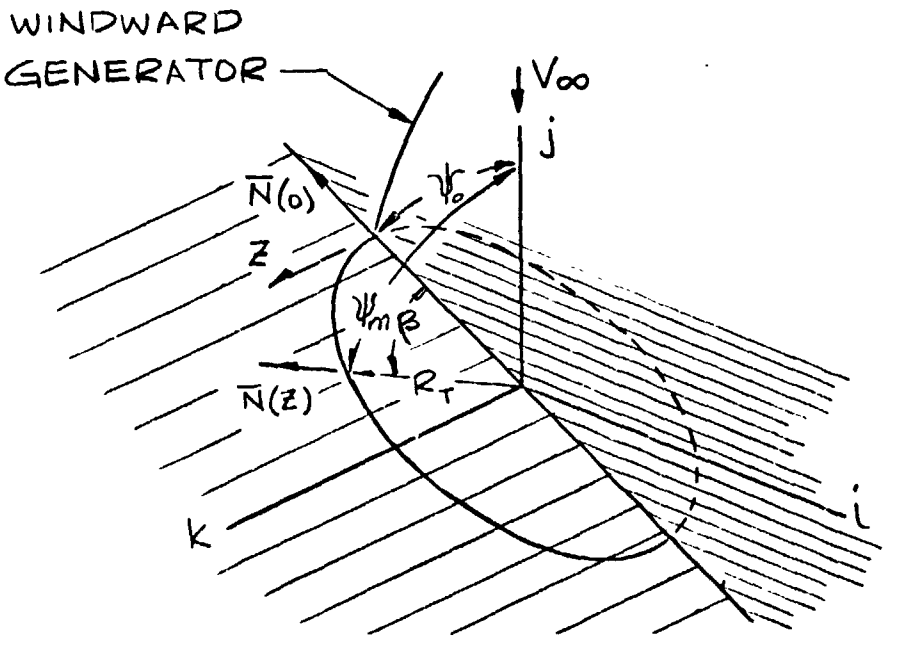

the tangent circle in the plane perpendicular to the windward streamline (generator), z = 0. A rotation in this plane by an angle β, which is equivalent to some displacement z from the plane of symmetry, results in a change in the angle ψ. This angle may be found by viewing the tangent circle both in planform and on edge. The point Q represents the tip of the radius

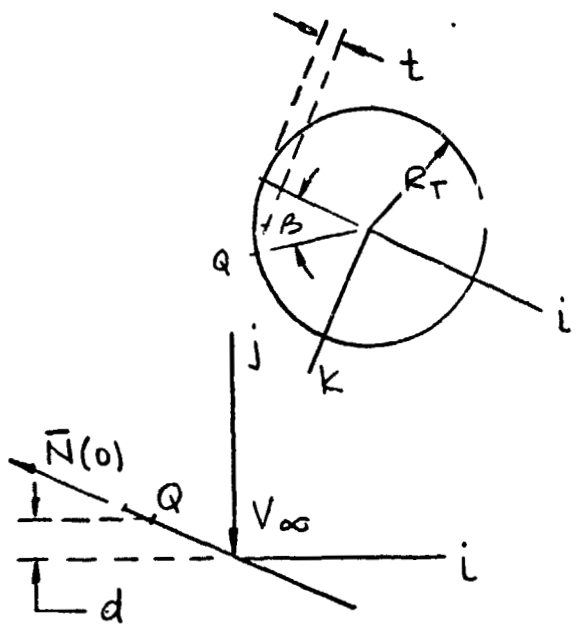


vector at some angle β. The angle this vector makes with the plane perpendicular to the velocity vector $\bar{V}$ is simply

$$\alpha = \sin^{-1} \frac{d}{R_T} \tag{A-3}$$

and thus
$$\psi(\beta) = 90^\circ - \alpha = 90^\circ - \sin^{-1}\left(\frac{d}{R_T}\right) \tag{A-4}$$

but from the above sketches we have the relation

$$\frac{d}{R_T \cos\psi(0)} = \frac{R_T - t}{R_T} \tag{A-5}$$

and
$$t = R_T(1 - \cos\beta) \tag{A-6}$$

thus
$$\psi(\beta) = 90^\circ - \sin^{-1}\left[\frac{1}{R_T}\left\{R_T\left(1 - (1 - \cos\beta)\right)\right\}\cos\psi(0)\right] \tag{A-7}$$

or
$$\psi(\beta) = 90^\circ - \sin^{-1}\left[\cos\beta\ \cos\psi(0)\right] \tag{A-7a}$$

Returning to the Newtonian pressure expression, Equation (A-2), it is now possible to find the pressure gradient in the direction normal tc the symmetry streamline.

$$\frac{\partial}{\partial m}\left[\frac{P(s,z)}{P(s,0)}\right] = \frac{\partial}{\partial m}\left[\frac{\cos^2\psi(s,z)}{\cos^2\psi(s,0)}\right] \tag{A-8}$$

or

$$\frac{\partial}{\partial m}\left[P(s,z)\right] = \frac{P(s,0)}{\cos^2\psi(s,0)}\,\frac{\partial}{\partial m}\left[\cos^2\psi(x,z)\right] \tag{A-8a}$$

where

$$\frac{\partial}{\partial m}\left[\cos^2\psi(\beta)\right] = \frac{\partial}{\partial m}\left[\cos^2\left\{90^o - \sin^{-1}\left(\cos\beta\,\cos\psi(0)\right)\right\}\right] \tag{A-9}$$

but

$$\cos(90^o - \gamma) = \sin\gamma \tag{A-10}$$

and

$$\sin(\sin^{-1}x) = x \tag{A-11}$$

therefore

$$\frac{\partial}{\partial m}\left(\cos^2\psi\right) = \frac{\partial}{\partial m}\left[\cos^2\beta\cos^2\psi(0)\right] = \cos^2\psi(0)\,\frac{\partial}{\partial m}\left(\cos^2\beta\right) \tag{A-12}$$

Now for small z and thus β, Equation (14) becomes in the limit

$$\frac{\partial}{\partial m}\left(\cos^2\psi\right) = \cos^2\psi(0)\left[-2\beta\,\frac{d\beta}{dm}\right] \tag{A-13}$$

with

$$\beta \approx \frac{z}{R_T} \quad \text{and} \quad m \approx z \tag{A-14}$$

thus

$$\frac{\partial}{\partial m}\left(\cos^2\psi\right) = \cos^2\psi(0)\left[-2\,\frac{z}{R_T}\,\frac{d\beta}{dz}\,\frac{dz}{dm}\right]$$

$$= \cos^2\psi(0)\left(-\frac{2z}{R_T^2}\right) \tag{A-15}$$

in the limit as z goes to zero.

If the local symmetry plane pressure in Equation (A-8a) is the Newtonian value then

$$\frac{P(s,0)}{\cos^2\psi(s,0)} = P(0,0) = P_T \tag{A-16}$$

and Equation (10a) becomes

$$\frac{\partial P}{\partial m} = -\frac{2z}{R_T^2}\cos^2\psi(0)P_T \tag{A-17}$$

where $\psi(0)$ and $\theta_B$ are equivalent quantities.

Thus, Equation (6-2) is replaced for non-spherical shapes by

$$\frac{d^2h_2}{ds^2} - \frac{1}{\rho u^2}\frac{\partial P}{\partial s}\frac{dh_2}{ds} + \left[\frac{1}{R_C^2} - \frac{2P_T}{\rho u^2}\frac{\cos^2\theta_B}{R_T^2}\right]h_2 = 0 \tag{A-18}$$